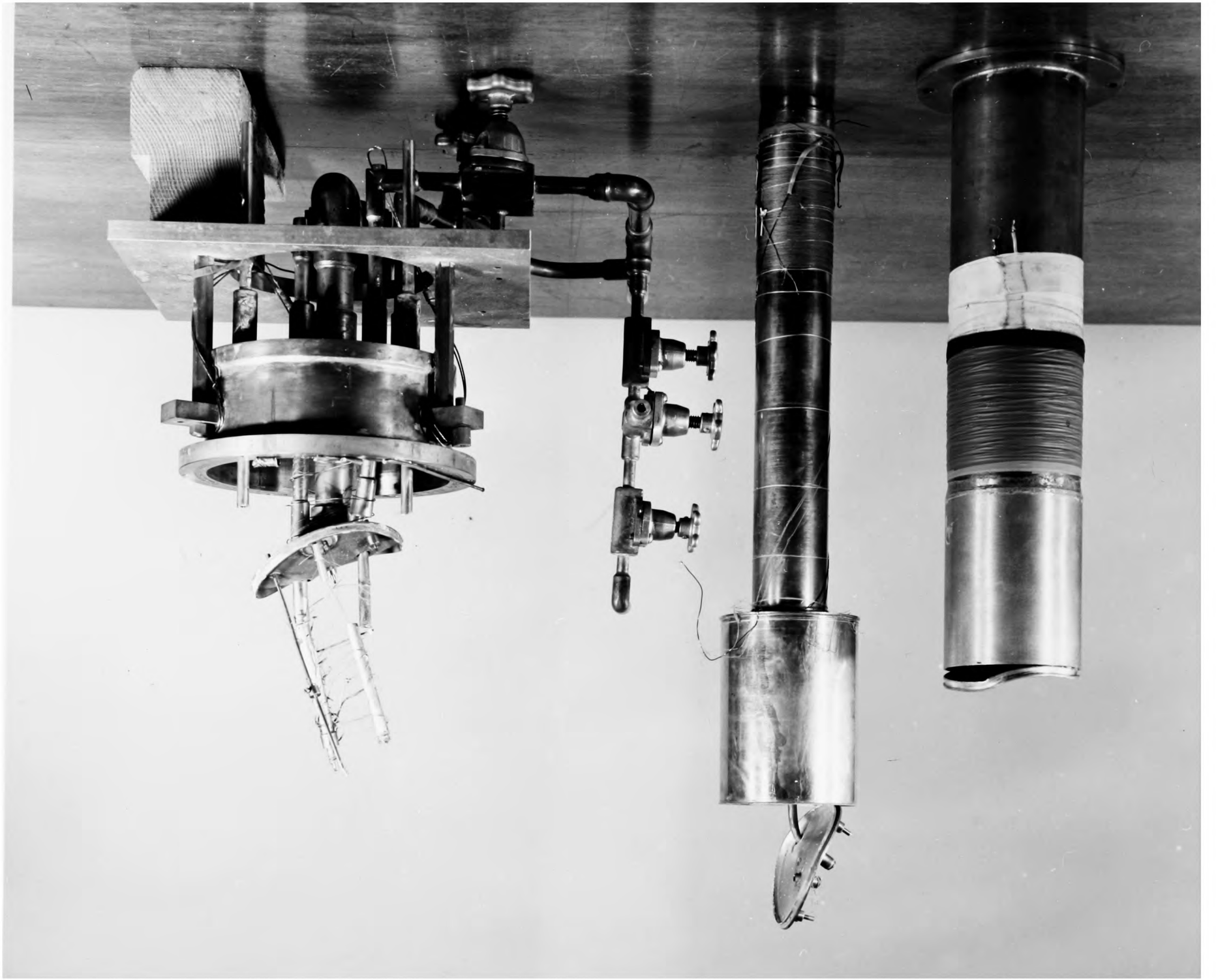
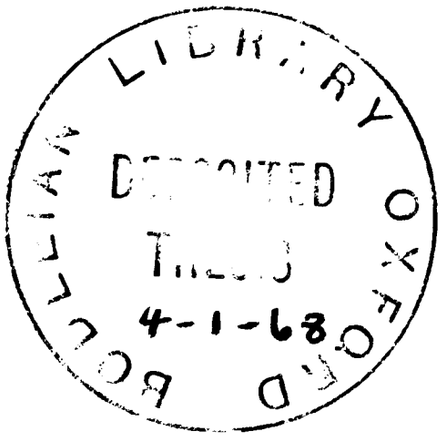


Frontispiece:

'An Exploded View of the Cryostat'.

(photograph by C. W. Band.)



EXPERIMENTS ON ORDERED SPIN SYSTEMS.

by

Margaret F. Cracknell.

(née Grant.)

(St. Hugh's College, Oxford.)

Thesis submitted in suplication for the Degree of Doctor of Philosophy, October 1967.

Abstract.

In this thesis the results obtained from several experiments in which radioactive nuclei were statically oriented in various hosts are described and discussed. The work is divided into eight chapters, the first four giving the theory and experimental details, and the remaining four being concerned with the results.

We commence with a brief introduction to the theory of magnetic and hyperfine interactions and describe the difficulties involved in the calculation of their strengths in metals. A discussion follows of the interpretation of measurements of the hyperfine field strength in metals and this short review concludes with an evaluation of the various experimental techniques which may be exploited to measure the hyperfine interaction.

A more detailed account follows of the particular technique used to obtain our results, namely that of static nuclear orientation. A phenomenological description of the hyperfine interaction is given, together with the theory of the angular distribution of gamma radiation emitted by oriented nuclei, and a discussion of the scope of gamma anisotropy measurements.

The cooling apparatus required to statically orient nuclei is described, together with the gamma radiation detection equipment and the data collection process. Also discussed are the corrections applied to all raw data and the procedure followed in analyzing the measurements in terms of a hyperfine magnetic field acting at the nucleus.

Measurement of the sense of any circularly polarised component in the gamma radiation emitted by oriented nuclei yields the sign of the hyperfine interaction, or hyperfine field in our case. The equations describing the gamma radiation polarization are presented, together

with a discussion of the theory of, and the apparatus required for, detection of the circularly polarised component via the dependence of the scattering cross-section for polarised electromagnetic radiation on the orientation of the spin of the scattering electron.

Gamma radiation anisotropy measurements were taken from four systems, namely ^{109m}Ag in iron, ^{54}Mn and ^{60}Co in palladium, and ^{60}Co in thermal neutron-irradiated cobalt. Circular polarization measurements were taken from the palladium host samples, and from a calibrating ^{60}Co in iron sample.

An alloy of 1% Pd in Fe was irradiated to form the 14hr ^{109}Pd isotope; this nuclide decays via beta emission (undetected) to a 40sec isomeric state, 88keV above the ^{109}Ag ground state. Anisotropy measurements of the electric octupole 88keV transition yielded an estimate of 340 ± 20kG for the hyperfine field at silver nuclei in iron, assuming complete re-orientation among the nuclear spin levels of the isomeric state. Hyperfine field measurements at diamagnetic nuclei dissolved in ferromagnets can only be interpreted collectively and we describe such an analysis, due to Shirley et al.[76].

Two differently prepared samples of ^{54}Mn in nominally pure palladium were examined and results from them were found to agree to to within the experimental errors. Up to 45% reduction was observed in the intensity of the axially emitted gamma radiation, measured in applied fields up to 5kG and at temperatures between 0.05 and 0.011°K. When analyzed assuming orientation parallel to the applied magnetic field, values for the 'apparent' hyperfine field were obtained which reduced in magnitude with reducing temperature and with reducing applied field at applied fields below ~4kG. This data was reanalyzed assuming the Mn ions to interact, describing this interaction by a

randomly oriented magnetic field. The theory for data analysis is given for a constant magnitude interaction and for a ''square-wave' distribution in magnitudes' interaction, and the results re-analyzed assuming the true hyperfine field to be a constant. The cut-off value of this 'square-wave form' interaction field was deduced for the two samples to be 0.4±0.1kG and 1.1±0.1kG and the hyperfine field to be 361±15kG. The different interaction field estimates were probably due to a different impurity content of the two samples. Both values correspond to interaction temperatures an order of magnitude above the temperature range of measurement and a later spectroscopic analysis of the initial palladium showed an impurity content high enough to cause magnetic ordering at about the deduced interaction temperatures. From circular polarisation measurements, where a 1% effect was observed, the sign of the hyperfine field at Mn nuclei in palladium was determined to be negative; the hyperfine field value is discussed in terms of the possible contribution from the polarization of the host's conduction electrons.

Four samples of ^{60}Co in palladium were examined. The two samples in nominally pure palladium, prepared in different ways and examined in applied fields up to 5kG and at temperatures between 0.05 and 0.012°K, were found to substantially agree to within the experimental errors. The 'apparent' hyperfine field results showed the same temperature- and applied field dependence as the MnPd data but with less accuracy, the axial gamma radiation reduction being always less than 10%. A Co-Co 'interaction field' analysis, as for the MnPd data, yielded estimates of the 'square-wave' form interaction of 1.4±0.2kG and $\geq$ 1.5kG, and the value for the hyperfine field at Co nuclei in Pd 110±8kG. Any comments concerning the interaction field estimates are

similar to those for the MnPd data. Anisotropy measurements from ^{60}Co in two palladium samples containing respectively 0.2% and 0.05% of stable cobalt, sufficient to achieve ferromagnetic ordering below 1°K, were taken in applied fields up to 16kG and at temperatures between 0.03 and 0.011°K. The 0.002CoPd sample yielded 'apparent' H_e values larger than the dilute samples, but was far from being magnetically saturated. The 0.0005CoPd sample yielded even larger 'apparent' H_e values, which indicated the approach to a saturation value of either $+200\pm20$kG or -240 ± 20kG in applied fields $\sim$20kG. Circular polarisation measurements yielded, from $\sim$1% 'effects', the surprising result that the hyperfine fields at ^{60}Co in one of the 'pure' samples and in the 0.002CoPd sample were positive. Thus the result from the 0.0005CoPd alloy is in agreement with n.m.r. data (H_e = 213±5kG.). Anisotropy measurements from one 'pure' sample were taken in applied fields up to 16kG and the results yielded a value of $+116\pm10$kG for the hyperfine field, and were consistent with saturation in applied fields $\sim$5kG. It is concluded that the hyperfine field at cobalt nuclei in palladium metal may well be a function of the cobalt concentration in the very dilute alloy range, possibly due to a variation in the degree of conduction electron polarization.

The last experiment reported herein involved the irradiation of a single crystal of cobalt metal at 4°K in a thermal neutron beam. The ^{60}Co nuclei so formed were cooled to $\sim$0.01°K and gamma radiation a anisotropy measurements taken. Some ^{58}Co diffused into the cobalt crystal acted as the thermometer. These measurements were repeated after the sample had been annealed at 20°K, then at 77°K and 300°K. Little change in the data with annealing temperature was observed, in contrast with resistivity measurements from similarly treated cobalt; particularly,

the hyperfine field value measured after annealing at $4^{\circ}K$ was only $6\pm4\%$ larger than that measured after annealing at $300^{\circ}K$. From our result it is argued that even after absorption of a thermal neutron and emission of $\sim$6MeV energy, the ^{60}Co nuclei occupy lattice sites, with any vacancy or interstitial more than one lattice constant distant.

TABLE OF CONTENTS.

Abstract. ..... i.

Chapter I: Magnetic and Hyperfine Interactions in Metals.

Introduction. ..... 1.

I.1. The Exchange Interaction. ..... 1.

I.2. The Hyperfine Interaction. ..... 4.

I.3. The Hartree-Fock Formalism. ..... 6.

I.4. Magnetic Interactions in Metals. ..... 9.

I.5. Hyperfine Interactions in Metals. ..... 14.

I.6. Measurement of the Hyperfine Interaction in Metals..... 15.

Conclusion. ..... 19.

Chapter II: The Nuclear Orientation Technique.

Introduction. ..... 20.

II.1. Mechanisms for Orienting Nuclei. ..... 20.

II.2. The Spatial Distribution of Radiation from Oriented Nuclei. ..... 22.

II.3. The Scope of Gamma Radiation Anisotropy Measurements. ..... 25.

II.4. Parameters for Analysis of ^{60}Co and ^{54}Mn Data. ..... 26.

Chapter III: Apparatus and Data Analysis for Anisotropy Measurements.

Introduction. ..... 27.

III.1. Sample Assembly. ..... 27.

III.2. Helium Reservoir. ..... 28.

III.3. Nitrogen Reservoir. ..... 29.

III.4. Superconducting Magnets. ..... 29.

III.5. Aluminium 'Windows'. ..... 30.

III.6. Magnetising Solenoid. ..... 30.

III.7. Counting Assembly. ..... 31.

III.8. Procedure. ..... 31.

III.9. Storage of Data. ..... 32.

III.10. Raw Data. ..... 32.

III.11. Corrections to the Anisotropy Data. ..... 33.

III.12. Sample Strengths. ..... 35.

III.13. Analysis of Anisotropy Measurements. ..... 35.

III.14. Estimation of Errors. ..... 36.

Chapter IV: Circular Polarimetry.

Introduction. ..... 37.

IV.1. The Circilar Polarisation of Gamma Radiation. ..... 37.

IV.2. The Scattering of Electromagnetic Radiation by Matter. ..... 38.

IV.3. Experimental Details of the Circular Polarimeter. .... 39.

IV.4. Storage and Analysis of Data. ..... 41.

Chapter V: ^{109m}Ag in Iron.

Introduction. ..... 42.

V.1. Samples. ..... 42.

V.2. Decay Scheme Parameters for ^{109m}Ag, 88keV Transition. ..... 43.

V.3. Thermometry. ..... 45.

V.4. Correction for Time Decay of the Activity. ..... 45.

V.5. Results. ..... 46.

V.6. Discussion. ..... 47.

Chapter VI: ^{54}Mn in Palladium.

Introduction. ..... 50.

VI.1. Sample Preparation. ..... 52.

VI.2. Thermometry. ..... 53.

VI.3. Results. ..... 54.

VI.4. Discussion. ..... 55.

VI.5. Attenuation Factors for Electronic Interactions. ..... 57.

VI.6. Analysis of Anisotropy using the Attenuation Factors. ..... 58.

VI.7. The Sign of the Hyperfine Field (^{54}Mn in Pd). ..... 61.

VI.8. Further Discussion and Conclusion. ..... 62.

Chapter VII: ^{60}Co in Palladium.

VII.1. Sample Preparation. ..... 67.

VII.2. Thermometry. ..... 68.

VII.3. Results. ..... 68.

VII.4. The Sign of the Hyperfine Field at ^{60}Co Nuclei in Palladium. ..... 71.

VII.5. Discussion. ..... 72.

VII.6. Conclusion. ..... 77.

Chapter VIII: Hyperfine Fields in Neutron Irradiated Cobalt.

Introduction ..... 79.

VIII.1. Special Features of the Cryostat. ..... 80.

VIII.2. Samples. 81

VIII.3. Parameters for Data Analysis. ..... 81.

VIII.4. Experimental Procedure. ..... 82.

VIII.5. Results. ..... 83.

VIII.6. Discussion. ..... 85.

VIII.7. Conclusion. ..... 87.

Appendices.

References.

Chapter I.

Magnetic and Hyperfine Interactions in Metals.

Contents:

Introduction.

I.1. The Exchange Interaction.

I.2. The Hyperfine Interaction.

I.3. The Hartree-Fock Formalism.

I.4. Magnetic Interactions in Metals.

I.5. Hyperfine Interactions in Metals.

I.6. Measurement of the Hyperfine Interaction in Metals.

Conclusion.

Introduction.

Magnetic ordering phenomena have long been understood (at least qualitatively) in terms of interactions between the elementary magnetic moments associated with atoms having unfilled inner electron shells (e.g. '3d' and '4f' transition series elements) which depend on the relative spin orientation and separation. When the energy of thermal disorder is less than the interaction energy, a transition to an ordered state takes place, in which neighbouring dipoles may be aligned mutually parallel, antiparallel, or in a more complicated array depending on the substance under investigation. Quantitative estimates of the gross properties of a solid associated with cooperative magnetic ordering, e.g. the magnetic susceptibility of the solid, the variation in the specific heat through the transition temperature, the change in temperature due to an adiabatic change in the external magnetic field, the variation in the degree of spontaneous magnetization with temperature, etc, compare well enough with experimental results to provide substantial data on the magnitude and sign of the interaction energy in various environments.

I.1. The Exchange Interaction.

The strength of this interaction between the atomic magnetic moments is much larger than the dipole interaction at the separations found in solids, and its origin was identified with the 'exchange' interaction between neighbouring electrons by Heisenberg(1928)[1]. This 'exchange' interaction arises in the following way. Electrons obey Fermi-Dirac statistics and so the total wave function describing a system of electrons must be anti-symmetric for permutation of the identical particles, and may be expressed as a product of the one-electron wave-functions if the electrons are non-interacting. It is easy to show that

a system of two non-interacting electrons, for which the one-electron wave-functions are separable into orbital and spin functions, can be described by two alternative product wave-functions one of which has a symmetrical orbital part in conjunction with an anti- symmetric spin part (corresponding to anti-parallel spin orientation of the electrons), the other vice-versa. If the Coulomb repulsion, always present between electrons, is included in the Hamiltonian for the system then two alternative values result for the total energy W (using first order perturbation theory), one associated with each of the two product wave-functions. Denoting the spins of the two electrons by $\underline{S}_1, \underline{S}_2$, we can define the 'exchange' energy or 'exchange integral' J by the equation

$$W = \text{Constant} + 2J\underline{S}_1 \cdot \underline{S}_2 \qquad \ldots\ldots\ldots\ldots \quad \underline{I.1}$$

and J is then the difference in the energy associated with the two possible states of the system, i.e. with parallel or anti-parallel spin orientation. Heisenberg showed that for two nearest neighbour identical one-electron atoms a,b, separated by a distance R, the exchange integral could be written as

$$J(a,b) = \iint d\underline{r}_1 \cdot d\underline{r}_2 \psi_b(\underline{r}_1)\psi_a(\underline{r}_2)\left\{\frac{e^2}{R} + \frac{e^2}{r_{12}} - \frac{e^2}{r_{1b}} - \frac{e^2}{r_{2a}}\right\}\psi_b(\underline{r}_2)\psi_a(\underline{r}_1) \cdot \quad \underline{I.2}$$

where $\underline{r}_1$, $\underline{r}_2$ are co-ords, ψ_a, ψ_b the normalised one-electron wave-functions.

Clearly the magnitude of this exchange energy depends on the degree of overlap of the one-electron wave-functions and so is critically dependent on the atomic separation, while the four terms of the perturbing potential (i.e. the Coulomb interaction) are of comparable magnitude and together determine the sign of J. From the definition (eq. I.1) a positive value of J can be seen to correspond to a ferromagnetic

ground state for the system, i.e. parallel spin orientation associated with less energy than anti-parallel orientation.

Large positive exchange energies are found in the ferromagnetic metals iron, cobalt, nickel and gadolinium (transition temperatures 1043°K, 1394°K, 631°K, 289°K respectively) and in many metallic alloys involving transition series elements. Large negative exchange energies are found in the anti-ferromagnetic chromium (475°K) and again many alloys; we omit discussion of non-metallic solids. In fact, for every substance containing elementary magnetic dipoles the exchange energy has a finite value and there will be a temperature, albeit very low, at which a (usually) co-operative transition takes place.

Quantitative theoretical estimates of the exchange integral (eq. I.2) for iron series atoms only recently became available with the advent of reliable calculations of their electronic structure (using computers); in particular, Stuart and Marshall (1960)[2] found J for the overlap of the magnetic (3d) electrons of two iron atoms to be positive, but a factor of ~70 too small to account for ferromagnetism in the metal, while Freeman et al. (1962)[3] found J for the overlapping 3d-electrons of two Co atoms and of two Co^{++} ions to be large but negative. It seems this 'direct' exchange interaction is <u>not</u> large enough to account for magnetic phenomena involving the elements of the 3d transition series, and the magnetic moments of other elements are associated with electrons evenly more closely bound to the nucleus, e.g. 4f electrons.

Various extensions of the exchange mechanism between magnetic ions in metals via the intermediary of polarised conduction electrons have been proposed in order to obtain quantitative agreement with experiment and these will be discussed in § I.4.

I.2. The Hyperfine Interaction.

The interaction between the electronic orbital and spin angular momentum and the angular momentum of the nucleus is analogous to the exchange interaction, though generally a factor $\sim 10^3$ smaller in magnitude, and is known as the hyperfine interaction. The hyperfine interaction was first observed in atomic spectra via the hyperfine splitting of the electronic energy levels of atoms, and Fermi (1930)[4] first derived the Hamiltonian $\mathcal{H}$ for the interaction between the nuclear magnetic moment $g_I\mu_N\underline{I}$ and the orbital $g\mu_b\underline{L}$ and spin $g\mu_b\underline{S}$ magnetic moments of a single atomic electron,

$$\mathcal{H} = -gg_I\mu_b\mu_N\left\{\frac{8}{3}\pi\delta(r)\underline{S}\cdot\underline{I} + \frac{(\underline{L}-\underline{S})\cdot\underline{I}}{r^3} + \frac{3(\underline{S}\cdot\underline{r})(\underline{I}\cdot\underline{r})}{r^5}\right\} \quad \ldots\ldots \underline{I.3}$$

The first term, in $\delta(r)$, is non-zero only for s-electrons (which have a finite probability of being at the nucleus) and is called the "Fermi contact" term; the other two terms are analogous to the classical interaction between dipoles and are zero for s-electrons because of the spherical symmetry of their wavefunctions.

If the nuclear precession time is much shorter than the electronic spin relaxation time, then there will be 2I+1 nuclear energy levels associated with each of the 2S+1 electronic energy levels, If the former is much longer than the electronic spin relaxation time then the nuclear spin will be unable to come to equilibrium with the instantaneous orientation of the electronic spin, and instead there will be only 2I+1 equally spaced nuclear energy levels with a splitting proportional to the time-averaged electronic spin. (For this splitting to be non-zero, the application of an external magnetic field may well be necessary in which case the relevant time is the electronic relaxation time in the external

field.) This type of energy level splitting is usually obtained in the one-electron atom since in the same magnetic field the nuclear precession time is $\sim 10^3$ longer than the electronic precession time, and it is analogous to the normal Zeeman effect in which the electronic energy levels of an atom are equally split by the interaction with an external magnetic field. In such cases, it is possible to express the hyperfine interaction in terms of an 'effective' or hyperfine magnetic field acting on the nuclear magnetic moment.

For a many-electron atom the hyperfine interaction may be expressed as a sum over terms of the form eq. I.3, in which case all 'paired' electrons give a net zero contribution, and then for ions having only unpaired s-electrons the hyperfine field H_c at the nucleus arises from the contact part of the Hamiltonian, the contact field H_c being given by

$$H_c = \left(8\pi/3\right) . g\mu_o \underline{S} \left|\psi_s(0)\right|^2 \qquad \ldots\ldots\ldots \text{I.4.}$$

where $\left|\psi_s(0)\right|^2$ is the density of the unpaired s-electrons at the nucleus. Again, in the many-electron atom the concept of a hyperfine field is only valid if the electronic spin system comes into internal equilibrium in the external magnetic field much faster than the time the nucleus takes to precess in the 'effective' field. For ions with a net spin but no unpaired s-electrons the hyperfine interaction is much larger (e.g. for Mn^{2+}, $3d^5\ {}^6S$, $H_c \sim 700$kG) than that expected from the unpaired d-electrons alone, and can be attributed to a net polarisation of the atomic core s-electrons by the unpaired spin of the free ion[5]; hence the sum of one-electron Hamiltonians does not describe such atoms adequately.

It should be clear that the exchange interaction and the hyperfine interaction are intimately connected phenomena, via the net polarisation

of all the relevant electrons, and that the problems involved in calculating either are indeed formidable. To illustrate this point more fully, we continue with a brief account of the principal theoretical approach to the problem of calculating electronic wave-functions in atoms, with emphasis on their ability to provide an adequate estimate of the hyperfine interaction.

I.3. The Hartree-Fock Formalism.

In order to calculate any physical observable one must first obtain the relevant wave-functions, i.e. the solutions to Schroedinger's equation, for the system in question. Exact solution of Schroedinger's equation has not yet proved possible for systems involving more than one electron, and so the true many-electron wave-functions must be approximated by an expansion in terms of some set of basis functions (and usually a truncated expansion due to computational difficulties); in the Hartree-Fock ('H-F') formalism the approximate many(n)-electron wave-function is taken to be a single, or linear combination of, 'Slater determinant'[6] where the 'Slater determinant' is the normalised determinant having n rows of the form

$$\psi_1(x_j)\psi_2(x_j)\ldots \quad \ldots\psi_n(x_j)$$

with j running from 1 to n, made up from one-electron wave-functions $\psi_i(x_j)$ of the space and spin co-ordinates x_j. The 'best' approximation to the true many-electron wave-function is determined by minimising the total energy of the system using the variational principle on individual ψ_i's, and attempts to apply this principle to other observables to improve on this many-electron wave-function have not so far been profitable.

In the conventional H-F calculations the one-electron wave-

functions are assumed to be separable into a product of spatial and spin functions, where the same spatial function describes both orientations of the spin angular momentum, and so no paired electrons of the ion, based on this model, will contribute to the exchange or hyperfine interactions. Secondly, the spatial part of the one-electron wave-function is assumed to be separable into a product of radial and angular wave-functions, the angular wave-functions are chosen to be the spherical harmonics and the radial part of the wave-function is the same for all electrons in the same shell; that is, the atom or ion is assumed to be spherically symmetrical, a condition which is usually not entirely fulfilled. These restrictions are placed on the one-electron wave-functions in order to reduce the total number of simultaneous equations requiring solution, and it seems their relaxation affects the computed total energy of the system by as little as $10^{-3}\%$.[7]

In an ion having net unpaired spin, the exchange interaction of this net spin with the spin of each electron would give rise to different spatial wave functions for the two possible orientations of each electron spin; this difference is all-important for calculation of the hyperfine interaction, and an approach in which the spatial restraint is relaxed, while the single determinant is treated as before, is known as the "Spin- or Exchange-Polarized" Hartree-Fock method. Much work is being devoted to examining the possibility of further refinements to the Hartree-Fock method of obtaining many-electron wave-functions, e.g. by including linear combinations of 'Slater determinants' and by considering correlation effects, but even in the lightest ions difficulties such as maintenance of the symmetry of the system render the analysis extremely complex.

At the moment only the exchange-polarized Hartree-Fock method has been used to obtain an approximate wave-function for atoms as large as Fe, Mn and Co, in which we are interested, and we reproduce in table I.1 some of the results obtained by Watson and Freeman(1961)[8] for the individual s-electron contributions to the contact part of the hyperfine field at the nucleus of the Mn atom.

Table I.1.

Electron	Contribution	Net contbn. (shell)
$(3d^5\uparrow)$ 1s ↕	2,502,840kG	-30kG
1s ↓	-2,502,870kG	
2s ↑	226,670kG	-1410kG
2s ↓	-228,080kG	
3s ↑	31,210kG	+740kG
3s ↓	-30,470kG	
4s ↑	1,750kG	+600kG
4s ↓	-1,149kG	
	Total	-100kG
Experimental value: Mn^{2+} ion		-650kG
	atom	0kG

We see that the net contribution to the hyperfine field due to the electrons from each shell arises from competition beween two very large terms, and that the contributions from each shell also compete, depending in sign on whether the ns-electrons can be regarded as being predominantly "inside" or "outside" the '3d' or unpaired electrons. To summarise, we quote Freeman and Watson (1965)[9] "...it is surprising that the exchange-polarization method is successful in reproducing the observed sign of H_c; it is even more remarkable that the observed order of magnitude is also

determined by the calculations."

In the exchange-polarized H-F method, the spatial part of the wave-function was assumed to be separable into radial and angular functions and the same radial function described all the electrons of one spin orientation within each shell; relaxation of this restraint, i.e. taking into account aspherical distortion of the inner 'shells' of an ion by distorted outer 'shells' or a crystalline electric field, also gives rise to a hyperfine interaction.[10]

The many-electron wave-function contains much more information than is necessary to predict the size of the hyperfine interaction and other physical observables which are associated with one- and two-electron operators, and the getting of this excess information is a luxury one can hardly afford for the heavier atoms. However, the known alternative method of dealing with one- and two-electron "reduced density matrices" has not yet been developed to the stage where wave-functions may be excluded from the formalism, and other possible alternative approaches have yet to be explored, so exchange-polarized H-F calculations remain the only source of theoretical estimates of the hyperfine interaction in atoms.

I.4. Magnetic Interactions in Metals.

In a metal the outermost electrons do not have the discrete energy levels characteristic of atoms but may possess energies within an approximately continuous and bounded range or 'band' and belong to no particular atom. The wave-functions describing these electrons are determined by the atoms concerned and by the spatial symmetry of the solid, and as already mentioned satisfactory wave-functions describing these shared electrons are scarcely obtainable even using the full H-F

restraints so calculation of the exchange or hyperfine interaction is not possible.

Two complementary explanations of the transition in solids from paramagnetism to ferromagnetism are in use. In the Heisenberg (1928)[1] approach, the magnetic electrons are regarded as being tightly bound to their respective atoms and the 'direct' exchange interaction between pairs of atoms calculated from the overlap of electronic wave-functions, is summed over the solid and compared with the thermal disordering energy. By suitable adjustment of the value for the exchange energy, this model can be used to explain many of the gross properties of magnetic solids but cannot account for the observed magnetic moment per atom in the magnetic state, which is not an integral number of Bohr magnetons. In the 'collective electron' model, investigated by Slater and Stoner[11] the magnetic electrons are 'shared' between the atoms of the solid as described in the previous paragraph, and the exchange interaction causes a relative displacement (w.r.t. energy) of the allowed energy 'bands' for the two possible orientations of the electron spin, the magnitude of the displacement being proportional to the relative population of the two spin states. This displacement, the density of electrons per unit energy range in the band, and the thermal energy together determine the degree of magnetization to be expected. On this "collective electron" model, the non-integral value of the magnetic moment per atom is easily accounted for.

It very soon became apparent that the 'direct' exchange interaction could certainly not explain the ferromagnetism of the rare-earth (4f) transition series metals, and later the magnetic transition in the 3d transition series metals, and so for some time attention has mostly been directed towards evaluation of the 'indirect' exchange interaction in metallic solids via the conduction electrons; we continue

here with a short history of the theory of this mechanism.

The possibility of a ferromagnetic interaction between nuclear spins in a diamagnetic metal via their double interaction with the conduction electrons was first discussed by Frohlich and Nabarro (1940)[12] in the context of the lowest temperature attainable by the adiabatic demagnetization of such a nuclear spin system. An analogous 'indirect' exchange interaction between the electronic 3d or 4f spins, via their 'direct' exchange with polarised conduction electrons was postulated by Zener (1951)[13] as a possible explanation of ferromagnetism in the transition metals; like Frohlich and Nabarro, Zener considered only the first order perturbation, that is assumed a uniform polarization of the conduction electrons, and arrived at a necessarily ferromagnetic interaction.

The indirect interaction between two nuclear moments in a diamagnetic metal was first calculated using second order perturbation theory by Ruderman and Kittel (1954)[14] and it was shown that the spin-spin interaction was not necessarily ferromagnetic, but varied in both magnitude and sign with the separation of the nuclei. This 'indirect' exchange mechanism was then applied to a system of electronic spins by Kasuya (1956)[15] and Yosida (1957)[16] (the s-d interaction) and the net result was considerable localization of the conduction electron polarization about the perturbing spin, and an exchange-type interaction between the d-electron spins which oscillated in sign and diminished rapidly with distance. (The Hamiltonian for the indirect exchange interaction between the ith and jth ions a distance R_{ij} apart is given by

$$\mathcal{H} = A_{ij}\underline{S}_i \cdot \underline{S}_j \qquad \text{where}$$

$$A_{ij} \propto \left[2k_F R_{ij}\cos(2k_F R_{ij}) - \sin(2k_F R_{ij})\right] / R_{ij}^4$$

and the conduction electron band is assumed filled in both spin states from $k = 0$ to k_F.)

Recent calculations of the ground state energy of a free-electron gas whose spins interact with the nuclear or ionic spins have been made by Vertogen and Caspers (1967)[17] "in the so-called R-K-K-Y (Ruderman-Kittel-Kasuya-Yosida) approximation" in which the third order correction tended to infinity; the conclusion was that the usual R-K-K-Y result quoted above is not correct and terms higher than second order must be taken into account.

The exchange interaction between conduction electrons and a 'localized spin' (the dilute alloy problem) has been treated using the 'double-time' Green's function by Kondo (1966, 1967)[18] and Nagaoka (1965, 1967)[19]. In particular they predict for a negative exchange energy J the formation at low temperatures of a 'spin compensated bound state', that is there appears a "quasi-bound state around the localized spin" in which the conduction electron polarization is opposite to that of the localized spin; the range of this polarization is somewhat greater ($\propto (\sin k_F R / k_F R)^2$) than the R-K-K-Y result.

The 's-d' interaction provides a mechanism of short range order in metallic alloys containing transition elements; a mechanism of long range order, via interaction of the 'localized' moments with a 'static spin density wave', was proposed by Overhauser (1960)[20]. Overhauser demonstrated that the paramagnetic state of a three-dimensional electron gas confined to a box, as calculated using the Hartree-Fock formalism, was unstable against the formation of a stationary spin density wave (hereafter S.D.W.) of (as in R-K-K-Y theory) wave vector $q = 2k_F$, the diameter of the Fermi sphere, and furthermore that this stationary S.D.W. state was associated with a lower total energy than the paramagnetic state,

hitherto believed to be the H-F ground state for such a system. (Recall that the equations describing a many-electron system were solved in the H-F formalism by minimising the total energy.) (The H-F formalism over-estimates the effect of exchange interactions, and a more accurate treatment of the problem may well suppress the static S.D.W.s or merely reduce their amplitude and the critical temperature below which they come into existence, but a theoretical investigation of this aspect of the problem has still to be effected.) If all the S.D.W. modes of the conduction electrons are partially exited, then there will be an associated increase in the energy of the system; however the localized magnetic moments will experience an exchange interaction with the spin polarization of the conduction electrons which affects the polarization itself, the net effect being a reduction in the energy of the system. Minimization of the total energy leads to evaluation of the (finite) amplitude of each S.D.W. mode, and hence to an ordering of, i.e. interaction between, the magnetic moments which may be long range depending on the relative S.D.W. amplitudes; the R-K-K-Y interaction is shown to be a special case resulting from these considerations. Much otherwise puzzling experimental data can be explained, at least qualitatively, by invoking the existence of a static S.D.W.; in particular the curious antiferromagnetism discovered in chromium metal where the wavelength of the magnetization is not a small integral number of lattice constants, can be attributed to the formation of a S.D.W.

We must mention here the less fundamental work of Friedel (1958, 1962)[21] in which the alloys of transition elements in various hosts are discussed in terms of the existence of 'virtual bound states'; these occur when the energy of the 'bound' (3d) electrons of the solute transition element is near to the Fermi energy of the conduction electrons so that a resonance phenomenon occurs and localized magnetic moments are

formed. The coupling between the localized moments varies in the same way as in the R-K-K-Y interaction, but originates in the phase-shift of the conduction electrons involved in the resonance and is a factor ~4 larger in amplitude.

No attempt has been made to present systematically the vast quantity of experimental data which supports these various approaches towards accounting for magnetic interactions, but a selection from these results will be presented in the later chapters. To a certain extent the various approaches seem to be complementary so the same data fits more than one scheme, and so far no conclusive evidence is available to rule out any of the possibilities. It may well prove that each is appropriate to a particular environment.

I.5. Hyperfine Interactions in Metals.

In a metal the electrons interact strongly and so the electronic spin system usually reaches internal equilibrium much faster than the nuclear precession time; the 2I+1 nuclear energy levels are equally split with a spacing proportional to the time-average of the electron spin and description of the hyperfine interaction in terms of an 'effective' field at the nucleus is valid. This is not true in an insulator where all electrons may be regarded as tightly bound to their respective ions and relax via the lattice - a slow process (~1 sec). Within each domain of a ferromagnet the electronic spins are partially aligned, the net magnetization being a function of temperature, and so there will be a single temperature dependent value for the hyperfine field at equivalent lattice sites. In a paramagnetic metal the net electronic spin and thus the hyperfine field splitting will time-average to zero at all temperatures in the absence of an external magnetic field,

while in its presence the hyperfine field is often directly proportional to the time average of the electron spin,[22] which may have Brillouin function dependence on ($H_{applied}$/Temp.), providing the electronic moments are localised and do not interact appreciably

Since the conduction electron polarization contributes significantly to the hyperfine interaction, its magnitude and sign may be probed by measuring the hyperfine fields at various nuclei in a wide range of metallic alloys and it is to this end that the nuclear orientation technique (see later) is applied in the experiments to be described in this thesis. Unfortunately, interpretation of hyperfine interaction measurements is somewhat complicated by the difficulty of separating the core-s-electron polarization contribution from the conduction electron contribution; there are also the much smaller external, demagnetizing, and Lorentz field contributions to be taken into account, as well as the direct dipolar field of the unpaired (d or f) electrons (zero for cubic symmetry) and the field due to any unquenched orbital angular momentum. Clearly, it is necessary to make a systematic analysis of hyperfine interaction measurements over a wide range of environments in order to differentiate these various contributions.

I.6. Measurement of the Hyperfine Interaction in Metals.

We continue with a brief enumeration of the various experimental techniques used to measure the hyperfine interaction in metallic solids, with emphasis on their versatility and limitations.

a. Nuclear Magnetic Resonance. The most straight-forward and accurate way of measuring the hyperfine interaction is by detection of the frequencies at which transitions between the various nuclear energy levels occur. A stable nuclide having an appreciable magnetic moment is

essential, and frequently lack of such an isotope precludes the application of this technique to many systems. Also at the frequencies involved the skin depth in metals is very small so the specimens must be powdered and the resonance occurs in the surface whose nature is of course unknown. The n.m.r. technique may be applied over a wide range of temperatures and applied magnetic fields, limited only by a high enough signal to noise ratio but of course the concentration of resonating atoms must exceed a lower limit depending on the method of detection. Any spread in the hyperfine field may be detected by a Fourier analysis of the spin echo signal received after switching off the r.f. power; also the sign of the hyperfine field may be determined from the applied field dependence of the resonance frequencies.

Resonant absorption by nuclei may be detected via the reduction in the degree of anisotropic emission of the (gamma or beta) radiation from statically oriented nuclei (see I.6c) as the nuclear energy level population is equalised by the incoming power. The temperature range is restricted to below that at which appreciable orientation of the nuclei occurs but the restriction on alloy concentration is removed, and also of course there are many more radioactive than stable nuclides having an appreciable nuclear magnetic moment, which widens the scope of the n.m.r. technique appreciably. However this technique has only recently been successfully applied[23] and not much data is available yet. Of course, resonant destruction of nuclear orientation has the added advantage over conventional n.m.r. experiments that the resonating nuclei are unambiguously identified.

b. The Mössbauer Effect. For a gamma radiation transition of low energy in the decay of a radioactive isotope to the ground state, the

recoil required to conserve momentum may involve the lattice of the solid as a whole and not only the individual nucleus. In this case the energy removed from the gamma radiation by the recoil will be vanishingly small, the lattice being a factor $\sim 10^{23}$ heavier than the individual atom ('recoilless emission'), and then there existe the possibility of re-absorption of the gamma quanta by excitation of the same isotope from the ground state ('resonant absorption'). Any hyperfine splitting of the levels of the initial or final nucleus alters the condition for resonant absorption and may be detected by imposing a small variable relative velocity between the source and absorber ($\sim$1mm/sec) and observing the successive destruction and creation of the absorption condition.

This technique for studying hyperfine interactions is limited to the isotopes and environments for which an appreciable degree of recoilless emission or resonant absorption take place (the principal isotopes used are ^{57}Fe, ^{119}Sn, and ^{197}Au while other possibilities are ^{67}Zn, ^{61}Ni, ^{161}Dy, ^{153}Eu); thus specific combinations of isotope and host may not provide a successful measurement of the hyperfine interaction but most types of environment may be successfully examined by the technique. The temperature range is usually limited to below $\sim 300^{\circ}$K and measurements can be made in all applied fields, though the attainable accuracy is limited by the natural width of the lines in the absorption spectrum ($\sim$16kG in the case of the ^{57}Fe isotope). The sign of the hyperfine field cannot be directly obtained from Mössbauer measurements.

If the nuclear energy levels are unequally split, though still well-defined (e.g. if there is some quadrupole splitting) this can still be detected unambiguously using the nuclear magnetic resonance and Mössbauer techniques.

c. Oriented Nuclei. At low enough temperatures the higher nuclear energy

levels will depopulate appreciably according to a Boltzmann distribution. The hyperfine contribution to the specific heat may be separated from the other contributions (electronic, lattice) and the average hyperfine field over the solid as a whole estimated in the case of Zeeman-type splitting though this not very accurately. This mode of detection is not very sensitive to a spread in the magnitude of the hyperfine interaction and also the dilution to which alloys may be studied is severely limited.

The hyperfine interaction can be deduced from the spatial dependence of radiation emitted by spatially aligned radioactive nuclei. Thus polarising fields are always necessary for the observation of a non-zero hyperfine field in polycrystalline samples and the temperature range is limited to that over which the nuclear depopulation occurs ($\sim 0.03 \rightarrow \sim 0.003^{\circ}K$). The dilution to which alloys can be studied is unlimited but initial sample purities normally place a lower limit $\sim$1ppm. This technique is not very sensitive to a spread in hyperfine field values, nor can non-linear energy level splitting be easily discerned. Again, detection of anisotropic emission can only be effected for those alloys in which the appropriate radioactive nuclide experiences an appreciable hyperfine splitting but the range of susceptible systems is considerably greater than that available to Mössbauer experiments. The sign of the hyperfine interaction can be deduced from measurements of the sense of the circular polarisation of the gamma radiation emitted by aligned nuclei.

The experiments to be reported in this thesis involved measurement of the anisotropic emission of gamma radiation from radioactive nuclei aligned in various systems and also in some cases of the sense of its circular polarisation.

The angular correlation by delayed coincidence of successive radiations from a nucleus which decays by a cascade can also provide a measure of the hyperfine interaction when the lifetime of the intermediate state is long enough for appreciable precession of the nuclear spin to take place in the hyperfine field; in effect the direction of the first emanation selects the axis of quantization of the nuclear spin and the theory is similar to that describing grossly oriented nuclei. Angular correlation experiments can be performed at any temperature and in any applied field, as Mössbauer experiments, but the scope of the technique is limited, as usual, by the availability of suitable nuclides.

We see from the foregoing account that the various techniques available for measurement of the hyperfine interaction are complementary rather than competive in scope.

Conclusion.

In this chapter we have attempted to introduce the hyperfine interaction and discuss the extent to which measurements of the hyperfine field in various solids may be interpreted.

Chapter II.

The Nuclear Orientation Technique.

Contents:

Introduction.

II.1. Mechanisms for Orienting Nuclei.

II.2. The Spatial Distribution of Radiation from Oriented Nuclei.

II.3. The Scope of Gamma Radiation Anisotropy Measurements.

II.4. Parameters for Analysis of ^{60}Co and ^{54}Mn Data.

Figure:

II.1. Decay Schemes for ^{60}Co and ^{54}Mn.

Introduction.

In chapter I we discussed the hyperfine interaction in metals and the contribution its measurement makes towards a deeper understanding of magnetic (electronic spin) interactions. In this chapter we continue with a short review of one particular technique for measuring the hyperfine interaction - observation of the spatial anisotropy of radiations emitted by statically oriented nuclei. This technique applied to ions of the 3d transition series dissolved in metals was used to obtain the results to be presented in chapters 5 to 8 of this thesis.

II.1. Mechanisms for Orienting Nuclei.

The electronic and nuclear energy levels of an ion in a paramagnetic crystal possessing axial symmetry about the z-axis and in the presence of both crystalline fields and an external magnetic field may be described by the phenomenological Hamiltonian of Bleaney (1951)[24] and of Abragam and Price (1951)[25] (using the usual notation)

$$\mathcal{H} = [-\underline{\mu}_n \cdot \underline{H}] + [\mu_b\{g_{/\!/} H_z S_z + g_\perp (H_x S_x + H_y S_y)\}] + [AS_z I_z + B(S_x I_x + S_y I_y)] + [D\{S_z^2 - \tfrac{1}{3}S(S+1)\}] + [P\{I_z^2 - \tfrac{1}{3}I(I+1)\}] \quad \ldots\ldots\ldots \text{II.1.}$$

In any particular environment one or other of these terms will predominate and so we discuss them in turn, with a view to orienting nuclei statically.

The first term expresses the direct interaction of the nuclear moment $\underline{\mu}_n$ with an external applied field $\underline{H}$ and is the "brute force" mechanism for acheiving static nuclear orientation, the first to be suggested.[26, 27] The orientation of nuclei by this method requires a static external field $\underline{H} \sim 100$kG in conjunction with a temperature $\sim 0.01^\circ$K, experimental conditions which are not readily attained. Substantial

orientation of the ^{115}In nucleus has however been achoived by this mechanism.[28]

The second and third terms, in which a (small) magnetic field $\underline{H}$ polarises the electrons which then interact with the nuclear spin I, comprise the 'Gorter-Rose' mechanism for alignment[29]; the nuclei of several paramagnetic ions have been so oriented in paramagnetic crystals, applied fields ~100G in conjunction with temperatures ~0.1 to 0.01°K being sufficient to produce a considerable effect[30]. In an isotropic substance where the external field defines the z-axis this Gorter-Rose mechanism leads to Zeeman-type splitting of the 2I+1 nuclear energy levels (as described in I.2 from a different viewpoint) and then the equilibrium population a_m of these energy levels is given by the normalised Boltzmann distribution (in the usual notation)

$$a_m = \exp.(-m\mu_n.\underline{H}_e/I_o kT)/\sum_m \exp.(-m\mu_n \underline{H}_e/I_o kT) \qquad \ldots\ldots\ldots \text{II.2,}$$

where the effective field at the nucleus, or hyperfine field, $\underline{H}_e$, is said to be positive if parallel to the applied field. In the rare-earth metals the largest contribution to the hyperfine field comes from the unpaired orbital (4f) electrons ($H_e \sim 10^6$G) but in the 3d transition series metals the orbital contribution is 'quenched' and then the largest contribution comes from the polarisation of s-type electrons ($H_e \sim 10^5$G) (the 'Fermi contact' interaction previously discussed). This Gorter-Rose machanism was used to orient the nuclei of diamagnetic ions in ferromagnetic metals by Samoilov et Al. (1959)[31] and later by Cameron et Al. (1966)[32] to orient the nuclei of paramagnetic ions in diamagnetic metals. Temperatures ~0.01°K in conjunction with applied fields of only ~1kG are sufficient to produce considerable orientation and all the experiments to be reported herein utilised this Gorter-Rose mechanism.

The earliest successful attempt to statically orient nuclei (^{60}Co in a tutton salt[33]) involved terms 3 and 4 of the Hamiltonian eq. II.1; the strong electric fields in a paramagnetic salt cause a net spin orientation of the electrons which then interact magnetically with the nuclear spin of the paramagnetic ions. This mechanism results in unequal splitting and coincidence of the $\pm I_z(=\pm m)$ levels, thus in alignment not polarization of the nuclei parallel to a crystal axis; single crystals containing the apropriate nuclide at $\sim$0.1 to 0.001°K are necessary for an appreciable effect. Many rare-earth ions have since been aligned by this mechanism, which was first suggested by Bleaney (1951).

The fifth term describes the interaction between the electric quadrupole moment of the nucleus and the (crystalline) electric field gradient at the nucleus and was first proposed as a possible source of oriented nuclei by Pound (1949).[34] Blok and Shirley (1966)[35] have recently oriented many nuclides (e.g. ^{140}La, ^{154}Eu, ^{159}Gd, ^{177}Lu, ^{177m}Lu) by this mechanism in a rare-earth ethyl sulphate lattice, which could not otherwise be oriented owing to the lack of an appreciable nuclear spin; also Dabbs et Al.(1956)[35a] oriented the ^{233}U nucleus at 1.1°K via term 5.

II.2. The Directional Distribution of Radiation from Oriented Nuclei.

From the foregoing we see that many nuclei can be oriented if placed in a suitable environment. A convenient way of detecting this static orientation is via the spatial distribution of any emitted radiation and in this section we give an explicit expression for the normalised intensity of gamma radiation emitted at an angle θ to the alignment axis by a partially oriented system of nuclei. A parallel discussion of the circular polarisation of the gamma radiation is reserved for chapter 4.

The direction in which radiation is emitted by a particular

radioactive nucleus, and the degree of polarisation of that radiation are functions of the initial nuclear spin and its orientation, the final nuclear spin, and the angular momentum carried away by the radiation. For an ensemble of nuclei whose nuclear spins are initially partly oriented spatially, this distribution must be summed over all possible values of the orientation of the initial spin to arrive at expressions for the gross spatial distribution and polarisation of the radiation; the details of this theory have been formulated by a number of workers firstly for special cases then for the general case with varying degrees of completeness[36-50]. The many relevant works have been reviewed extensively by Grace and Blinstoyle (1958)[51] and the scope of the technique discussed in detail. We restrict our following account to gamma radiation, as the other radiative products (α and β particles) were not observed during the experiments to be described.

Suppose we have an ensemble of nuclei in which the nuclear energy levels associated with magnetic quantum number m have an initial population distribution given by a_m (normalised)[52], the total angular momentum of each parent nucleus is I_o, the radioactive decay is by a cascade in which some alternative routes compete i.e. 'mixed' and the radiation observed is immediately preceeded by unobserved transitions which change the population distribution from the initial value. We consider first a simple 'unmixed' decay cascade $I_o \xrightarrow{L_1} I_1 \rightarrow \ldots\ldots I_{n-1} \xrightarrow{L_n} I_n \rightarrow \ldots$ where the gamma radiation L_n is the observed transition. The angular distribution of this radiation $W(\theta)$ (normalised to be 1 for a system of randomly oriented spins) may be expressed in terms of tabulated angular momentum coupling coefficients as a series sum in Legendre polynomials

$$W(\theta) = \sum_{\nu} B_\nu U_\nu F_\nu P_\nu(\cos\theta) \qquad \ldots\ldots \text{II. 5.}$$

where $B_o=1=U_o=F_o=P_o$ and[50]

$$B_\nu(I_o,a_m) = \sum_m (2I_o+1)^{\frac{1}{2}} a_m (-)^{I_o-m} (I_o I_o m-m | I_o I_o \nu 0) \qquad \ldots\ldots \text{II.4.}$$

The Wigner coefficients $(I_o I_o m-m | I_o I_o \nu 0)$ are given by Tinkham (1964)[53] and have been tabulated by Simon[54].

U_ν is the product of U_ν^i over the i transitions preceeding that observed and expresses the attenuation of the initial orientation by these unobserved transitions; for the ith transition $I_{i-1} \xrightarrow{L_i} I_i$,[50]

$$U_\nu^i = \left[(2I_{i-1}+1)(2I_i+1)\right]^{\frac{1}{2}} (-)^{I_{i-1}+I_i-L_i} W(I_{i-1},I_{i-1},I_i I_i;\nu L_i) \ldots\ldots \text{II.5}$$

where $W(I_{i-1} I_{i-1} I_i I_i;\nu L_i)$ is a Racah coefficient, tabulated by Biedenharn (1952)[55] and by Simon et Al. (1954)[56].

The F_ν are angular correlation functions of the angular momenta involved in the observed transition $I_{n-1} \xrightarrow{L_n} I_n$ and for gamma radiation are given by[51]

$$F_\nu(L_n I_n I_{n-1}) = (-)^{I_n - I_{n-1} - 1} (2I_{n-1}+1)^{\frac{1}{2}} (2L_n+1) C(L_n L_n \nu; 1-1).$$

$$W(I_{n-1} I_{n-1} L_n L_n;\nu I_n) \qquad \ldots\ldots \text{II.6.}$$

(The $C(L_n L_n \nu; 1-1)$ are Wigner coefficients in the notation of Biedenharn and Rose (1953)[57].)

These F - functions have been tabulated by Biedenharn and Rose (1953)[57] and by Ferentz and Rosenzweig[58] and are non zero only for even $\nu \leq 2L_n$, thus limiting the number of terms in eq. II.3.

The $P_\nu(\cos\theta)$ are of course the Legendre polynomials and given by[59]

$$P_\nu(\cos\theta) = (\tfrac{1}{2})^\nu \sum_{s=0}^{\mu} \frac{(-)^s (2\nu-2s)! (\cos\theta)^{\nu-2s}}{(\nu-s)!\, s!\, (\nu-2s)!} \qquad \ldots\ldots \text{II.7.}$$

where $\mu=\frac{1}{2}\nu$ if ν even, $=\frac{1}{2}(\nu-1)$ if ν odd.

The U_ν^i and F_ν are modified when the decay is via a 'mixed' transition, that is when two or more possible modes of decay compete with each other. For an observed transition in which the relative amplitudes of transitions involving angular momentum changes of L_n and L_n+1 between states I_{n-1} and I_n are $1:\delta$ respectively

$$F_\nu = \left[F_\nu(L_nI_nI_{n-1}) + \delta^2F_\nu(L_n+1,\ I_nI_{n-1}) + 2\delta F_\nu(L_nL_n+1, I_nI_{n-1})\right]/(1+\delta^2)$$

.....II.8.

where the 4-variable F_ν's can be obtained from eq. II.6 using the transformations

$$(2L_n+1) \longrightarrow \left[(2L_n+1)(2L_{n+1}+1)\right]^{\frac{1}{2}}$$

$$C(L_nL_n\nu;1-1) \longrightarrow C(L_nL_{n+1}\nu;1-1)$$

$$W(I_{n-1}I_{n-1}L_nL_n;\nu I_n) \longrightarrow W(I_{n-1}I_{n-1}L_nL_{n+1};\nu I_n)$$

and are tabulated by Biedenharn and Rose (1953)[57].

For an unobserved 'mixed' transition

$$U_\nu^i = \left[U_\nu^i(L_i) + \delta^2U_\nu^i(L_i+1)\right]/(1+\delta^2) \qquad .....II.9.$$

i.e. the cross terms due to interference of the components vanish.[51]

For a particular decaying nucleus the equations II.3$\longrightarrow$9 reduce to an expression containing only the variables a_m (or $\mu H_e/T$) and θ and a sufficient quantity of information is usually obtained by restricting the measurements to the axial($\theta=0^\circ$) and equatorial($\theta=90^\circ$) directions.

II.3. The Scope of Gamma Radiation Anisotropy Measurements.

Apart from the magnitudes of the hyperfine fields at nuclei in many varied environments (the sign can only be determined from measurements

of the sense of circular polarisation of the gamma radiation) much information relating to the radioactive nucleus may also be obtained from gamma anisotropy measurements. In particular the magnitude of the magnetic moment of the nucleus may be determined if the hyperfine field is known from other measurements[60]; if there are competing modes, associated with different angular momentum changes, for the β or γ emission then the relative probabilities i.e. 'mixing' ratios of these alternative transitions may be obtained from a 'best fit' of eqs. II.3, 8 and 9 to the experimental data[61]; if the initial nucleus were placed in a very strong known (crystalline) electric field gradient then the electric quadrupole moment could be found[62]. Such information is invaluable for testing the validity of the various nuclear models and often cannot be obtained by any other technique.

II.4. Parameters for Analysis of ^{54}Mn and ^{60}Co Data.

Most of the experiments in this thesis involved orientation of the nuclei ^{54}Mn or ^{60}Co and so we give here their magnetic moments and all non-zero products $U_\nu F_\nu$. The decay schemes are shown in fig II.1[63]. For ^{54}Mn the 0.835Mev gamma ray is monitored and for ^{60}Co the 1.17 and 1.34Mev gamma rays are monitored jointly. Both the beta decays involve removal of one unit of angular momentum and all the gamma transitions are pure electric quadrupole; because the ^{60}Co gammas are emitted as a 'stretched' cascade both share the same numerical values for the products $U_\nu F_\nu$.

Table II.1.

	μ	U_0F_0	U_2F_2	U_4F_4
^{54}Mn	3.29±0.06nm[65]	1	-0.4949	-0.4467
^{60}Co	3.754±0.008nm[64]	1	-0.4206	-0.2429

Decay Schemes for $^{54}_{25}Mn$ and $^{60}_{27}Co$.

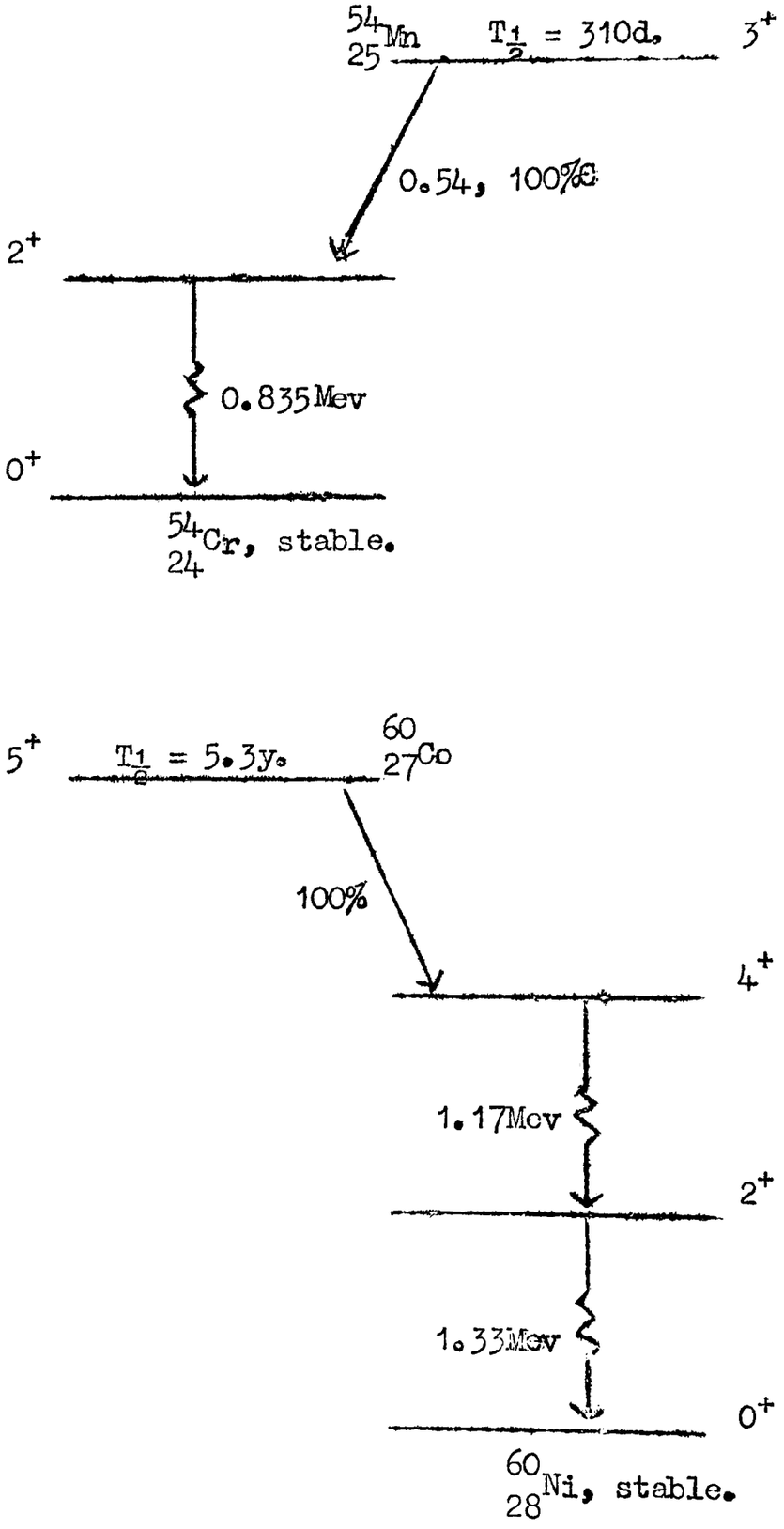


Figure II.1.

Chapter III.

Apparatus and Data Analysis for Anisotropy Measurements.

Contents:

Introduction.

III.1. Sample Assembly.

III.2. Helium Reservoir.

III.3. Nitrogen Reservoir.

III.4. Superconducting Magnets.

III.5. Aluminium 'Windows'.

III.6. Magnetising Solenoid.

III.7. Counting Assembly.

III.8. Procedure.

III.9. Storage of Data.

III.10. Raw Data.

III.11. Corrections to the Anisotropy Data.

III.12. Sample Strengths.

III.13. Analysis of Anisotropy Measurements.

III.14. Estimation of Errors.

Figures:

Frontispiece: Photograph of Cryostat.

III.1. Diagram of Cryostat.

III.2. Sample Assembly with Superconducting Magnet.

III.3. Helium Consumption in Cooling Cryostat from 4.2 - 1.3°K.

III.4. Field Profile of Mo-Rh Superconducting Magnet.

III.5. Field Profile of Nb-Zr Superconducting Magnet,

III.6. Magnetising Solenoid Around Cryostat.

Conclusion.

The Cryostat.

(photograph by C. W. Band.)



Introduction.

As discussed in chapter II, suitable experimental conditions for static orientation of nuclei are a temperature $\sim 0.01^{\circ}K$ and a specimen with an axis of symmetry; to detect this orientation it is convenient to use a radioactive isotope and observe the spatial distribution of the radiation emitted.

Most of the experiments described in this thesis were performed using to attain the low temperatures a cryostat designed by Dr I. A. Campbell. The somewhat unusual design was specifically to cater for the experiment described in chapter VIII, in which a single crystal of cobalt metal was irradiated by a beam of thermal neutrons while at a temperature of $\sim 1^{\circ}K$ and and the principal requirements were thus that the cryostat be portable between the laboratory and the neutron beam, some 15miles away, and also that there be a 'window' to the sample transparent to thermal neutrons. In the experiments described in chapters V, VI, and VII polycrystalline samples were used, the axis of symmetry being then defined by the application of a magnetic field.

A photograph of the dismantled cryostat appears at the beginning of this chapter and scale diagrams are shown in figs III.1 and III.2. Also shown as a frontispiece to this thesis is an "exploded view of the cryostat" - the product of a solid air block (not the author's) - included because of the extra detail it shows.

The experiments to be presented herein were the first for which this cryostat was used and so we describe it in some detail in what follows.

III.1. Sample Assembly.

The samples used consisted of between 0.05 →1grams of various

Legend: Figs III.1, III.2.

1. Sample, soft soldered to copper rod.
2. Copper fins, hard soldered to copper rod and embedded in chromic potassium alum - the whole encased in tufnol.
3. Heat shield, a brass cylinder and tufnol reservoir containing chromic potassium alum or manganous ammonium sulphate.
4. Brass 'cradle' from which 2. and 3. are suspended by linen threads.
5. Liquid helium reservoir, pumped to 1.3°K via 6.
6. Pumping tube for helium gas.
7. Syphon inlet tube to helium reservoir.
8. Brass helium reservoir and brass 'outer' (room temperature) jacket.
9. Stainless steel support tubes (3) for helium reservoir.
10. Liquid nitrogen reservoir made from copper.
11. Copper extension to nitrogen reservoir.
12. 'Inner' jacket pumping tube, for helium 'exchange' gas providing thermal contact between helium and chrom. alum.
13. 'Outer' vacuum space (for heat insulation).
14. Aluminium 'windows' - i) greased cone joint to helium reservoir
    ii) 'push' fit greased joint to nitrogen can
    iii) 'araldite' seal to brass outer jacket.
15. For most of the experiments a small superconducting magnet is mounted on the inner jacket cap, as shown in the enlarged view of the sample assembly, fig III.2.

THE CRYOSTAT. (x½ vert., x½ horiz.)

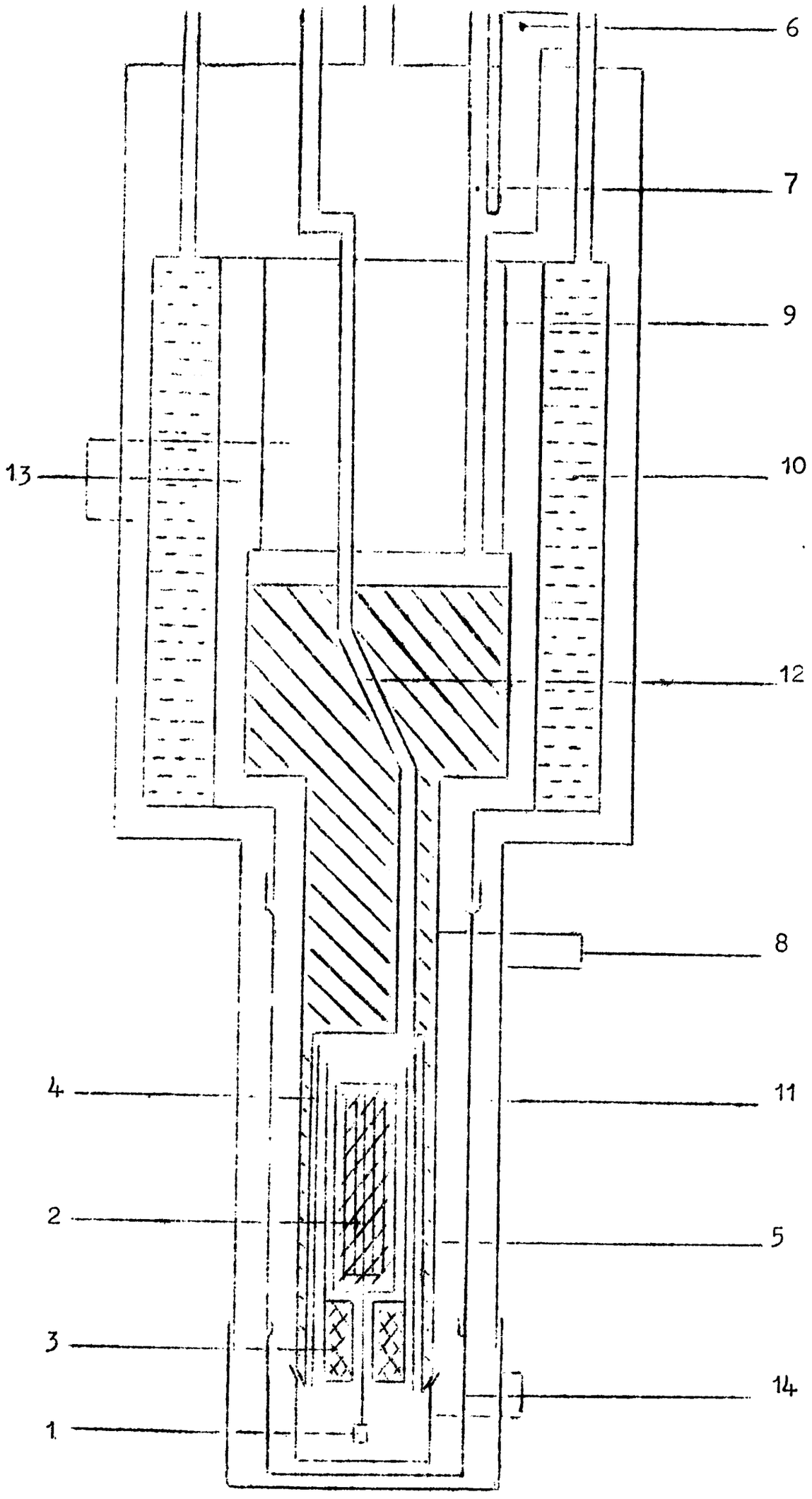


Figure III.1.

SAMPLE ASSEMBLY WITH SUPERCONDUCTING MAGNET.

(full scale)

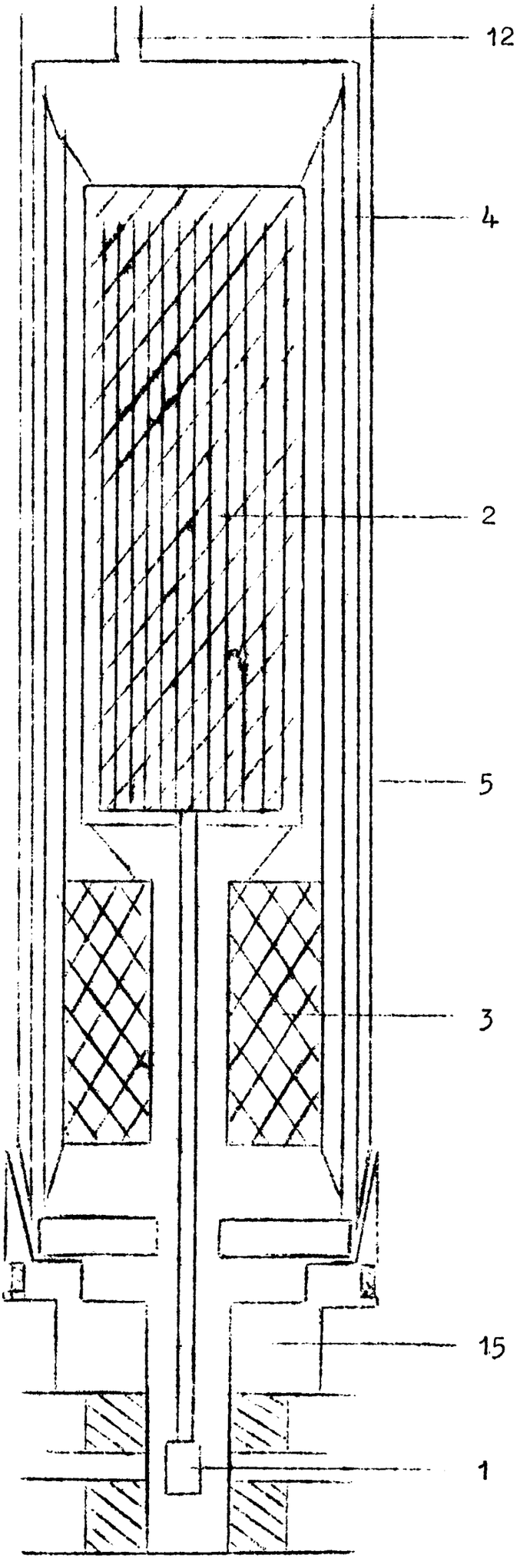


Figure III.2.

metals 'doped' with the appropriate radioactive isotope and cut to size according to the activity required; further preparation details are given in the appropriate chapters. The sample and cooling agent, a paramagnetic salt, were some distance apart so a polarising field might be applied to the sample without warming the demagnetised salt. The thermal link between these two was effected by soldering the sample to a copper rod (~3mm diam, ~8cm long) itself hard-soldered to a system of copper fins (~1900sq. cm of contact area) embedded in the salt. Optimum dimensions for this link have been discussed by Compton (1965)[66]. There are many available paramagnetic salts[67] but for the desired temperature range (0.01 - 0.02°K) chromic potassium alum ($Cr_2(SO_4)_3.K_2SO_4.24H_2O$) has the largest heat capacity. Between 100-150grams of chrom. alum were used in the experiments and with the heat sheild the heat leak to the sample was typically ~30ergs per min, corresponding to a rise in temperature from ~0.12 to 0.14°K in ~two hours.

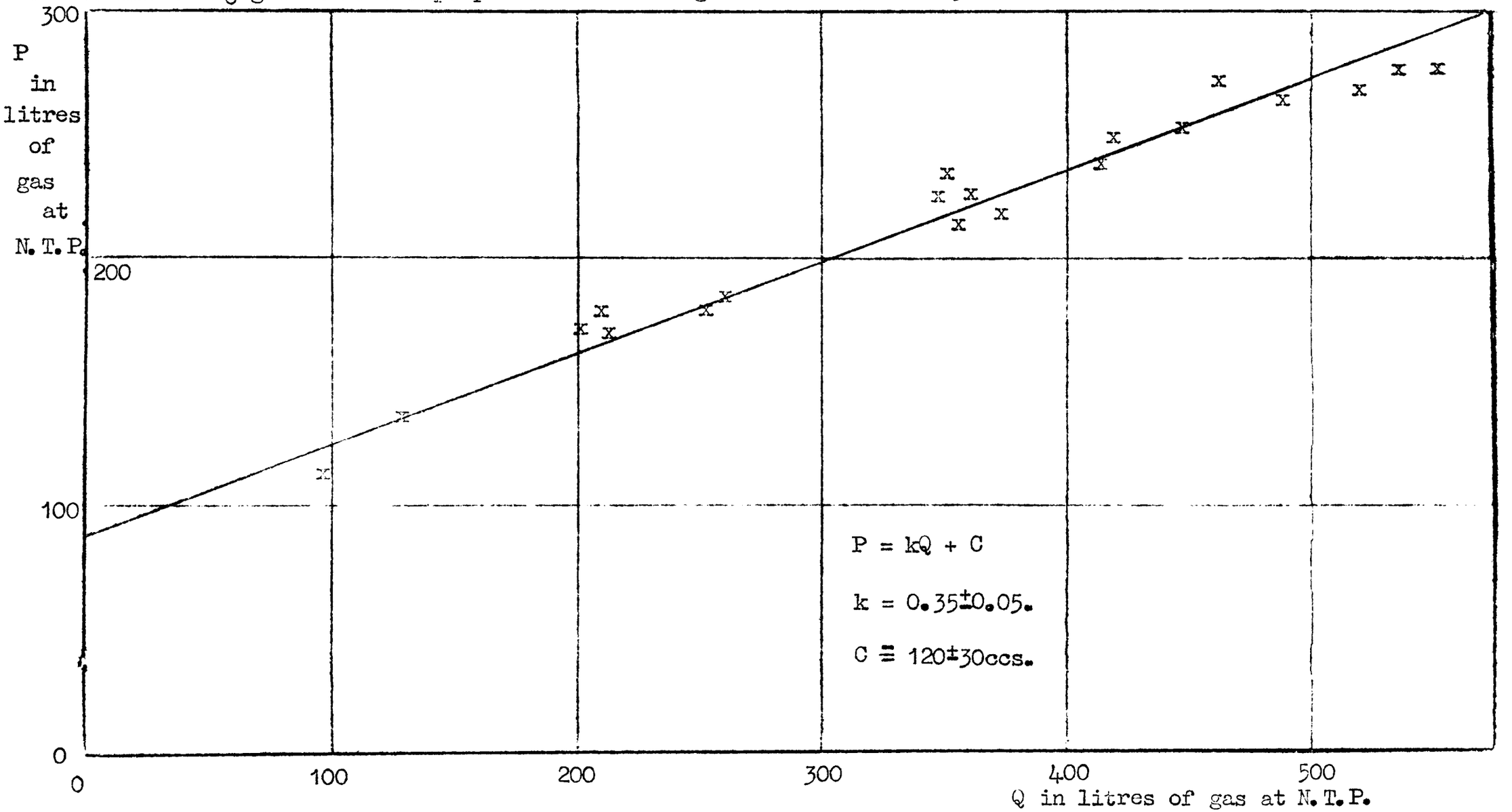
The sample assembly was surrounded by the walls of the helium reservoir at 1.3°K, with which thermal contact could be maintained using helium exchange gas.

III.2. Helium Reservoir.

This reservoir had a capacity of 1150ccs and in the ambient state helium liquid 'boiled-off' at the rate of ~30ccs/hr at 4°K, ~35ccs/hr at 1.3°K. To achieve this low heat leak it was necessary to provide a thermal link (strips of copper wire) between the one gas-cooled support tube and the other four support tubes. These can be seen clearly in the photographs of the cryostat. From accumulated performance data, fig III.3, we can deduce that ~1/3rd of the helium in the reservoir was consumed in pumping (using a rotary vacuum pump) the rest of the liquid helium down to

HELIUM CONSUMPTION IN PUMPING CRYOSTAT FROM $4.2^{\circ}K$ TO $1.3^{\circ}K$.

P = volume of H_e gas at N.T.P. pumped off in cooling remainder Q and cryostat to $1.3^{\circ}K$ from $4.2^{\circ}K$.



$1.3^{\circ}K$ ($\sim$0.13cm Hg), and a roughly constant quantity $\sim$120ccs of helium was consumed in cooling the cryostat and sample assembly from $4^{\circ}K$ to $1.3^{\circ}K$.

III.3 Nitrogen Reservoir.

The nitrogen reservoir encircled the helium reservoir, had a capacity of 1.7litres and the ambient boil-off rate was $\sim$250ccs/hr of liquid N_2 (with liquid helium in the helium reservoir). A copper shield was attached (with Wood's metal solder) to this reservoir to complete the shielding of the helium reservoir from room temperature radiation.

III.4 Superconducting Magnets.

When necessary, the symmetry axis was defined by an external field from a superconducting magnet. The helium reservoir in this portable cryostat was enclosed so magnet and leads were suspended in the vacuum jacket and only a small current could be supplied. Accordingly it was wound from 0.002ins Molybdenum-Rhenium alloy wire onto a pre-shaped dural 'cap' and carried a maximum current of 0.85amps, i.e. a maximum field $\sim$5kG at the sample. This small superconducting magnet was wound in sections - two main coils with a gap between to facilitate the emergence of gamma rays in the $\theta = 90^{\circ}$ direction and a 'compensating' coil wound in the opposite sense to the main pair, which served to reduce the field on the salt to $\sim$5G/amp. A few extra turns were wound in the central 'window' to make the field constant over the sample and the field profile is given in fig III.4.

For some of the experiments in chapter VII polarising fields up to 16kG were obtained from a higher current superconducting magnet mounted in a cryostat of different design (discussed by Campbell (1964)[68]). In particular the supply leads carrying up to 15amps passed into the helium bath in which the magnet was immersed. The design of this larger magnet is very similar to the Mo-Rh magnet (see fig III.5 for the field profile)

AXIAL FIELD PROFILE OF Mo-Rh SUPERCONDUCTING MAGNET.

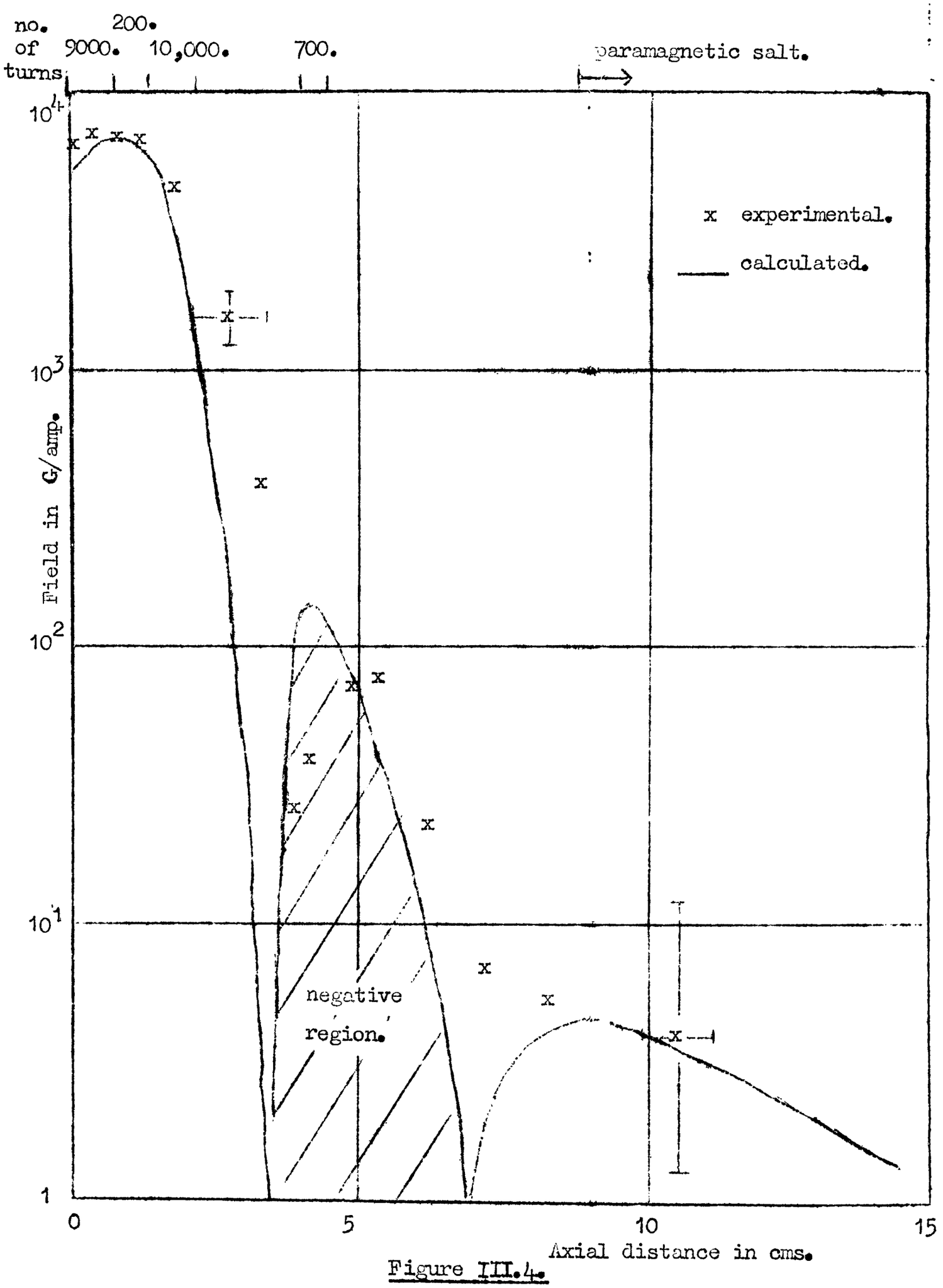


Figure III.4.

AXIAL FIELD PROFILE OF Nb-Zr SUPERCONDUCTING MAGNET.

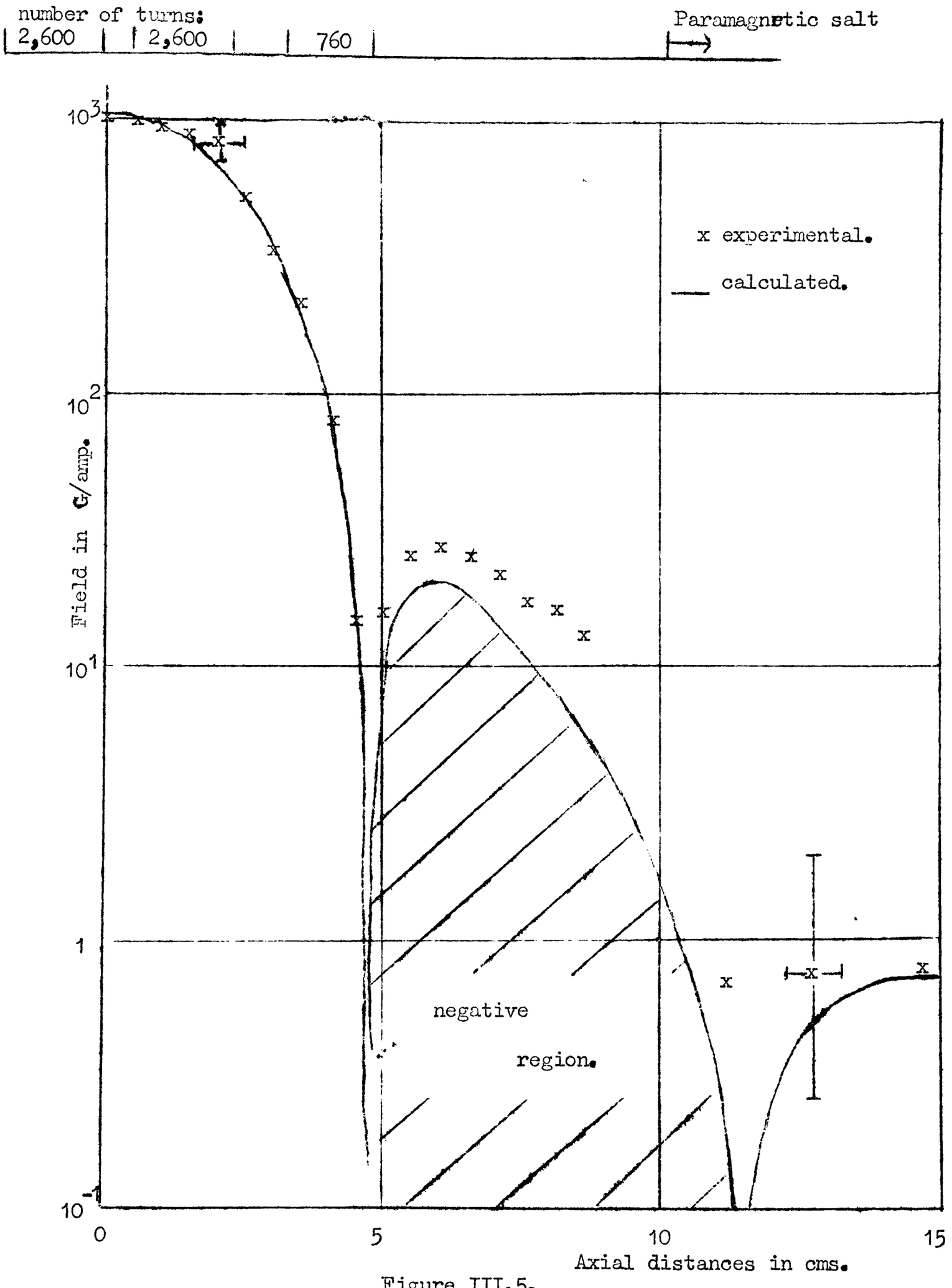


Figure III.5.

and it was wound from a Niobium-Zirconium alloy wire.

(The experimental points in figs III.4 and III.5 were obtained using a magnetometer for relative measurements, a calibrated pick-up coil for absolute measurements and also were calculated using a computer program[69].)

III.5 Aluminium 'Windows'. (to the thermal neutron beam.)

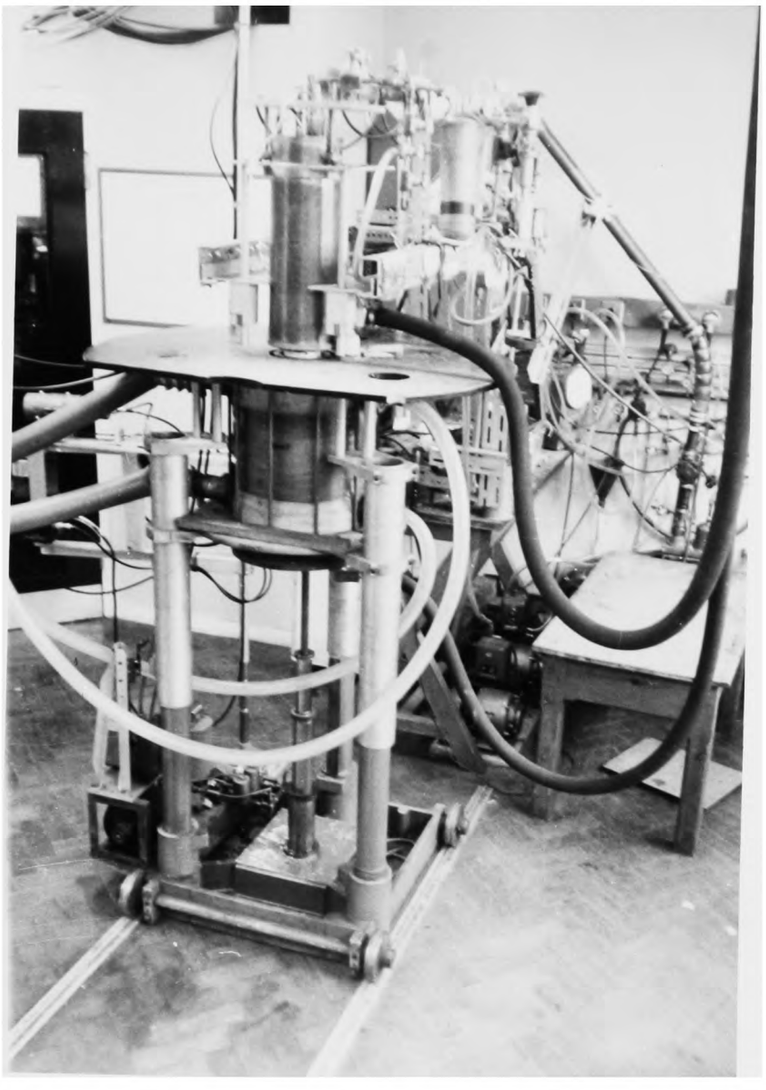
These were made from 'pure' aluminium tube and rod supplied by Blackburns (London) Ltd. The impurity content was 0.1%Cu, 0.4-1.5%Mg, 0.6-1.3%Si, 0.6%Fe, 0.4-1%Mn, 0.1%Zn, 0.5%Cr, and 0.2%Ti; the radioactive products from neutron capture by Al, Cu, Mg, Mn, and Si all have short half-lives ($<$13hrs) compared with the irradiatiom time, while the neutron capture cross-sections of the other impurity elements are very small campared with the ^{59}Co cross-section.

The soldering of aluminium is a difficult process and even if successful in the first instance the joints quickly deteriorate; this difficulty was by-passed by using an 'araldite' seal between the aluminium and brass parts of the outer jacket, making the vacuum spaces around the nitrogen and helium reservoirs common, and relying on a greased cone joint to separate the vacuum space from the exchange gas ($<10^{-1}$mmHg pressure)

III.6. Magnetising Solenoid.

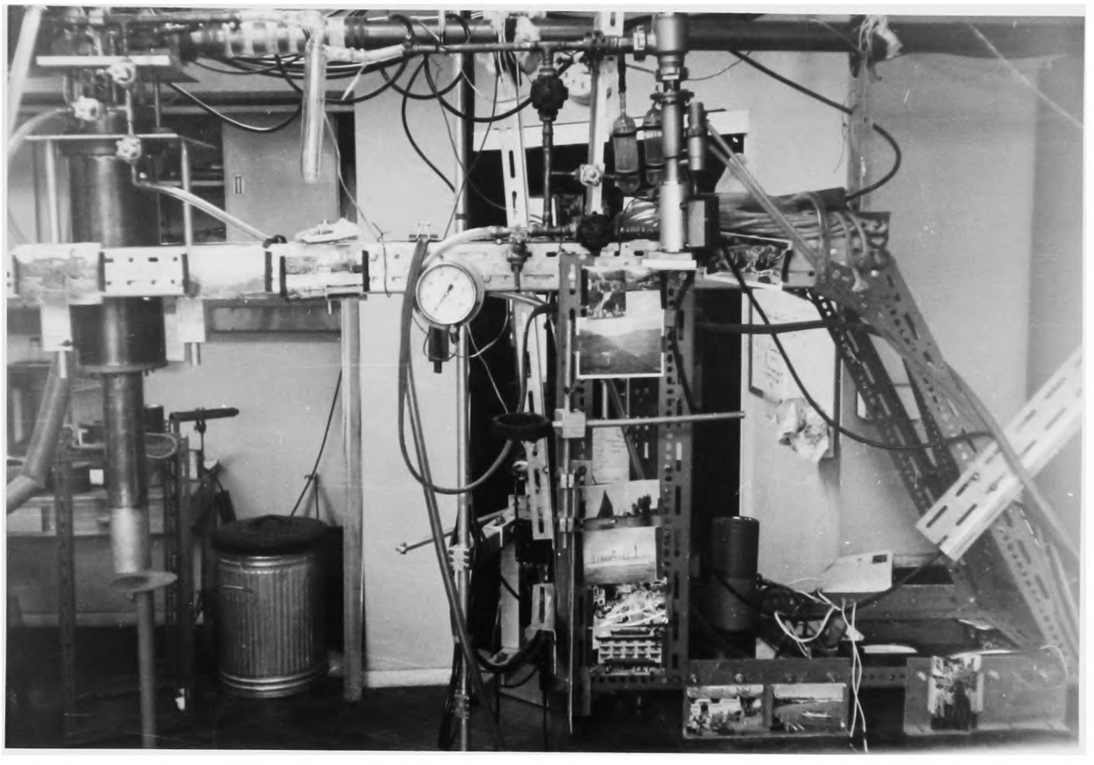
In order to magnetise the chrom. alum a water cooled copper solenoid external to the cryostat was used. This magnet, designed by Mr M.Wood, gave 35±3.5kG over a cylindrical volume 10cms long by 10cms diameter which was found to be sufficient to cool the salt to $\sim$0.011°K from 1.3°K. Fig III.6 shows this magnet in position around the cryostat.

The current supply for this magnet came from a 2MW d.c. generator, previously used to supply power for Manchester city's street lighting.

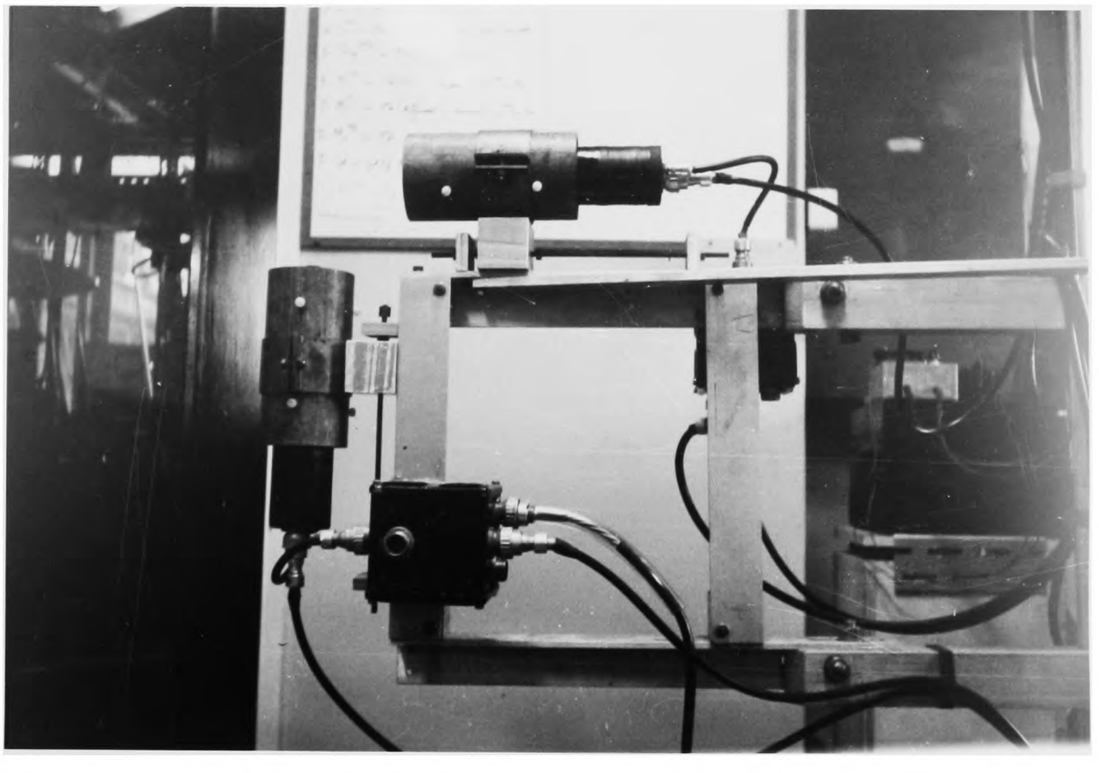


MAGNETISING SOLENOID AROUND CRYOSTAT.

Figure III.6(a).



The Cryostat with Ancillary Equipment.



The Counters, with Shielding.

Figure III.6(b).

III.7. Counting Assembly.

The two gamma radiation counters used, at angles corresponding to $\theta = 0^{\circ}$ and 90° in eq. II.3, were of the usual design: a NaI(Thallium activated) scintillation crystal together with a photomultiplier tube supplied with ~1000volts high tension. These counters gave an energy resolution of ~10% and had an efficiency depending on the energy of the incident gamma radiation[70].

The signals from each photomultiplier tube, proportional in magnitude to the energy of the incident gamma radiation, were amplified then fed to two voltage 'discriminators' whose output was counted. These discriminators only gave an output pulse (of constant magnitude) when an input pulse falling within a preset voltage range was received, and thus picked out a finite range in energy of the incident gamma radiation which of course usually corresponded to the gamma ray energy of the particular isotopes under investigation. A small drift in the high tension supply to the photomultiplier tubes caused considerable variation in the part of the energy spectrum 'passed' by the discriminators; this defect was eliminated by the addition of a feedback stabiliser to the counting equipment by Dr G. V. H. Wilson (see appendix A), which locked the 'window' onto a peak in the energy spectrum, rendering long counting times possible.

III.8 Proceedure.

The general proceedure for cooling to $0.01^{\circ}K$ is a fairly standard technique, involving sucessive use of liquids nitrogen, hydrogen and helium, then the adiabatic demagnetization of a paramagnetic salt[68]. After demagnetization the copper solenoid was removed, the counters swung into position on their frame, the superconducting magnet supplied with current and the electronics checked for stability then set to count. Sometimes the

current to the superconductor was varied while counting 'cold'. After 2 to 3 hours counting the cooling salt was warmed to 1.3°K by passing a.c. through a copper coil wound on the outside of the cryostat 'tail' (so as to cause heating of the copper fins by eddy currents); then the isotropic gamma ray intensity was counted for 1 to 2 hours to normalise the data. Care was taken not to alter the geometry of the sample plus counters throughout this counting cycle.

III.9. Storage of Data.

The sample under investigation usually incorporated two radioactive isotopes, one in the environment to be probed, the other for measuring temperature and thus in an environment where the nuclear energy level splitting was known. Hence a total of four gamma ray counting rates (two each from the axial and equatorial directions) required simultaneous and continuous monitoring. This was effected using a 400 channel pulse height analyser (in scalar mode) programmed to accept output from the four discriminators in channels 001, 101, 201, 301 for a multiple of 100secs, then in channels 002, 102, 202, 302 for an equal time, then in the third member of each subset, and so on. At the end of a counting cycle the data in the store could be printed onto paper tape. This automation in data collection made very long experiments possible.

The pulse height analyzer in analyzer mode was particularly useful in setting the discriminators' window width and bias and hence the stabilizer onto the correct peaks in the gamma ray energy spectrum. It was possible to compare the whole spectrum with the 'window' using a coincidence circuit.

III.10. Raw Data.

The raw data was obtained as the number of gamma rays emitted in a

fixed time for succesive intervals of time and each gamma 'peak' was counted separately. The value of the observed anisotropy $W(\theta,T)$ was obtained from this data by first averaging several adjacent channels at temperature T and angle θ, then dividing this average by the mean of the many adjacent channels taken after the sample had been warmed to $\sim 1.3^{\circ}K$.

III.11. Corrections to the Anisotropy Data.

The observed anisotropy must be corrected for contributions to the observed count rate not arising from the gamma transition concerned.

a. Background. This contribution to the count rate arises from cosmic radiation or any stray radiation from nearby sources (the latter reduced to a minimum where possible). The background counting rate fluctuated slightly with time and electronic settings and estimates of its maghitude were found by observing the count rate in each spectrum window, in the absence of the sources, at the end of each experiment. An average value was used in the correction of the data.

b. Overlap. When two gamma rays of different energy occur in the same spectrum considerable scattered radiation from the higher energy peak finds its way into the spectrum 'window' of the lower energy peak. Typically, the overlap from the 1.34 and 1.17Mev ^{60}Co transitions into a 'window' at 0.835Mev (^{54}Mn) was $\sim 30\%$ of the peak counting rate and this radiation was anisotropic with temperature, possessing some fraction of the anistropy in the 'peak'. Separate experiments must be performed to estimate this fraction, and the percentage of overlap is obtained from the slope of an overlap vs peak counting rate curve for varying strengths of peak radiation; this percentage was measured at the end of each experiment.

c. Pile-up. This is the analogue to overlap, but arises from different

causes. It is the contribution from the lower energy gamma ray to the counting rate in the higher energy window. The finite resolution time or finite width of the pulses in the electronic circuitry gave spurious 'coincidence' between two of the lower energy gamma rays which arrived within a short time interval of each other, and so raised the energy of the pulse to the higher energy 'window', where it was counted. The probability of such an event is proportional to the square of the lower energy counting rate, and the pile-up fraction can be estimated from measurements of the counting rate in the two 'windows' using varying strengths of the lower energy source; it was found for a source of ^{54}Mn (0.835Mev) to be less than 1% in the ^{60}Co ($\sim$1.3Mev) 'window'. Coincidences between the lower energy radiation and the scattered radiation from the higher energy peak also lead to a pile-up contribution, which can only be estimated and is usually $\sim\frac{1}{3}$ of the low-low coincidence contribution (see §III.12).

Of course this 'pile-up' will exhibit some anisotropy, theoretically more than double the 'effect' in the lower energy peak; however if an experiment is performed using only the lower energy source, the anisotropy of the pile-up radiation turns out to be only $\sim$1.5 times the anisotropy of the lower energy peak. The pile-up correction is of the order of the estimated error, so this discrepancy is by no means unnerving!

d. Dead Time Correction. The dead time of the 400 channel analyzer was 20μsecs per pulse counted and was much longer than the dead time of any other component in the counting circuitry. For a total counting rate from all four inputs of $\sim$1000cps the total dead time was less than 2%; the correction to the anisotropy depends on the difference between the total counting rates 'cold' and 'warm' and was correspondingly smaller so

neglected in the analysis. Although this neglect introduces a small systematic error into the data, it will affect the axial and equatorial H_e/T's oppositely and so in part be cancelled by averaging the two values.

III.12. Sample Strengths.

The optimum sample strengths must be chosen with a view to minimising the background, overlap and pile-up corrections and keeping the dead time correction neglible. For comparable anisotropy of the two peaks in the gamma ray spectrum, a ratio of 3:1 for the intensities of the lower to higher energy peaks minimises these corrections (360cps and 120cps for a total input of ~1000cps to the analyzer). If one peak is much more anisotropic than the other, then its intensity should be depressed below this ratio.

III.13. Analysis of Anisotropy Measurements.

Most of the data analysis was carried out using the computer K.D.F.9 together with programs written by Dr G.V.H.Wilson. These programs firstly tabulated the theoretical curves of the 'effects', $\epsilon(0) = 1-W(0)$, $\epsilon(90) = W(90)-1$, vs. H_e/T and $1/T$ for the two isotopes, using attenuation factors for the Legendre polynomials in eq. II.3 to take into account the finite detector aperture[70]; then by a quadratic interpolation procedure the values of H_e/T, $1/T$ were deduced for a given set of uncorrected 'effects'. The true values of H_e/T, $1/T$ were then tabulated from the corrected data, obtained using the equations in appendix B. Since the magnitudes of the corresponding axial and equatorial 'effects' were usually in the ratio 2:1, and the absolute accuracy was of the same order for both, the average values of H_e/T, $1/T$ for each point were computed from the axial and equatorial values weighted in the ratio 4:1. This procedure was the backbone to all anisotropy data analysis in this thesis.

III.14. Estimation of Errors.

Sources of error in the evaluation of the true anisotropy for both sample and thermometer were:

a. the finite count rate.

b. the uncertainty in the fractional contribution to the count rate by background, overlap and pile-up.

c. the uncertainty in the anisotropy of the overlap and pile-up contributions to the countrate as a function of the relevant peak anisotropy. and

d. the uncertainty in the positioning of the counters and polarising magnet with respect to the sample.

The magnitude of a and b could easily be estimated, due allowance must be made for c and d and then the consequent errors in the deduced values of H_e/T, $1/T$ may be found; comparison of values of H_e/T, $1/T$ within each counting cycle and from different counting cycles served as a check on the completeness of these error estimates.

Conclusion.

In this chapter we have described the apparatus used to obtain the results presented in chapters 5 to 8 of this thesis, and also discussed the analysis of the data and the estimation of errors.

Chapter IV.

Circular Polarimetry.

Contents:

Introduction.

IV.1. The Circular Polarisation Of Gamma Radiation.

IV.2. The Scattering of Electromagnetic Radiation by Matter.

IV.3. Experimental Details of the Circular Polarimeter.

IV.4. Storage and Analysis of Data.

Figures:

IV.1. Circular Polarimeter: a. Scattering Angles;
b. Apparatus.

IV.2. Spectra: a. ^{60}Co; b. Polarimeter 'Window'; c. Spectrum of Radiation Scattered by Polarimeter.

Introduction.

Knowledge of the sign of the hyperfine interaction, or hyperfine field in our case, is essential for the proper interpretation of any experimental data and can be determined from gamma anisotropy measurements only by varying the applied field, a technique which requires much larger fields than available in the present case. However, gamma radiation emitted by oriented nuclei contains both plane and circularly polarised components (c.f. polarisation of the Zeeman lines in optical spectra) and the sign of the hyperfine field may be deduced from the sense of the circular polarisation, which depends on the directions of the applied and hyperfine magnetic fields. The sense of the circular polarisation of electromagnetic radiation may be determined from the dependence of its scattering cross-section by electrons on the orientation of the electron spin angular momentum. We describe in this chapter the relevant theory of such measurements and the apparatus required to effect them.

No attempt was made to evaluate quantitatively the scattered radiation measurements taken (results reported in chapters VI and VII), as we were only interested in the sign of the hyperfine field; also to avoid errors of interpretation, the data from the sample under investigation was compared with similar data from a sample for which the sign of the hyperfine field was known, rather than evaluate the results from first principles.

Only the isotopes ^{54}Mn and ^{60}Co, for which all gamma transitions are pure electric quadrupole, were involved in circular polarisation measurements, so we restrict the following discussion to this case.

IV.1. The Circular Polarisation of Gamma Radiation.

The polarisation of electromagnetic radiation emitted at an angle

θ to the nuclear quantization axis can be expressed as the sum of linearly and circularly polarised components

$$W(\theta)\underline{\varepsilon}_o = A\underline{X}_l + B\underline{X}_c \qquad \ldots\ldots\ldots \text{IV. 1.}$$

where $\underline{X}_l$ and $\underline{X}_c$ are the linear and left-circular polarisation vectors respectively ($-\underline{X}_c$ is the right-circular polarisation vector), and the coefficients A and B are functions of the angle θ and of the population distribution amoung the 2I+1 magnetic energy levels of the nucleus.[44] The explicit expressions for A and B for the case of a pure electric quadrupole transition are given in appendix C; in particular, the magnitudes of the two coefficients are identical for any pair of angles $\theta = \theta_o$, θ_o+180^o, and the sign of B only changes. It can also be shown that the sign of B for a fixed angle θ_o depends on the sign of the difference $(a_{m_I}-a_{-m_I})$ in the population of the pairs of energy levels associated with magnetic quantum numbers $\pm m_I$, that is on the direction of the hyperfine field relative to the applied field. Thus a direct comparison of data for angles θ_o and θ_o+180^o leads to the relative sign of the hyperfine fields at each nucleus.

IV.2. The Scattering of Electromagnetic Radiation by Matter.

The differential scattering cross-section of electromagnetic radiation (by electrons) may be written as [71-74]

$$(d\sigma/dw) = (d\sigma_o/dw) + P_l(d\sigma_l/dw) - fP_c(d\sigma_c/dw) \qquad \ldots\ldots \text{IV. 2.}$$

where P_l and P_c are respectively the degree of linearly and circularly polarised radiation, f is the fraction of polarised electrons, $dw=\sin\phi d\phi d\psi$ (an element of solid angle), and

$$(d\sigma_o/dw) = C\left[(1+\cos^2\phi) + (k_o-k)(1-\cos\phi)\right]; \quad (d\sigma_l/dw) = C\sin^2\phi;$$

$(d\sigma_c/dw) = C(1-\cos\phi)\left[(k+k_o)\cos\phi\cos\theta + k\sin\phi\sin\theta\right]$; $C = \frac{1}{2}N(e^2/mc^2)^2k^2/k_o^2$.

N is the total number of electrons per atom of the scattering element, and fig IV.1(a) defines θ, ϕ and the wave vectors $\underline{k}_o$ and $\underline{k}$ of the incident and scattered radiation with respect to the direction of polarisation $\underline{s}$ of the electrons ($\underline{k}_o$, $\underline{k}$, $\underline{s}$ coplanar to reduce the number of variables).

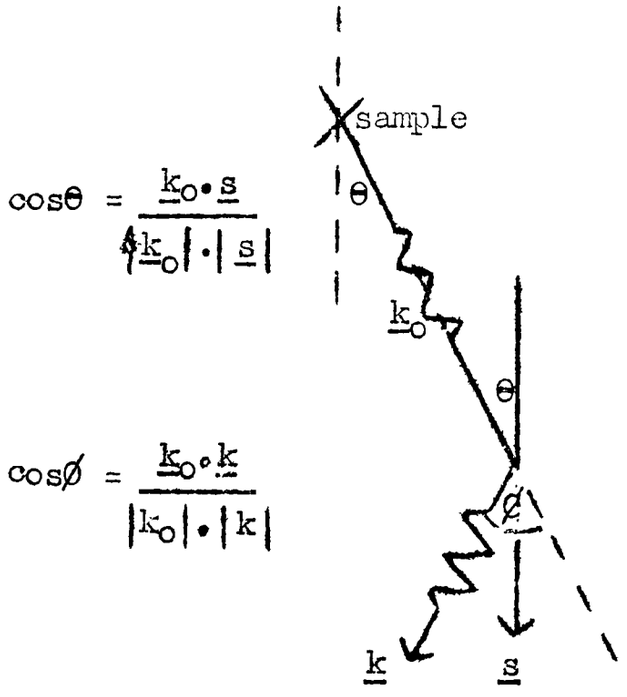
If all the variables in eq. IV.2 remain constant save the angle θ which is allowed to take on only the values $\theta_1, \theta_1+180^\circ$, then all terms remain constant in magnitude and the sign of only the circular polarisation term changes with the angle. (The angles θ in the two equations IV.1 and 2 can of course be changed by 180° independently.) Thus for gamma radiation containing an appreciable fraction of circular polarisation the intensity of scattered radiation should change if the direction of polarisation of the electrons is reversed or if the applied field at the sample is reversed, and the detection of any circular polarisation in the gamma radiation is based on these two facts. The values of θ, ϕ which give the maximum effect may be determined from simultaneous consideration of eqs. IV.1,2 remembering that these angles are related via the energies of the incident k_o and scattered k radiation. This problem is discussed by Wheatley et Al.(1955)[75] who show the range of angles $20^\circ < \theta < 30^\circ$ and $40^\circ < \phi < 60^\circ$ correspond to a broad maximum in the quantity $P_c(d\sigma_c/dw)/(d\sigma_o/dw)$.

In designing the apparatus it must be remembered that the formulae given refer to a coplanar scattering process, a condition obtained experimentally by using a cylindrically symmetric scattering system and placing the source and detector on axis.

IV.3. Experimental Details of the Circular Polarimeter.

The apparatus used to detect the circular polarisation of gamma

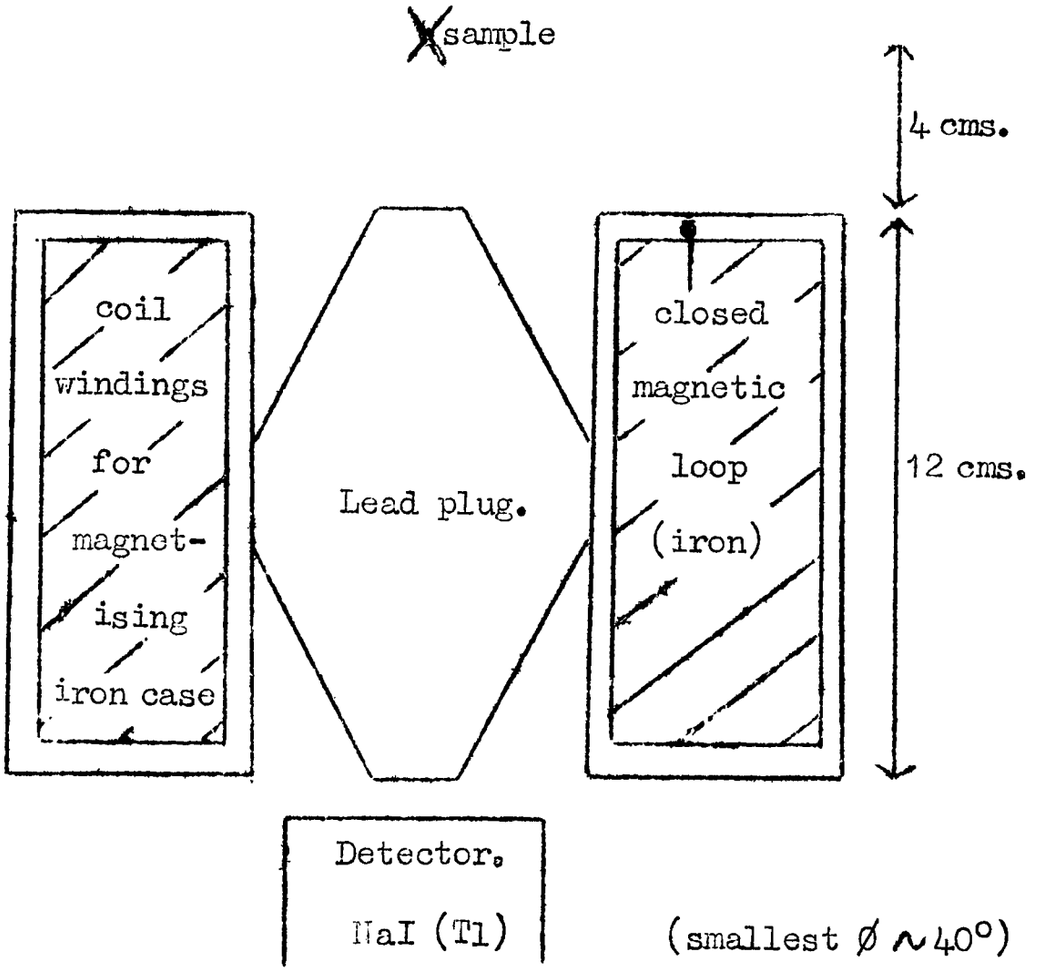
THE CIRCULAR POLARIMETER.



$$\cos\theta = \frac{\underline{k}_o \cdot \underline{s}}{|\underline{k}_o| \cdot |\underline{s}|}$$

$$\cos\phi = \frac{\underline{k}_o \cdot \underline{k}}{|\underline{k}_o| \cdot |\underline{k}|}$$

a. Scattering Angles.



b. Apparatus.

Figure IV.1.

radiation is shown schematically in fig. IV.1(b) and consisted of a NaI(Tl) crystal detector coaxial with the sample and its applied magnetic field, a lead plug of appropriate dimensions interposed between the two so that no radiation having a scattering angle ϕ less than 40° could be detected, and a cylinder of magnetised soft-iron surrounding the lead plug to scatter the radiation into the detector. (For iron, $\sim$2.1 polarised electrons out of 26 implies f = 0.075 in eq. IV.2.) The iron cylinder was magnetised by a coil of copper wire, carrying $\sim$1amp, wound about the iron cylinder. As already described, reversal of either the direction in which the iron was magnetised or of the applied magnetic field at the sample should cause a change in the intensity of the radiation reaching the detector. Since a changing contribution to the magnetic field at the sample from the magnetised iron could give a spurious intensity change by altering the degree of anisotropy of the gamma radiation, the magnetic flux was trapped in a closed iron loop about the coil windings. With this arrangement the field at the sample ($\sim$5kG from the superconducting magnet) changed by less than 10G when the current through the iron magnetising coil was reversed. The spectrum 'window' of the detector was set to accept only gamma radiation falling in the appropriate energy range, which of course included the highest energy detected by the counter - see fig IV.2. Unfortunately during the measurements stabilisation of the high tension supply was not possible, there being no suitable 'peak' in the energy spectrum; hence spurious intensity changes due to both H.T. 'drift' and to sample temperature variation ('warm-up') could be troublesome over a long counting cycle.

The first sucessful measurement of the sense of circular polarisation of gamma radiation was by Wheatley et Al. who measured the sign of the magnetic moment of the ^{60}Co nucleus; using apparatus very similar to ours and taking extensive precautions to shield the counters

POLARIMETRY SPECTRA.

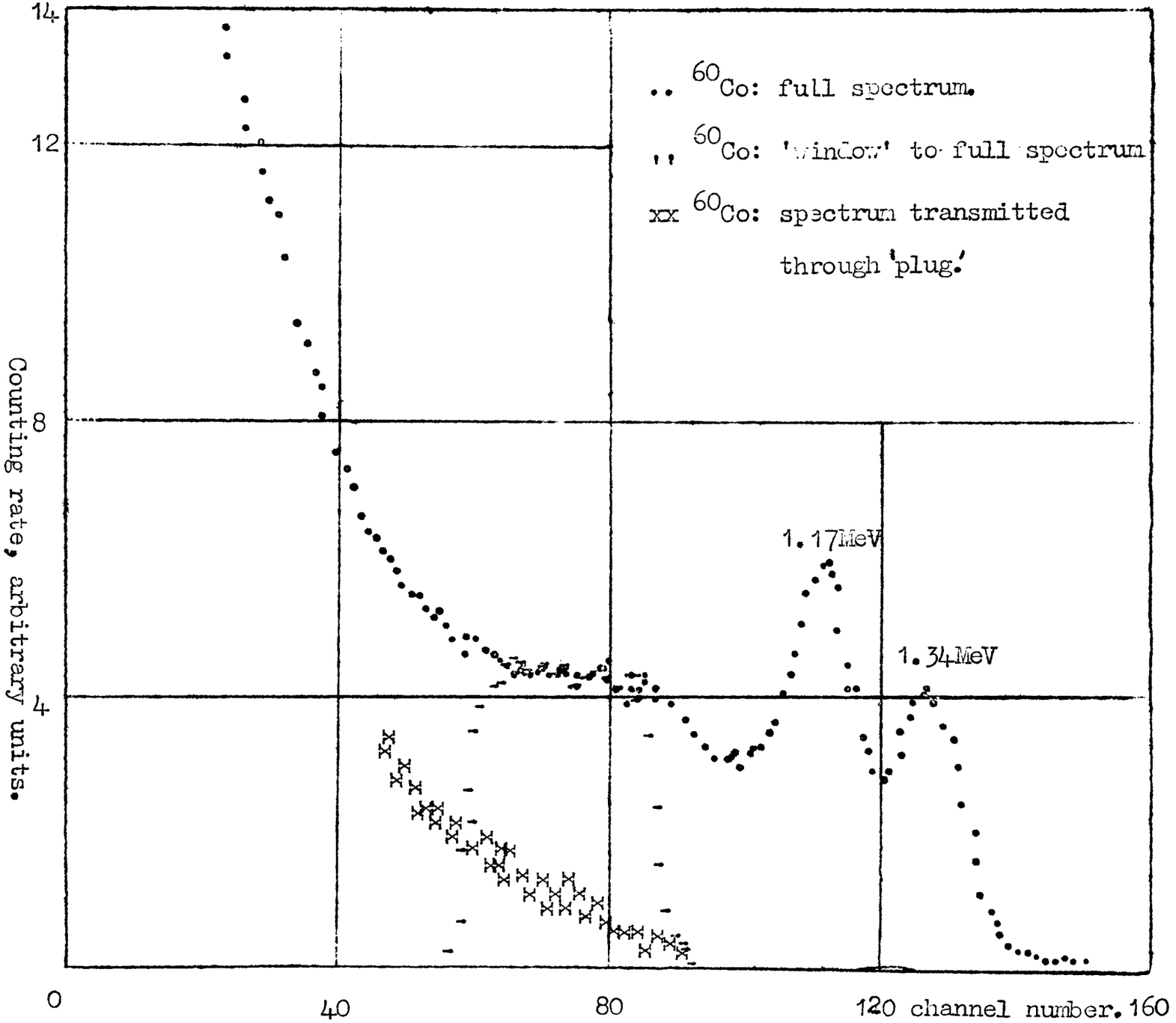


Figure IV.2.

from stray radiation etc (which we omitted to do) they observed a maximum change in the forward scattering countrate on reversal of either $\underline{s}$ or $\underline{H}_a$ of $2\pm0.5\%$, which agreed to within experimental errors with the expected change.

IV.4. Storage and Analysis of Data.

In view of the small intensity change to be expected, and to minimise the risk of a spurious result, during the counting cycle the direction of the current polarising the iron reversed for each succeeding storage channel of the analyzer (every 100secs) and after each set of say eleven channels (must be an odd number so the centers of time of the odd and even channels coincide) the direction of the magnetic field at the sample was also reversed, careful note being kept of the correspondence between the directions of the two polarising fields and the channel number. The number of counts in the even and odd channels were then averaged separately, and the results are quoted as the ratio of these two averages for the various combinations of direction of $\underline{s}$ and $\underline{H}_a$, no further analysis being carried out on this data.

The intensity changes observed were $\sim 1.5\pm0.5\%$, and in view of the fact that no corrections for background radiation etc were applied, this is in excellent agreement with the expected $\sim 2\%$.[66]

During these measurements of circular polarisation the equatorial counter could be used in the conventional fashion to monitor the temperature of the sample via the anisotropy $W(90^\circ)$; of course only one isotope would be included in the sample.

Having discussed the theory of all the measurements we now continue in the next four chapters to present and discuss some of the results.

Chapter V.

^{109m}Ag in Iron.

Contents:

Introduction.

V.1. Samples.

V.2. Decay Scheme Parameters for ^{109m}Ag 88keV Transition.

V.3. Thermometry.

V.4. Correction for Time Decay of the Activity.

V.5. Results.

V.6. Discussion.

Figures:

V.1. Decay Scheme of ^{109m}Ag with Parent Nuclei.

V.2. Spectrum of Irradiated Sample of 'first' Pd in Fe Alloy.

V.3. Spectrum of Irradiated Sample of 'second' Pd in Fe Alloy.

Introduction.

The results to be presented in this chapter play only a very small part in the systematic study of the hyperfine interaction at the nuclei of diamagnetic elements dissolved in the ferromagnetic metals iron, cobalt and nickel; it is in this type of environment that the technique of static nuclear orientation has been, to date, most extensively applied[76], since the first successful experiment on this system (Au in Fe) by Samoilov et Al (1959)[31].

When this experiment was first attempted the nuclear moment of ^{109m}Ag was unknown, and only an approximate value for the hyperfine field at silver nuclei dissolved in iron was available. However, by the time a reliable estimate of $|\mu||H_e|$ was obtained, values of these parameters were available and it was only possible to provide an independent estimate of the hyperfine field from these measurenemts.

The special difficulty associated with this experiment was the heavy absorption, in the walls of the cryostat and in the sample itself, of the low energy (88keV) gamma radiation emitted by the ^{109m}Ag nucleus; this had prevented a successful experiment in the conventional glass or brass cryostat and was part of the reason for the delay in obtaining a a good result.

V.1 Samples.

The 40sec. isomeric state of ^{109m}Ag is populated by the β^- decay of 14hr. ^{109}Pd and the β^+ decay of 470dy. ^{109}Cd - see fig V.1.[63] An attempt was made to diffuse the cadmium isotope (b.pt. metal=767°C) into iron by coating the iron with $^{109}CdCl_2$ solution, sealing it in a quartz tube under ½ atmosphere of (reducing) hydrogen, and baking the whole at 1000°C for several hours. Unfortunately no appreciable cadmium activity

DECAY SCHEME OF ^{109m}Ag WITH PARENT NUCLEI.

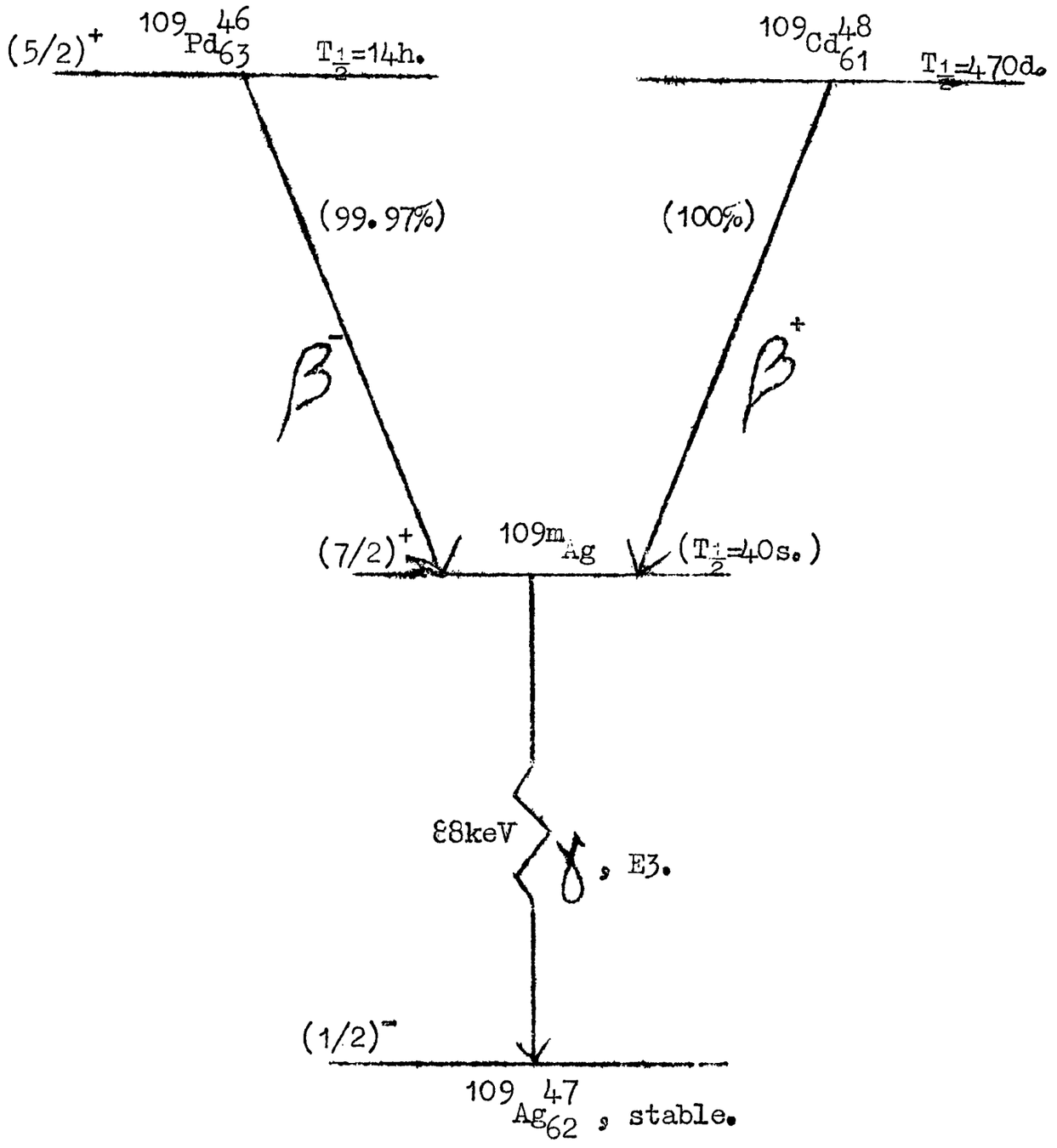


Figure V.1.

diffused into the iron in this way and so the isomeric state had to be approached from the 14hr. palladium isotope. Because of the short lifetime of this isotope the samples were prepared by irradiating pieces of a 1% Pd in Fe alloy at room temperature in a thermal neutron beam of 10^{12}n.cm.$^{-2}$sec.$^{-1}$ for about two hours (at A.E.R.E., Harwell, Berks.). Some ^{59}Fe ($t_{\frac{1}{2}} \sim 45$dys) activity was also formed, increasing the background intensity, but this is minimised by using the sample as soon as possible after irradiation.

Two separate alloys were irradiated, both being manufactured from spectroscopically pure elements; the first, supplied by Johnson Matthey Co. Ltd., was found to be heavily contaminated with (probably) iridium during manufacture, while the second alloy prepared much later by Metals Research (Cambridge) Ltd proved satisfactory. Each sample used consisted of platelets of the irradiated alloy weighing $\sim$50mg, size $\sim$2mm by 5mm by 0.5mm (to minimise the demagnetizing factor) and in number sufficient to give the required activity (4 to 6 pieces). In view of the results from the investigation of irradiation damage in cobalt metal, presented in chapter VIII, annealing of the alloy after irradiation was not considered necessary.

V.2. Decay Scheme Parameters for ^{109m}Ag.

The population distribution among the magnetic energy levels of the ^{109m}Ag nucleus immediately before emission of the 88keV gamma ray is governed by the relation between the lifetime $t_{\frac{1}{2}}$ (=40secs.) of the isomeric state and the nuclear-spin-lattice relaxation time T_1:

a. if $T_1 \ll t_{\frac{1}{2}}$ then total reorientation of the ^{109m}Ag nucleus at the temperature of the lattice will occur;

b. if $T_1 \gg t_{\frac{1}{2}}$ there will be no reorientation in the isomeric state, that

is the orientation of the parent nucleus ^{109}Pd will govern the population of the ^{109m}Ag nuclear energy levels;

c. if $T_1 \sim t_{\frac{1}{2}}$ then partial orientation of the ^{109m}Ag nucleus will take place, of a degree dependent on the lattice temperature T_1 since $T_1 \propto T_1^{-1}$.

Since no measurement of T_1 for diamagnetic nuclei in iron is available, to describe the spatial distribution of the gamma radiation emitted by the ^{109m}Ag nucleus the parameters μ, H_e, U_γ and F_γ in eq. II.3 must be considered for all possible situations.

a. Total Reorientation: Parameters for ^{109m}Ag. The 88keV gamma transition gives pure electric octupole radiation from the excited state of the ^{109}Ag nucleus, spin 7/2, magnetic moment 4.31 ± 0.04nm.[77], to the ground state spin 1/2 and there are no preceding decays to be taken into account. Hence the parameters U_γ, F_γ in eq. II.3 take the values:

$$U_\gamma = 1.$$

$$F_0=1, \quad F_2=-0.81832, \quad F_4=0.17904, \quad F_6=0.65279, \quad F_{\gamma>6}=0,$$

while in the temperature range with which we are concerned

$$\mu(^{109m}\text{Ag}) H_{e(\text{Ag in Fe})} / IkT \sim 0.5 \qquad \text{for which}$$

$$B_0(0.5) = 1, \quad B_2(0.5) \sim 0.4, \quad B_4(0.5) \sim 0.02, \quad B_6(0.5) \sim 0.0005,$$

so the term in $\gamma=6$ can be neglected in view of its smallness.

b. No Reorientation: Parameters for ^{109}Pd. The parameters F remain as in a. while the U_γ's now describe the disorentation caused by the preceding beta decay $\Delta J_\beta = 1$ and are given by

$$U_0=1, \quad U_2=0.8748, \quad U_4=0.5803, \quad U_{\gamma>6}=0.$$

The B_γ's are functions of the population distribution among the (6) levels of the ^{109}Pd nucleus, spin 5/2, of the hyperfine field at Pd

nuclei in Fe, 600±10kG,[78] and of the unknown moment of the ^{109}Pd nucleus.

c. Partial reorientation. In this case the gamma radiation anisotropy might be described by the sum of that from the two possible parent nuclei ^{109m}Ag and ^{109}Pd in the appropriate ratio. Since T_1 is inversely proportional to T_1 this ratio will change with T_1 and is not easy to determine. Data taken over a wide temperature range, if analysed using either set of parameters a or b will give a temperature dependent hyperfine field if $T_1 \sim t_{\frac{1}{2}}$ and thus indicate whether c. is likely to represent the true picture.

V.3. Thermometry.

The isotope ^{54}Mn, having a convenievtly simple gamma transition much different in energy from the ^{109m}Ag isotope was used for thermometry. The octupole radiation from the ^{109m}Ag was highly anisotropic ($W(0) \sim 0.6$ at $\sim 0.025^{\circ}K$) and so the ^{54}Mn was placed in an environment such that its gamma radiation was also highly anisotropic, to minimise overlap and pile-up corrections. For the Metals Research alloy the experiments described in chapter VI were in progress so ^{54}Mn in pure palladium was used.

V.4. Correction for Time Decay of the Activity.

The counting cycle usually involved two hours of 'cold' measurements followed immediately by one hour of 'warm' measurements for normalisation; hence time decay corrections (^{109}Pd, $t_{\frac{1}{2}}$ = 14hrs.) were essential. To extrapolate from the measured 'warm' count rate to the true normalising count rate at any particular time during the 'cold' part of the counting cycle a least mean squares fit was performed on the 'warm' count rate to an equation of the form

$$N = N_0(1-\lambda t) + C.$$

N_0 is the ^{109}Pd count rate at time t=0, λ is related to the half life of

^{109}Pd and C is the total (non Pd) background (this procedure has the advantage that C is automatically derived). The ratio of the 'cold' count rate to the true normalised count rate determined in this fashion gives the true observed anisotropy which could then be treated as in chapter III. Since the decay of a radioactive isotope follows an exponential and not a linear law there will be an error in this procedure given to a first approximation by the fraction

$$N_o\lambda^2t^2/(N_o+C)$$

which was $<$ 1% for all times t concerned and therefore negligible.

The procedure used in obtaining the data was as described in chapter III, an applied magnetic field of $\simeq$5kG being used to magnetically saturate the iron.

V.5. Results.

1. The Johnson Matthey Alloy.

The first sample irradiated, made from this alloy, was found to be heavily contaminated with an isotope emitting $\sim$320 and $\sim$480keV gamma radiation, see fig V.2, and later identified from anisotropy and lifetime measurements as 74dy ^{192}Ir (alloys containing 1% Ir in Fe, and others, were ordered with the 1% Pd in Fe). The Iridium concentration was estimated at $\sim$ 2.5ppm.Fe.

It was not considered profitable to analyze further the anisotropy measurements made with this sample.

2. The Metals Research Alloy.

The gamma radiation spectrum of this alloy immediately after irradiation is shown in fig V.3. Apart from the intense 88keV radiation a pronounced peak is visible in the region of the ^{54}Mn thermometer, i.e.

SPECTRUM OF IRRADIATED SAMPLE OF 'FIRST' Pd IN Fe ALLOY.

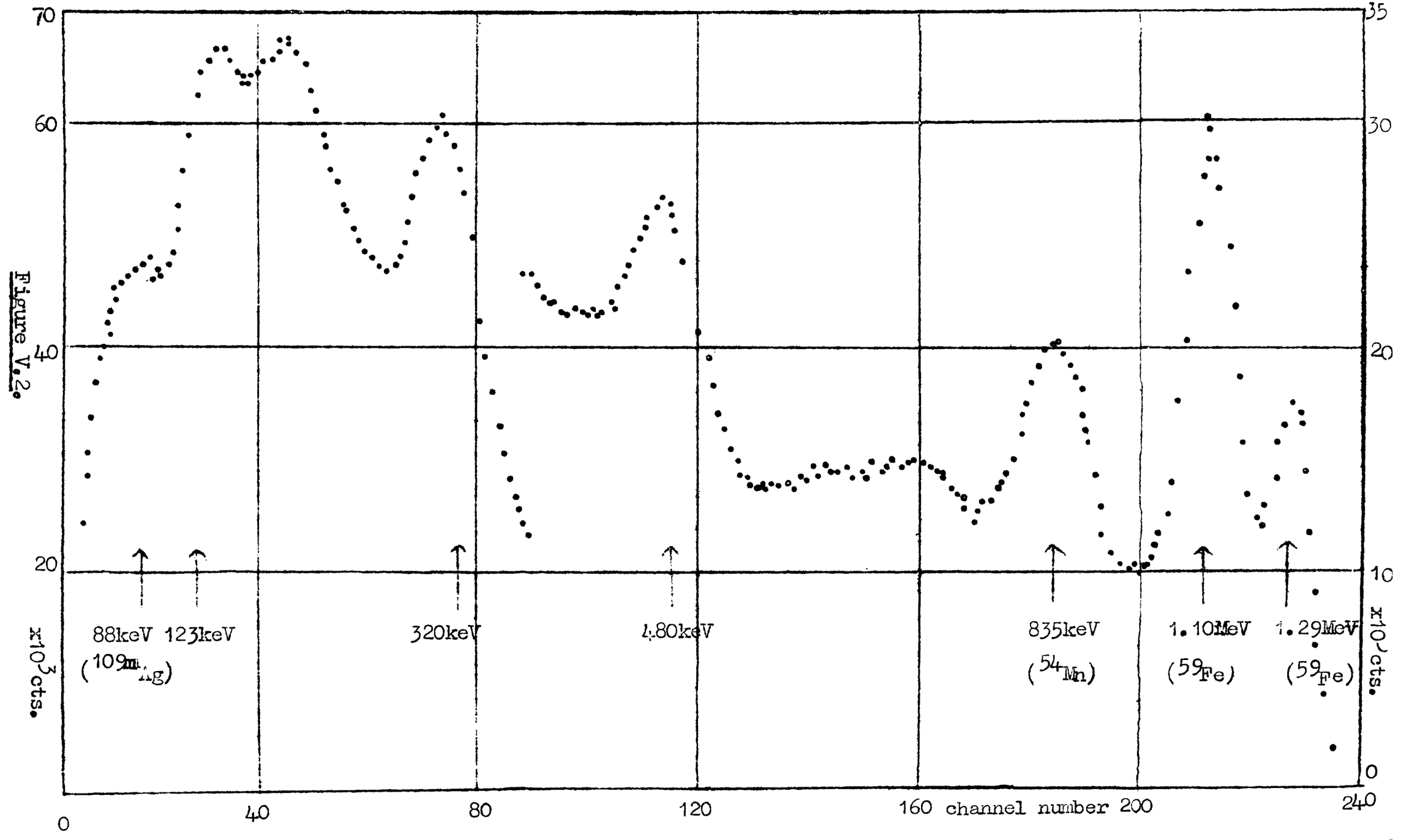


Figure V.2.

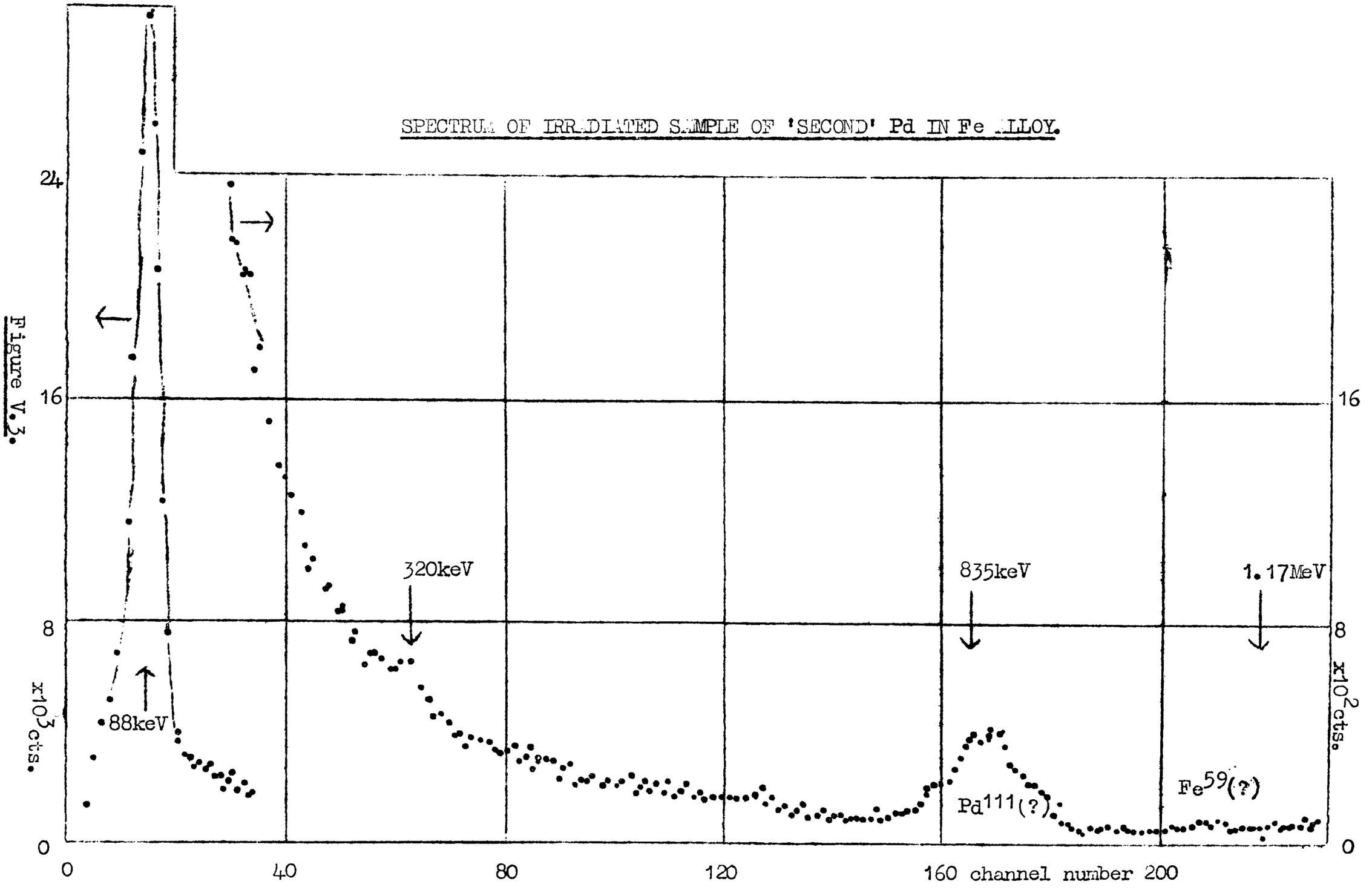

SPECTRUM OF IRRADIATED SAMPLE OF 'SECOND' Pd IN Fe ALLOY.
24
16
8
0
x10³ cts.
x10² cts.
88keV
320keV
835keV
1.17MeV
Pd¹¹¹(?)
Fe⁵⁹(?)
0
40
80
120
160 channel number 200

Figure V.3.

at 0.835MeV; its source was identified with the 5.5hr. ^{111}Pd isotope, and the radiation decayed to less than 1% of the intensity of the ^{54}Mn in Pd thermometer before measurements were made so it was not necessary to correct for this.

From three successful counting cycles the final value of the hyperfine field at silver nuclei in iron deduced assuming total reorientation of the ^{109m}Ag nucleus (V.2a) was

$$|H_e(\text{Ag in Fe})| = 340 \pm 20 \text{kG}.$$

Analysis of the anisotropy measurements assuming no re-orientation of the ^{109m}Ag nucleus (V.2b) yields an estimate for the magnetic moment of the ^{109}Pd nucleus of

$$\mu(^{109}\text{Pd}) = 2.66 \pm 0.17 \text{nm}.$$

In this particular experiment the temperature range was only from 0.022°K to 0.030°K and any temperature dependence in the hyperfine field values which would indicate c to hold is within the experimental errors.

V.6. Discussion.

The magnitude for the nuclear moment of the ^{109}Pd nucleus deduced assuming V.2b to hold is much larger than the Schmidt limit of 1.93nm calculated from the single-particle (shell) model of the nucleus (odd neutron), yet it is an experimental fact[79] that the nuclear moments of all but very light isotopes lie within the two possible values of the Schmidt limit (-1.913 to +1.366nm for ^{109}Pd). Thus we may assume that V.2a holds, i.e. that the ^{109m}Ag nucleus reorients before emitting the 88keV gamma ray. This conclusion is supported by the results of a similar experiment in which measurements of the angular distribution of the gamma

radiation emitted by the isomeric state of the nucleus ^{191m}Iridium in iron ($t_{\frac{1}{2}}$ = 4.7sec.) indicated that a nuclear-spin-lattice relaxation time less than 5secs may be expected for this alloy system[80].

The value for the hyperfine field at silver nuclei in iron obtained from our measurements is thus 340±20kG and this value may be compared with the results of similar measurements of the hyperfine field at the nuclei of ^{104}Ag ($t_{\frac{1}{2}}$ = 69min.) and ^{110m}Ag ($t_{\frac{1}{2}}$ = 253dys, but a very complex decay scheme) dissolved in iron, 350±100kG and 279±20kG respectively[81]. (The revised value for the nuclear moment of ^{110m}Ag, by Schmelling et Al. (1967)[82], has been used in the above results.) The discrepancy of ~ three standard deviations between the result for ^{109m}Ag and that for ^{110m}Ag may be due to systematic or underestimated errors in any or all of the measurements contributing to the quoted values.

The dominant contributions to the hyperfine field at nuclei are generally regarded as arising from the polarization of the core s-electrons and the conduction s-electrons, as we have seen in chapter I. The hyperfine field at the nuclei of many elements with paired inner-shell electrons (diamagnets, e.g. Cu, Ag and Au) in the ferromagnetic metals Fe, Co and Ni is found to be approximately proportional to the host moment[83] and each graph so obtained extrapolates to the origin. This circumstance raised the question as to whether the hyperfine field arose principally from the conduction electron polarization, any core polarisation contribution being much smaller. Shirley and Westenbarger (1965)[84] made a systematic analysis of this possibility for nuclei dissolved in iron by assuming

$$H_e \propto n\, p\, H(0)$$

where n is the number of conduction electrons per atom (≈ 1), p the conduction electron polarisation, and H(0) the hyperfine field due to

the contact interaction with the outermost electron in the atomic state. $H(0)$ they calculated from experimental data for each atom, and fitted much of the known data for diamagnetic atoms to the value $np = 0.07$ implying $\approx 7\%$ polarisation of the conduction electrons, a reasonable value; unfortunately np cannot as yet be calculated ab initio.

Such a systematic analysis of hyperfine field measurements awaits more experimental data to facilitate further development; however, hyperfine fields at several diamagnetic nuclei in iron could be predicted from the above analysis and are being sought experimentally.

Chapter VI.

^{54}Mn in Palladium.

Contents:

Introduction.

VI.1. Sample Preparation.

VI.2. Thermometry.

VI.3. Results.

VI.4. Discussion.

VI.5. Attenuation Factors for Electronic Interactions.

VI.6. Analysis of Anisotropy using the Atenuation Factors.

VI.7. The Sign of the Hyperfine Field (^{54}Mn in Pd).

VI.8. Further Discussion and Conclusion.

Figures:

VI.1. Apparent H_e at ^{54}Mn in Pd - both samples at H_a = 5kG.

VI.2. Temperature Dependence of Apparent H_e for melted ^{54}MnPd.

VI.3. Temperature Dependence of Apparent H_e for diffused ^{54}MnPd.

VI.4. 'Saturation' curves: $H_e(H_a)/H_e(5kG)$ vs H_a, both samples.

VI.5. Attenuation Analysis: Angles Identified for Axial and Equatorial Cases.

VI.6. Attenuation Factors for Single Value and 'Square Wave' Fields.

VI.7. Anisotropy vs 1/T, Theoretical Attenuated Curves plus some ^{54}MnPd (melted) data.

VI.8. H_e vs 1/T using Attenuated Expressions for Anisotropy for Several Values of the Interaction Strength.

VI.9. Effect of a 'Spread' in True H_e Values on the Observed H_e.

Introduction.

Metallic palladium has long been of interest to the solid state physicist in view of the details of its electronic structure; in the atomic state palladium has a filled electronic '4d' shell (10 electrons) and an empty '5s' shell, while in the metallic state the '4d' and '5s' electronic energy bands overlap with approximately 0.6 electrons believed (from susceptibility measurements[84-86] of alloys with diamagnetic elements) to be in the '5s' band. Palladium metal has no magnetically ordered phase[87,88] whereas the analogous member of the '3d' transition metal series, nickel, exists in a ferromagnetically ordered phase below 630°K. Moreover an anomalous temperature dependence of the large paramagnetic susceptibility of pure palladium metal has been observed[89], as also a similar temperature variation of the magnetic field for nmr at fixed frequency of ^{105}Pd in Pd[90], but no corresponding anomaly was found in the specific heat[91-95]. This curious combination of specific heat and susceptibility data can be accounted for using the density of states curve calculated on the assumption of an 'exchange' interaction between the $4d^9 5s^1$ states[96-98] but neutron paramagnetic scattering measurements place an upper limit of 5.10^{-13}secs on the life-time for association of such states with any particular atom in the pure metal[90,99]. To summarise, palladium metal is almost but not quite a ferromagnet.

How near palladium metal is to being a ferromagnet can be seen from the fact that alloys with the 3d 'transition' metal ions are ferromagnetic at very high dilution; for example a 0.1at.% CoPd alloy is known to have a Curie temperature of 7°K[100] and a 1.25at.%FePd alloy to have a Curie temperature of 66°K[101]. Also the magnetic moment per solute atom in these alloys increases with dilution to between 10 and 12μ_b in both the para- and ferromagnetic phases - much greater than can be

attributed to the transition atoms alone. This large moment has been shown by neutron diffraction experiments[102,103] to be the sum of the small moments induced at up to 200 neighbouring palladium sites; indeed one theory concerning the ferromagnetism of these alloys attributes its occurrence to a ferromagnetic interaction between the conduction electrons which consequently leads to ferromagnetic ordering of the magnetic ions themselves[104]. A long-range conduction-electron polarisation has also been observed (using the epr technique) in the alloy system GdPd[105-109] but is oppositely directed to the Gd magnetic moment, and correspondingly the magnetic moment per Gd ion falls considerably below the value of $7\mu_b$ for an isolated Gd atom ($4f^7$) in the very dilute alloys.

The spin values associated with the iron nuclei in dilute FePd as determined by various experimental techniques are in some disagreement. The spin on the Fe site in a ferromagnetic sample was determined by neutron diffraction to be 3.5 ± 0.4[103] while specific heat measurements resulted in 1.1 ± 0.3[110] from the entropy associated with the transition to the ferromagnetic state (more concentrated FePd alloys gave the value 3.1 per Fe atom); the cobalt in palladium system shows similar behaviour[103,111]. Also Mössbauer measurements on very dilute paramagnetic FePd alloys[112] led to the conclusion that the large local moment of $\sim 12\mu_b$ associated with each iron atom acts as one unit having a spin of 6.5 ± 1.5. One suggested explanation of the specific heat data, where the magnetic anomaly is not λ-shaped but spread over a wide temperature range, is that the local fields in the ferromagnet are random; in fact some Mössbauer spectra from alloys containing $> \frac{1}{2}\%$ Fe in Pd can be interpreted in terms of line-broadening and superposition of spectra for zero and a finite hyperfine field, over the transition temperature region[113]; for the paramagnetic samples unbroadened six line spectra were observed.

It seems that the ferromagnetism observed in CoPd and FePd alloys is of an entirely different character from that of the transition metals.

There is no iron nuclide suitable for nuclear orientation experiments; however orientation of both ^{54}Mn and ^{60}Co nuclei is easily detected and we report here preliminary results from the orientation of ^{54}Mn nuclei in palladium, saving the results of similar experiments on ^{60}Co nuclei in palladium to the next chapter, since they are best analyzed in the light of results from the MnPd system.

Little work has so far been done on the MnPd alloy system, beyond determination of the structure of the antiferromagnetic compounds Mn_2Pd_3, MnPd and $MnPd_3$[114-116] and a measurement of the g-shift of Mn in palladium metal[117] which was found to be large and positive, corresponding to a conduction electron polarisation parallel to the manganese moments.

VI.1. Sample Preparation.

Two MnPd alloys were used for the experiments to be described herein, to check complete solution, though manganese is known to dissolve readily in palladium at all concentrations[118].

a. Melted Sample. Carrier free $^{54}MnCl_2$ in 0.1N.HCl solution was dried onto a piece of etched (etching solution: equal parts ethanol and aqua regia) and rolled palladium wire (nominal impurities 5ppmSi, 2ppmFe, <1ppmCu,Mg) and reduced under H_2 at 1200°C for 12hrs in an alumina furnace tube and crucible. Since hydrogen gas is heavily absorbed by palladium and known to affect its magnetic properties[119] an atmosphere of nitrogen was used to melt the sample (1600°C for 20mins) and cool it slowly to room temperature. (M.Pt Pd = 1550°C, Mn = 1260°C.) The ball of metal obtained was then flattened, etched and annealed at 900°C for two hours under nitrogen, and cut into pieces having the required activity for use. The manganese content

was estimated as 0.1 to 0.2ppm from activity to weight measurements.

Since a clean furnace tube was not available at the time of preparation there is a strong possibility this sample was contaminated.

b. Diffused Sample. The palladium used for this sample was received in the form of sponge (nominal inpurities 5ppmSi, 1ppmFe, 2ppmAl, < 1ppmMg, Ca, Cu, Ag) and had to be melted (under vacuum), rolled and etched before the $^{54}MnCl_2$ solution could be dried on to it. The chloride was reduced under H_2 at 900°C, then the ^{54}Mn was diffused into the metal at 1200°C for 36hrs and cooled to room temperature, all in a vacuum ($< 5.10^{-4}$mmHg) and using a clean furnace tube and crucible. The activity level was observed before and after etching to check solution of the manganese and the concentration estimated at 0.4ppm.

After completion of the experiments and data analysis, §VI.5 and 6, the diffused sample was analyzed by C.S.I.R.O. (Australia) and found to contain 1000ppm Fe and 1000ppm Si. Also the original palladium wire used for the 'melted' sample was found to contain 1300ppm (0.13%) Fe; it has not yet proved possible to obtain a similar analysis of the melted sample. Thus, though the experiments were intended to investigate the hyperfine field in a paramagnetic host, it is likely that both the samples were magnetically ordered below ~1°K.

Measurements of the degree of anisotropy of the gamma radiation emitted by both samples were taken over a range of temperatures (~0.05°K to 0.012°K) and applied magnetic fields (~0.5kG to 5kG).

VI.2. Thermometry

For applied fields large enough to magnetically saturate iron (> ~4kG), ^{60}Co in Fe was used to monitor the sample temperature (H_e at ^{60}Co nuclei in Fe = -290.1kG[120]) while for lower applied fields it was

necessary to remove the iron otherwise it affected significantly the applied field at the sample - see fig VI.4. Thus to measure the sample temperature at low fields it was necessary to use the 5kG calibration and alternate the field between 5kG to measure temperature and the lower values to measure the hyperfine field, temperature being obtained by interpolation between the nearby high field points. Of course the accuracy of this latter procedure was greatly dependent on the magnitude of the heat leak to the sample.

VI.3. Results.

Using the parameters for ^{54}Mn and ^{60}Co given in §II.4, the anisotropy data obtained from both samples was firstly analyzed as described in chapter III, applying corrections for overlap, background, pile-up and finite detector aperture. The results for the 'apparent' hyperfine field thus observed at ^{54}Mn nuclei dissolved in palladium metal in applied fields of 5.4kG and over the available temperature range were next compared for the two samples, as a check on their preparation, and found to agree to within the experimental accuracy - see fig VI.1. (Each experimental point generally represents $\sim\frac{1}{2}$hr of counting time.)

Figures VI.2 and 3 show the variation with temperature and applied magnetic field of the 'apparent' hyperfine field at ^{54}Mn nuclei in the diffused and melted samples respectively. That this 'apparent' hyperfine field decreases with decreasing temperature at any particular applied magnetic field is clearly shown, also that this temperature dependence is greater the smaller the applied field.

At the lowest temperatures the observed axial effect was as high as 45% in $\sim$5kG applied field; thus the data was obtained with considerable accuracy over a wide range of T and H_a, in contrast with the case of ^{60}Co

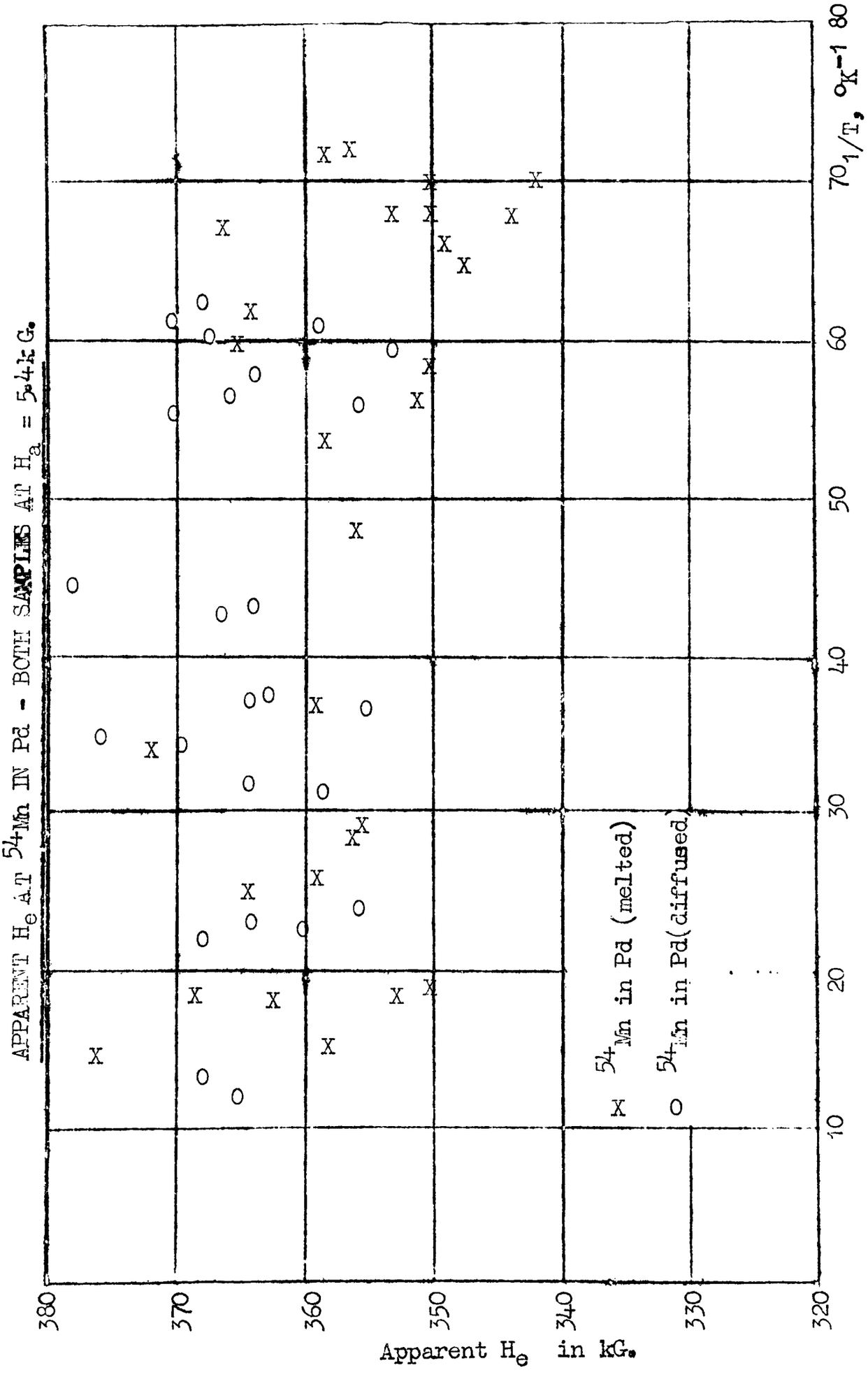

APPARENT H_e AT ^{54}Mn IN Pd - BOTH SAMPLES AT H_a = 5.4 kG.
$70_{1/T}$, $^oK^{-1}$
80
60
50
40
30
20
10
380
370
360
350
340
330
320
Apparent H_e in kG.
^{54}Mn in Pd (melted)
^{54}Mn in Pd (diffused)

Figure VI.1.

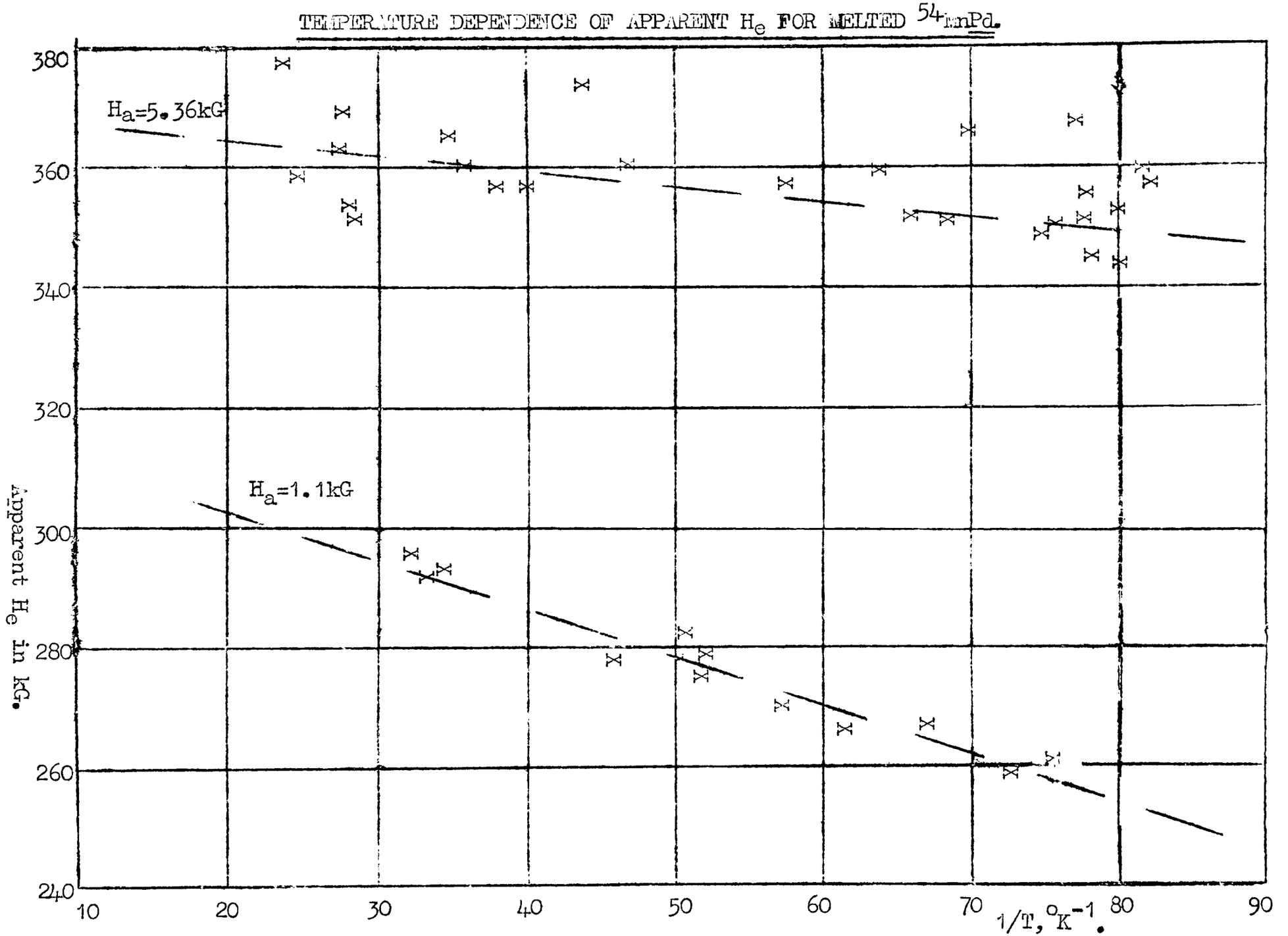

TEMPERATURE DEPENDENCE OF APPARENT H_e FOR MELTED ^{54}MnPd.
H_a=5.36kG
H_a=1.1kG
Apparent H_e in kG.
380
360
340
320
300
280
260
240
10
20
30
40
50
60
70
80
90
1/T, °K^{-1}.

Figure VI.2.

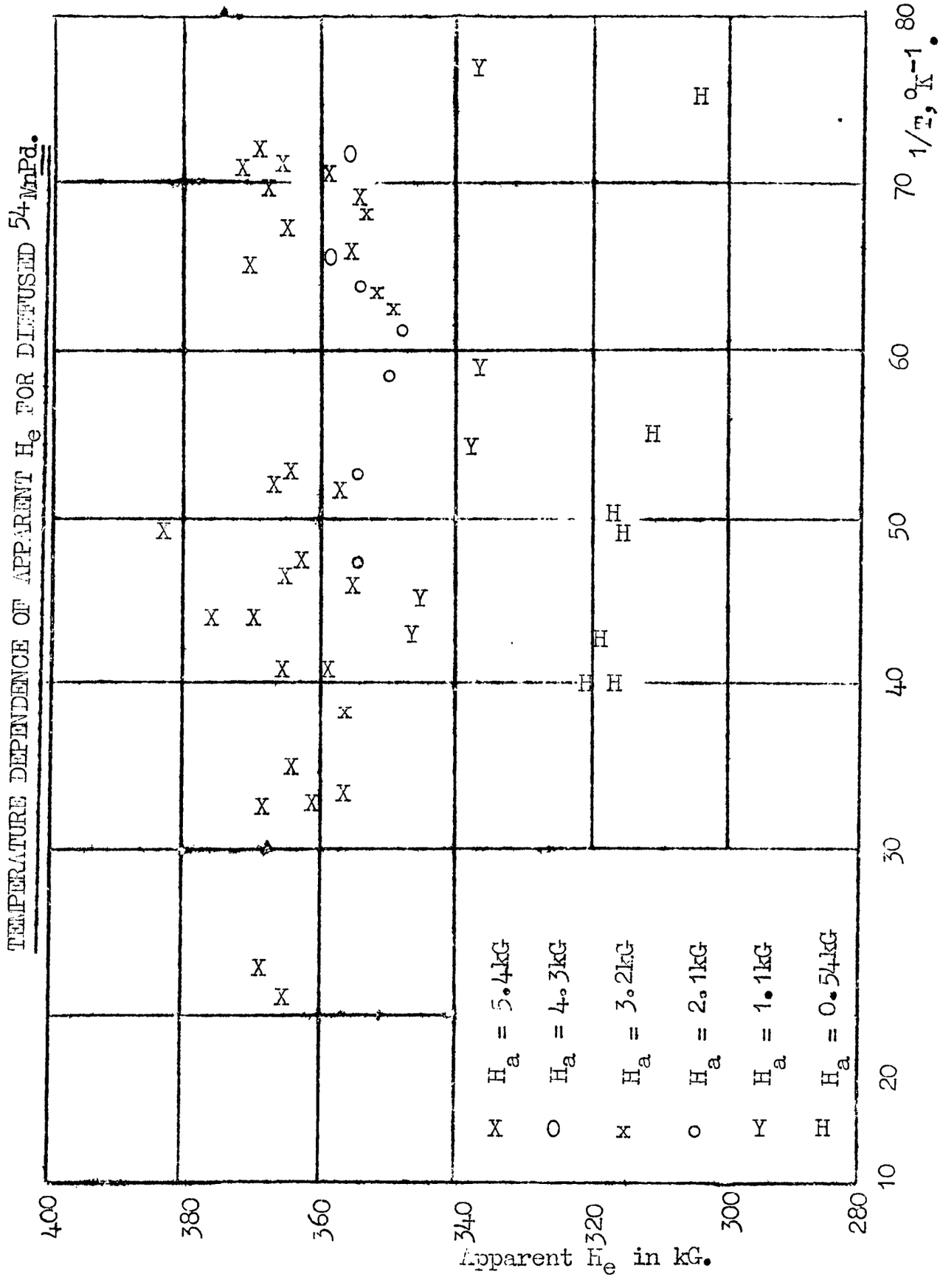

TEMPERATURE DEPENDENCE OF APPARENT H_e FOR DIFFUSED ^{54}MnPd.
Apparent H_e in kG.
400
380
360
340
320
300
280
10
20
30
40
50
60
70
80
1/T, °K^{-1} •
X H_a = 5.4kG
O H_a = 4.3kG
x H_a = 3.2kG
o H_a = 2.1kG
Y H_a = 1.1kG
H H_a = 0.54kG

Figure VI.3.

in palladium (chapter VI) where the largest axial affect observed was less than 10%. For this reason the 'internal field' analysis which follows is presented with the ^{54}Mn data.

VI.4. Discussion.

We have already discussed in chapter I how the concept of a hyperfine field is only valid when the electronic spin system attains equilibrium much faster than the nuclei precess and that the magnitude of this hyperfine interaction is proportional to the time-average of the electron spin only in certain cases. These assumptions have been justified experimentally for the hyperfine field at ^{57}Fe nuclei dissolved in palladium metal[112] between 1.5 and 4°K and by analogy are assumed true, in the following account, for the hyperfine field at ^{54}Mn and ^{60}Co nuclei in the same host.

A system of non-interacting paramagnetic ions aligns parallel to an applied magnetic field according to a Brillouin function of $g_s u_b SH/kT$ and one would expect ~70% alignment in an applied field of ~30G of a system of ions for which $S = 5/2$ and $g_s = 2$ at 1/50°K. Thus if the manganese ions in the palladium host metal were non-interacting then a single value would have been observed for the hyperfine field at all temperatures and applied fields involved in the data of figs VI.2 and VI.3, corresponding to a saturated electronic spin system. If the non-interacting spin system were simply not saturated then lowering the temperature of the sample in a constant magnetic field would increase the net magnetization and thereby increase the apparent hyperfine field, which is contrary to the observed trend. The simplest explanation of the observed temperature dependence of the 'apparent' hyperfine field is that the electronic moments interact appreciably, while each electronic moment is

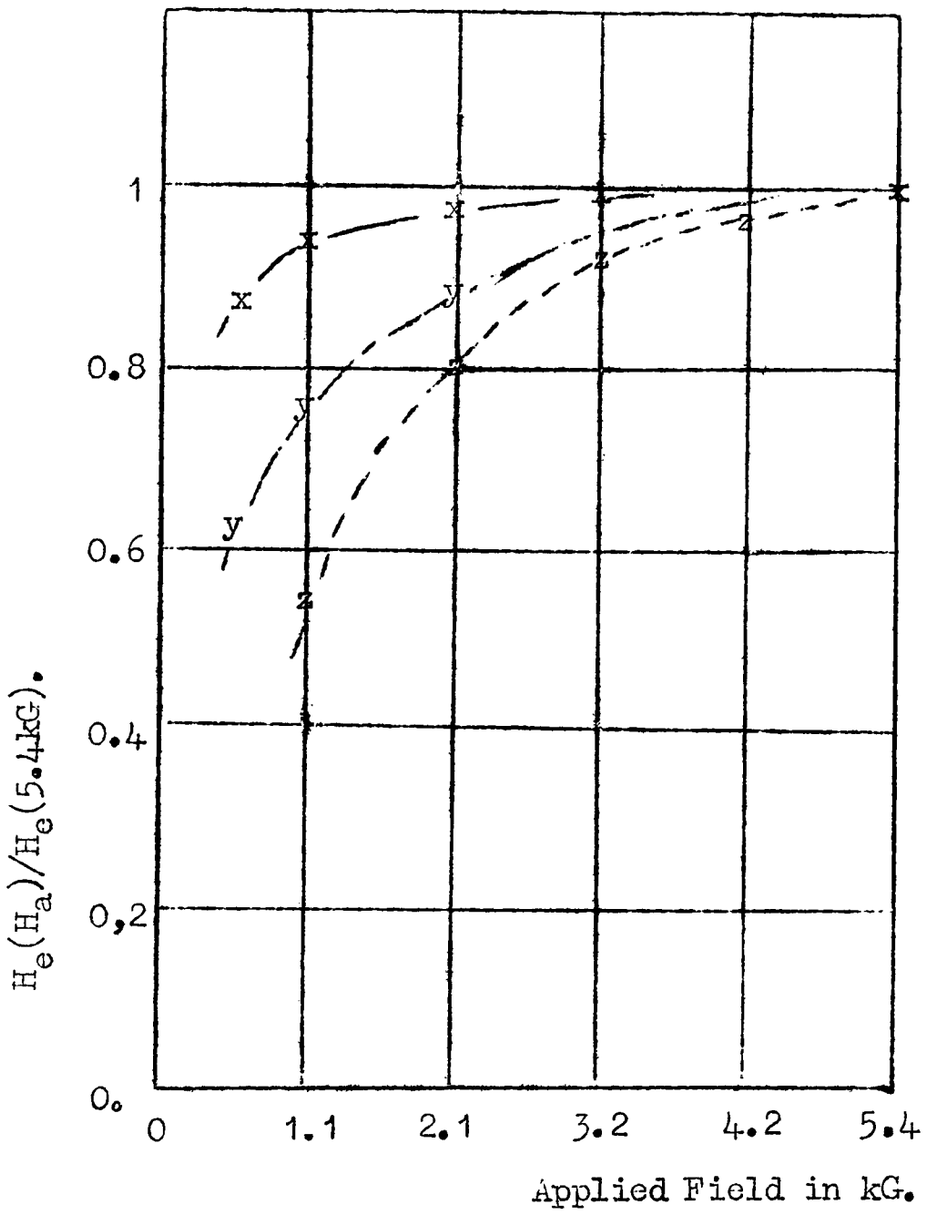
completely saturated in the resultant of the applied magnetic field and the 'local' magnetic field describing this interaction. In this case eq. II.3 describing the angular dependence relative to the applied magnetic field of the emitted radiation must be modified to take this non-axial alignment into account and the net result is an attenuation factor associated with each of the Legendre polynomials $P_\nu(\cos\theta)$, reducing the fractional anisotropy at all temperatures. Analyzing the anisotropy data using the unattenuated eq. II.3 would yield too low a value for the hyperfine field at each temperature, and this discrepancy would increase as the temperature fell owing to the effective divergence of the attenuated and unattenuated expressions for the anisotropy and so the 'apparent' hyperfine field would decrease with decreasing temperature - the trend observed. At a fixed temperature the 'apparent' hyperfine field would of course tend to increase with increasing applied field as the electronic moments align parallel to the external axis, and this can be seen in the data of fig VI.4 in which the ratio between the 'apparent' hyperfine field at various applied fields and at 5.4kG applied field is plotted against the applied field (data from the temperature region 0.017 to 0.014°K).

(In fig VI.4 the discrepancy between the two curves for the melted sample can be explained by assuming the ^{60}Co in iron thermometer 'concentrates' magnetic flux in its own volume at low applied fields, thus reducing the magnetic field 'felt' by the palladium, and the discrepancy between the two curves for the melted and diffused samples alone by assuming a greater impurity content in the melted sample.)

Inter-electronic interactions can be deduced from hyperfine field measurements only if the interaction is 'static' that is fluctuates much more slowly than the nuclei precess. In the following analysis we also assume the interaction strength to be independent of temperature and for

e interaction, evaluate the attenuation factors

SATURATION CURVES: ^{54}Mn IN Pd.



x ^{54}Mn in Pd (diffused) - alone.

y ^{54}Mn in Pd (melted) - alone.

z ^{54}Mn in Pd (melted) - with ^{60}Co in Fe thermometer.

The difference at low H_a between y and z is due to distortion of the magnetic field 'felt' by the $^{54}MnPd$, caused by the unsaturated iron 'sucking in' magnetic flux.

Figure VI.4.

for the Legendre polynomials in eq. II.3.

VI.5. Attenuation Factors for Electronic Interactions.

The distribution of transition ions in the alloys with which we are concerned is random, so we consider first an interaction between these ions which has a constant magnitude, the simplest case, and describe it in magnetic field units H_l. We assume the electronic moments, and thus the nuclear spin quantization axes, are aligned parallel to the resultant of this 'local' field H_l and the applied magnetic field H_a. The gamma ray intensity is monitored in the directions parallel and perpendicular to the applied field and so the observed radiation originates from a range of angles ϕ in the axial direction and α in the equatorial direction (see fig VI.5). The Legendre polynomials $P_\nu(\cos\phi)$ and $P_\nu(\cos\alpha)$ in eq. II.3 must be averaged over these angles to give the correct expuession for the gamma radiation

$$\overline{W(\theta)} = \sum_{\nu \text{ even}} B_\nu(\mu H_e/kT)U_\nu F_\nu \overline{P_\nu(\cos\theta)} \qquad \ldots\ldots\ldots\text{VI.1.}$$

Setting $a = H_l/H_a$ and considering the axial direction first we have

$$\cos^2\phi = (1/a + \cos\theta)^2/((1/a)^2 + 1 + 2\cos\theta/a) \qquad \ldots\ldots\ldots\text{VI.2.}$$

and

$$\overline{P_\nu(\cos 0)} = (1/4\pi)\int_0^{2\pi}\int_0^{\pi} P_\nu(\cos\phi)\sin\theta\, d\theta\, d\psi = A_\nu^c(0)P_\nu(\cos 0) \ldots \text{VI.3.}$$

with

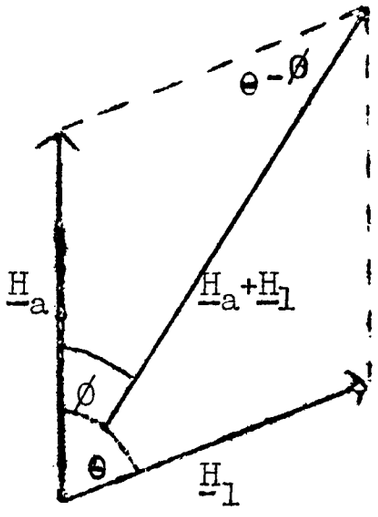
$$A_2^c(0) = (5-3a^2)/8 - 3(1-a^2)^2\log((1-a)/(1+a))/16a$$

$$A_4^c(0) = \left\{30(1-a^2)^2 - 35(1-a^2)^3\right\}\log((1-a)/(1+a))/64a + \\ + (105a^4 - 190a^2 + 81)/96 \qquad \ldots\ldots\text{VI.4}$$

The first of these attenuation factors was previously calculated by

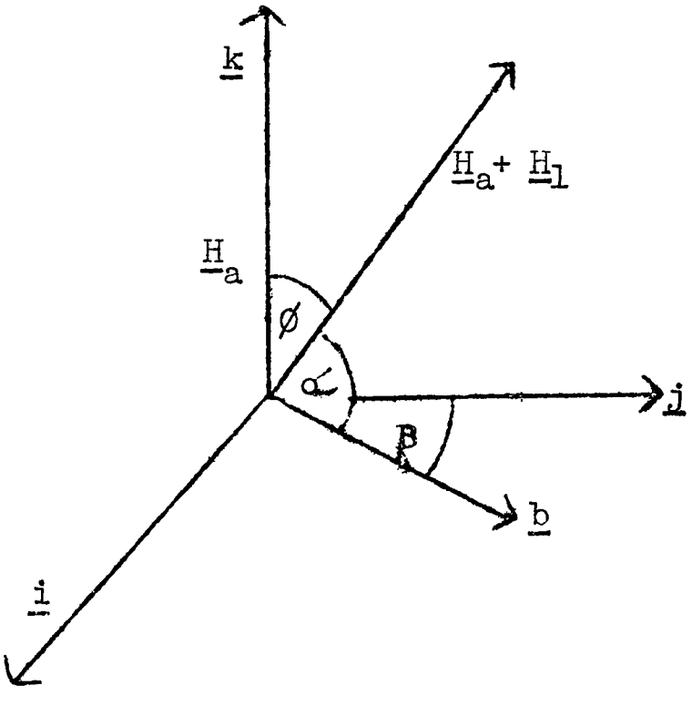
ATTENUATION ANALYSIS.

Identification of Angles for Axial and Equatorial cases.



(ψ = angle between H_1 and axis fixed in plane $\perp H_1$)

a. Axial.



b. Equatorial.

Figure VI.5.

In the equatorial direction for each value of ϕ the radiation is observed over angles β from 0 to 2π , thus over a range of angles α in fig VI.5. We have

$$\underline{b}.(\underline{H}_a + \underline{H}_l)/|\underline{H}_a + \underline{H}_l| = \cos\alpha = \sin\phi\cos\beta \qquad \ldots\ldots\ldots VI.5.$$

and

$$\overline{P_\nu(\cos 90)} = (1/4\pi)\int_0^{2\pi}\int_0^{\pi} P_\nu(\cos\alpha)\sin\theta d\theta d\beta = A_\nu^c(90)P_\nu(\cos 90) \qquad \ldots\ldots\ldots VI.6.$$

and on integration it turns out that

$$A_\nu^c(90) \equiv A_\nu^c(0)$$

as given above.

A single value for the magnitude of a random interaction is somewhat unlikely. To explain the low temperature specific heat of some dilute random alloys Marshall[121] proposed a distribution in random fields which took the form of a sum over two distorted, cut-off Lorentzians centred at $\pm H_l$ respectively (based on the assumption that the magnetic ions interact via the R-K-K-Y mechanism). For our analysis this can be approximated by a 'square wave' distribution, that is equal probability of all values H_l up to a maximum cut-off value and calculation of the attenuation factors for this case involves only integration over $H_l \pm aH_a$ from zero to some cut-off value $H_{max}=AH_a$ of the eqs VI.4, i.e.

$$A_\nu^s = (1/H_{max})\int_0^{AH_a} A_\nu^c dH_l \qquad \ldots\ldots\ldots VI.7.$$

This integration was performed numerically using the computer KDF9, and the variation of these attenuation factors with a, A is shown graphically in fig VI.6.

VI.6. Analysis of the Anisotropy using the Attenuation Factors.

From the high applied field data we get an approximate value for

ATTENUATION FACTORS FOR SINGLE VALUE AND 'SQUARE WAVE' FIELDS.

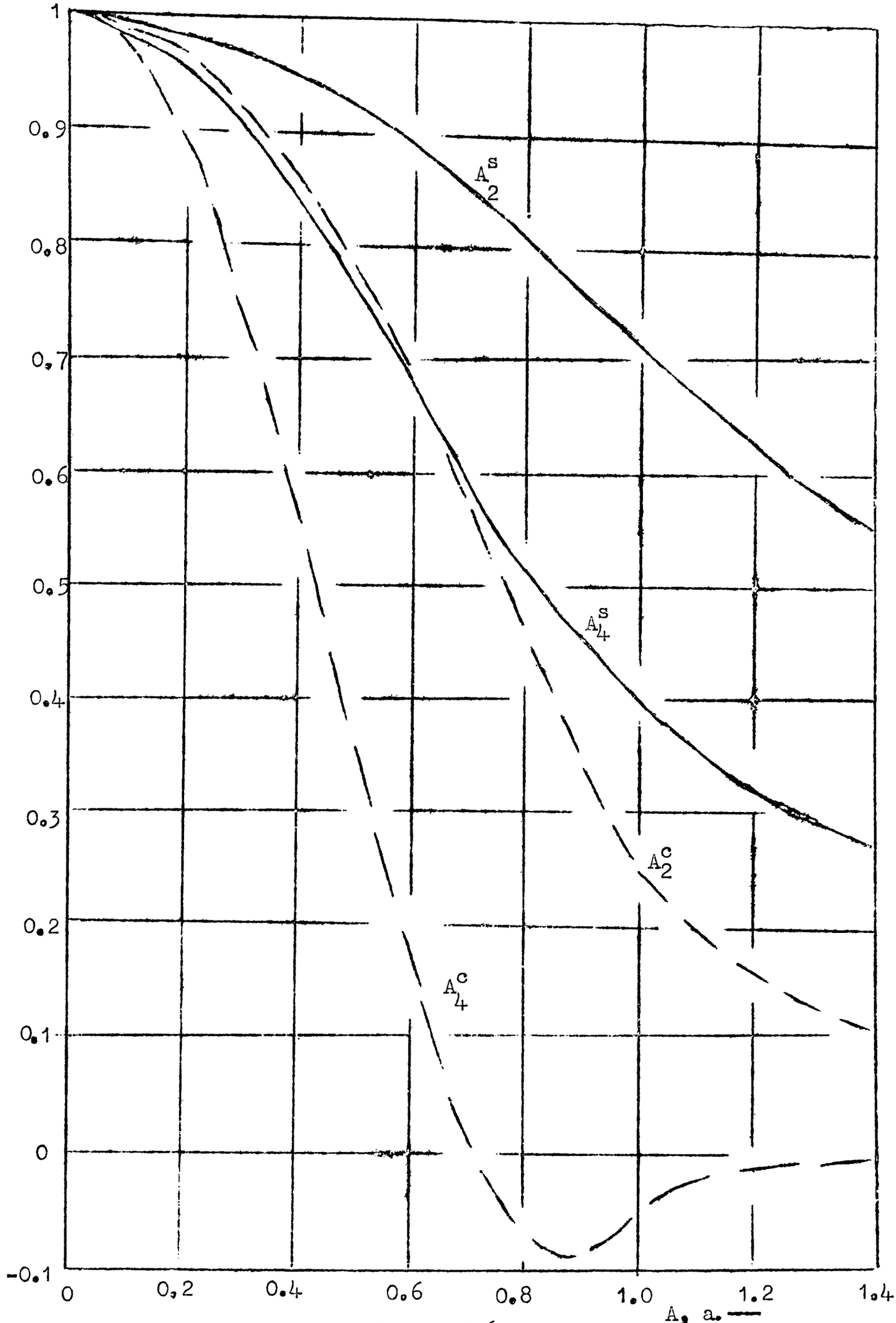


Figure VI.6.

the hyperfine field of 364kG. Fitting some of the low field (melted sample) data to the attenuated axial anisotropy as shown in fig VI.7 yields the following estimates of the strength of the random interactions using the single and square wave descriptions respectively.

Table VI.1a

H_a	H_1	H_{max}	
5.4 kG	0.8±0.3 kG	0.9 ±0.3 kG	
1.1 kG	0.6±0.1 kG	1.0 ±0.15kG	H_e=364kG
0.54kG	0.4±0.05kG	0.95±0.1 kG	

It can be seen that the square wave form of the interaction describes the data more consistently than the single value and in fact we continue the more detailed analysis using only the square wave attenuation factors.

The hyperfine fields at all ^{54}Mn nuclei present as a very dilute solute in palladium metal should, at all temperatures and in all applied fields used to obtain the data, have the same value, corresponding to saturation of the electronic spin system. The data was analyzed to determine this value by the procedure outlined in chapter III, only using the attenuated expression for the anisotropy with various cut-off values of the local field H_{max}. Fig VI.8 shows how the temperature dependence of the hyperfine field so derived changes sign as we pass through the most appropriate value of H_{max} for the data taken at H_a = 1.1kG from the melted sample and a summary of all the experimental data after this analysis is given in tables VI.2 and 3.

In taking the data the applied magnetic field was supplied by a superconducting magnet and only measured by monitoring the supply current. Hence remanent fields may well be appreciable, particularly in the low applied field region, and less weight should be given to the data for applied fields below 1kG. Further experiments either measuring the

AXIAL ANISOTROPY V.S. 1/T:

Some Experimental Data with Theoretical Attenuated Curves.

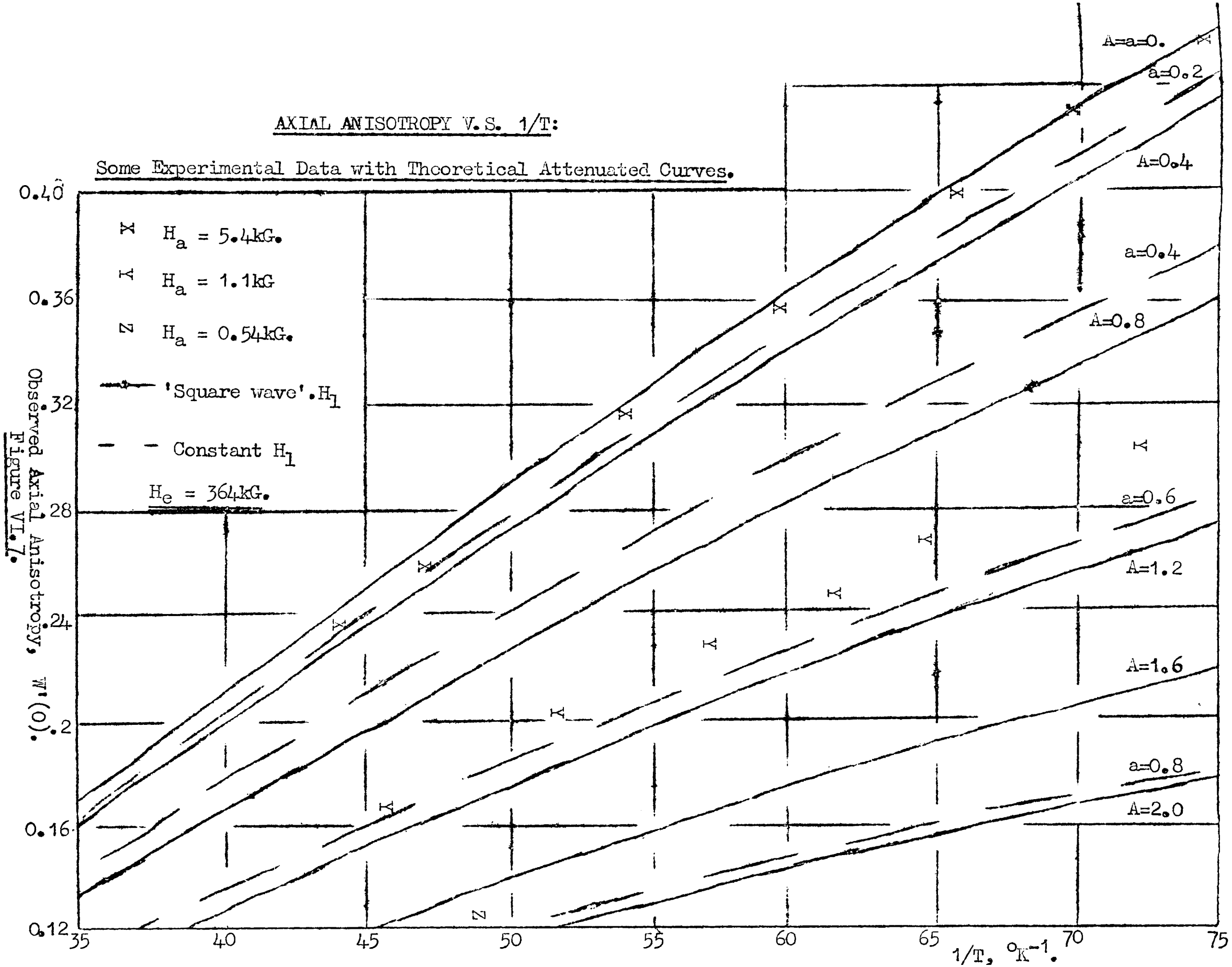


Figure VI.7.

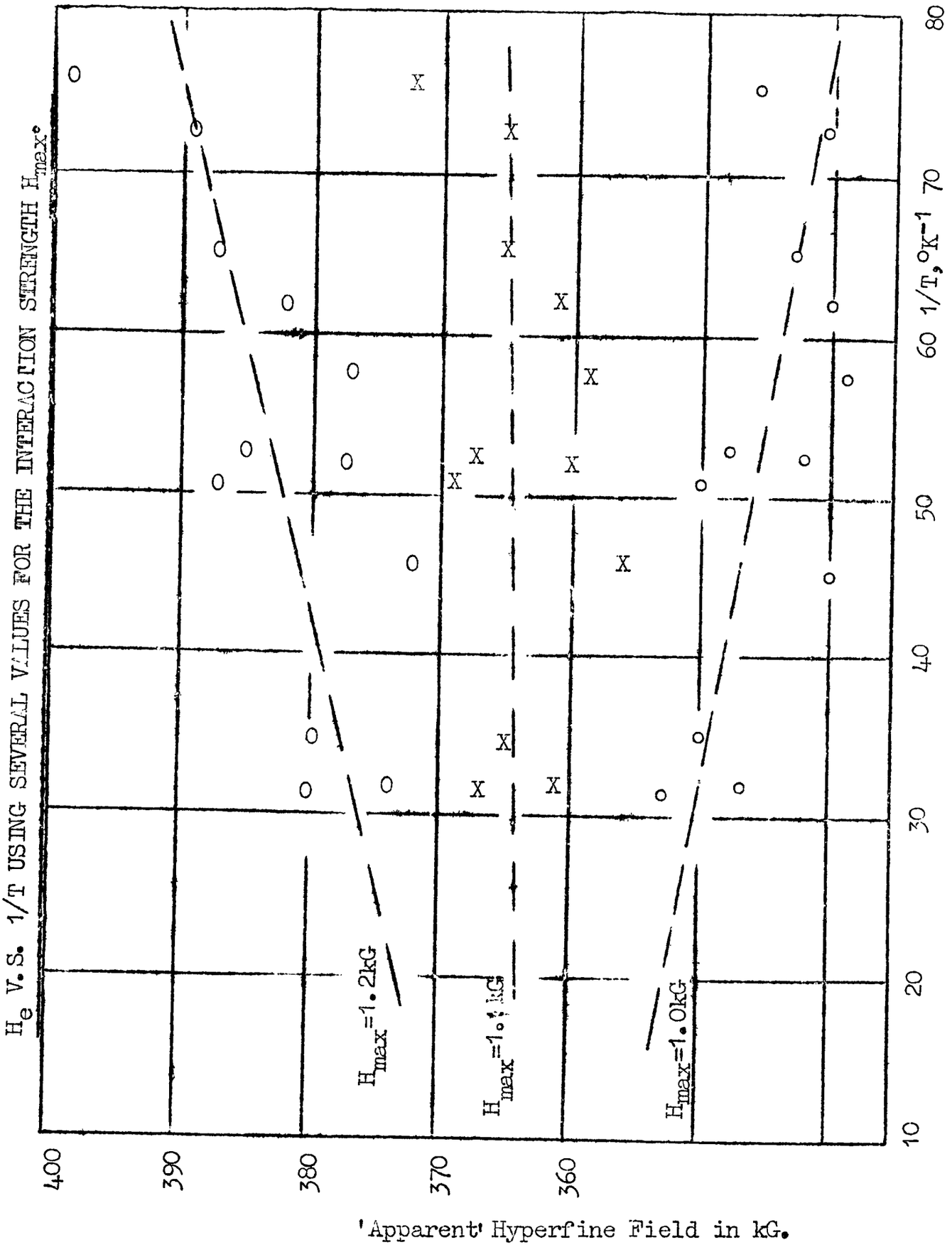

H_e V.S. 1/T USING SEVERAL VALUES FOR THE INTERACTION STRENGTH H_{max}.
H_{max}=1.2kG
H_{max}=1.1kG
H_{max}=1.0kG
400
390
380
370
360
10
20
30
40
50
60
70
80
1/T, °K⁻¹
'Apparent' Hyperfine Field in kG.

Figure VI.8.

Table VI.2.

H_e values: ^{54}Mn in Pd (melted).

H_{max} \ H_a	5.4kG	1.1kG	0.54kG
1.5kG	371kG	451kG	556kG
1.4kG	369kG	428kG	514kG
1.3kG	368kG	404kG	481kG
1.2kG	367kG	384kG	451kG
1.1kG	366kG	365kG	419kG
1.0kG	365kG	346kG	391kG
no. of points	27	12	1

H_{max}= 1.1±0.1kG; H_e= 366±20kG.

Table VI.3.

H_e values: ^{54}Mn in Pd (diffused).

H_{max} \ H_a	4.3kG	3.2kG	2.1kG	1.1kG	0.54kG
1.0kG	365kG	364kG	377kG	458kG	645kG
0.6kG	362kG	359kG	360kG	373kG	454kG
0.5kG	360kG	356kG	357kG	362kG	403kG
0.4kG	359kG	355kG	355kG	352kG	368kG
0.3kG	359kG	354kG	354kG	346kG	342kG
0.2kG	358kG	353kG	353kG	341kG	326kG
no. of points	3	4	5	4	8

H_{max}= 0.4±0.1kG; H_e= 356±10kG.

(Errors quoted include all sources and the hyperfine field values given have been corrected for the applied field assuming the positive sign measured in §VI.7.)

magnetic field during the experiment or using a conventional magnet or a superconducting magnet wound from type I wire are planned to obtain more reliable low field data.

In the calculation of the above attenuation factors we did not consider the case of very small resultant fields, when the electronic moments are incompletely aligned. If the hyperfine field is proportional to the net magnetisation which itself follows a Brillouin function dependence on temperature and the resultant magnetic field, then the expression for the anisotropy involves quite complicated integrals, e.g.

$$\overline{W(0)} \rightarrow (1/4\pi)\sum_{\nu} U_\nu F_\nu \int_0^{2\pi}\int_0^{A}\int_0^{\pi} B_\nu \left[\mu_n H_e \left(\sum_{m_j} m_j e^{-m_j \Delta E/kT} \right)/kT \sum_{m_j} e^{-m_j \Delta E/kT} \right] \cdot P_\nu(\cos\phi) \sin\theta \, d\theta \, da \, d\psi \qquad \ldots\ldots\ldots \text{VI.8.}$$

where $\Delta E = 2\mu_b |H_a| (1 + a^2 + 2a\cos\theta)^{\frac{1}{2}}$; $\cos^2\phi = (\cos\theta + 1/a)^2 / (1 + 1/a^2 + 2\cos\theta/a)$

and these have not yet been calculated. The anisotropy will be further attenuated only in the region where $H_a \sim -H_1$ and this attenuation will become more important as the applied field itself is reduced; thus for this reason also, less weight must be given to the low field data in tables VI.2 and VI.3.

VI.7. The Sign of the Hyperfine Field (^{54}Mn in Pd).

The sense of the circular polarisation of the gamma radiation from ^{54}Mn nuclei aligned in palladium was measured using the equipment described in chapter IV and compared with the same for the ^{60}Co nucleus in iron. The data is summarised in table VI.4. We can see that the signs of the products μH_e for both nuclei must be the same; the nuclear moments are both known to be positive and the hyperfine field at ^{60}Co nuclei in Fe is known to be negative; hence we may deduce the hyperfine

Table VI.4.

H_a	$C(^{54}Mn)$	$C(^{60}Co)$
+5kG	0.982±0.007	0.992±0.004
-5kG	1.004±0.003	1.010±0.003
+5kG	0.996±0.003	0.987±0.004
-5kG	1.010±0.005	1.004±0.002
+5kG	0.991±0.005	0.988±0.002
-5kG	1.007±0.009	1.011±0.002

(C = counting rate when polarimeter field is negative / ditto positive.)

field at ^{54}Mn nuclei in palladium metal also to be negative, and the values of H_e quoted in tables VI.2 and 3 have been corrected accordingly for the applied field.

VI.8. Further Discussion and Conclusion.

a. The Hyperfine Field. We have determined the hyperfine field at the nuclei of fully saturated ^{54}Mn ions dissolved in palladium metal to be

$$H_e(^{54}Mn \text{ in Pd}) = -361 \pm 15 kG.$$

for two samples to within the experinental accuracy, the principal magnetic impurity contents being ~1000ppm Fe in both samples.

It is expected that the manganese atom gives up two electrons to the conduction band in palladium; the hyperfine field at an isolated Mn^{2+} ion is known to be -650kG (see §I.3) so this value is consistent with a conduction electron contribution of ~+300kG. This quantity has the sign expected though no theoretical estimate of its magnitude is available.

b. The Random Interaction. We have fitted the anisotropy data for $^{54}MnPd$ to theoretical curves by assuming an interaction between the Mn

electronic moments which is expressible as a magnetic field, is randomly directed, and whose magnitude has a 'square wave' distribution i.e. has equal probability of being anything from zero to a cut-off value. For the two samples the values of the cut-off field were determined to be

$\underline{\underline{H_{max} = 0.4 \pm 0.1 kG}}$ - principal impurity 1000ppm Fe.

$\underline{\underline{H_{max} = 1.1 \pm 0.1 kG}}$ - principal impurity $>$1300ppm Fe.

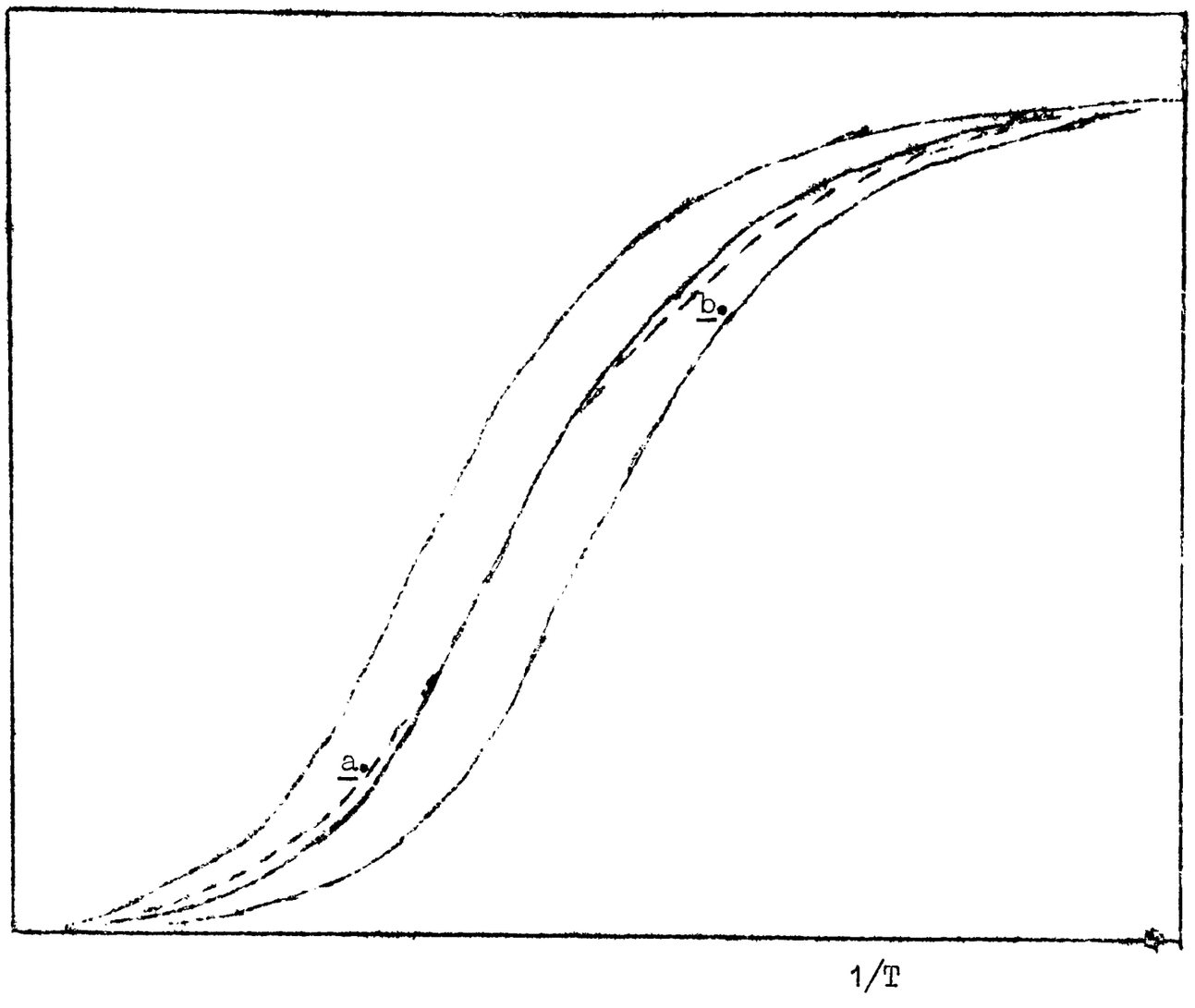
Kitchens et Al. (1965)[122] have also interpreted in terms of electronic 'interactions' the observed temperature dependence of hyperfine fields at ^{57}Fe nuclei in noble metals containing between 10 and 1000ppm Fe. Their data was obtained using the Mössbauer effect (actual hyperfine field at nuclei unambiguously measured) and the interaction strength was determined from the deviations of the hyperfine field from a Brillouin function dependence upon H_a/T and was expressed in temperature units s. The interaction strengths were in the range $s/\mu = \sim(1 \rightarrow 4)/\mu_b$ which is equivalent to interaction fields between 14$\rightarrow$55kG (using the relation $H_1 = ks/\mu$) - nearly two orders of magnitude larger than the interactions observed here in dilute FePd alloys. Kitchens et Al. did not observe any interactions between iron ions in very dilute FePd alloys and this can be explained by assuming our values of $\sim$1kG were below the limit of sensitivity of their data. However the degree to which our results may be compared with the Mössbauer data is in some doubt; in two alloys of copper containing nominally 200ppm and 1000ppm Fe respectively Kitchens et Al. observed an identical interaction field $\sim$50kG whereas Compton[66] using the technique of nuclear orientation observed an interaction field of $\sim$1kG between manganese ions dissolved in copper containing 80ppm Fe. (It should be borne in mind that the values for the hyperfine field at the ^{57}Fe nucleus in the two copper samples were quite small, $\sim$-40kG, and just failed to agree to within the experimental error, and that the

applied fields used limited the values of the total hyperfine field to the range -40 → +20kG; the hyperfine field at the manganese nuclei in copper was ∿-280kG.) This discrepancy in interaction strengths would seem too large to be explained by a temperature-dependent interaction and indeed considerable effort has gone into explaining the apparently concentration-independent Mössbauer data in terms of a 'spin density wave' ground state for copper, the iron ions interacting with the spin density waves[123].

Re-interpretation of the Mössbauer and nuclear orientation data on the Fe-Cu system is presently being attempted[124], at least qualitatively, by assuming the analyses in terms of a simple interaction between the magnetic ions to be incorrect. The approach under consideration assumes that over some finite temperature range a 'spin compensated bound state'[125,126] forms, in which the conduction electron polarisation 'concentrates' about the magnetic ions, screening out their magnetic moments at large distances. This type of analysis receives some support from the fact that for both the Mössbauer and nuclear orientation data the temperature range of measurement was an order of magnitude below the 'interaction' temperature deduced. However, since the conduction electron polarisation in the MnPd and CoPd systems is parallel to the solute magnetic moments such an interpretation in our case may be ruled out.

A significant 'spread' in the hyperfine field values can lead to an apparent decrease in the 'observed' hyperfine field with decreasing temperature in a nuclear orientation experiment, as illustrated in fig. VI.9; we can estimate the possible spread in the value of the hyperfine field at the Mn nuclei in palladium from the line width of the ^{105}Pd nuclear magnetic resonance in pure Pd (9±2kG[90]) and from the Mössbauer spectra of ∿1% FePd alloys[113] in which line-broadening

EFFECT OF A 'SPREAD' IN TRUE H_e VALUES ON THE OBSERVED H_e.



The solid curves are W(0) v.s. 1/T for three equally spaced values of the hyperfine field H_e. The dashed curve is the mean value of W(0) v.s. 1/T from a system in which $\frac{1}{3}$ of the nuclei each experience one of three equally spaced values of the hyperfine field.

If one used the family of solid curves to analyze the data from a sample truly described by the dashed curve, then for points in the region a. a value of H_e higher than the mean value would be obtained, while for points in the region b. a value of H_e lower than the mean value would be obtained.

Figure VI.9.

compatible with a contribution of between 5 and 7kG to the hyperfine field at the ^{57}Fe nucleus due to one nearest neighbour iron atom was observed. Thus it would seem that any 'spread' in the hyperfine field at Mn nuclei in ~0.1% FePd would not be large enough to account for the observed temperature dependence. Of course, any 'apparent' temperature dependence caused by a 'spread' in H_e would not reduce with increasing H_a as does the temperature dependence observed.

It is likely that our alloys were magnetically ordered over the temperature range of measurement, though samples known to be ferromagnetic (CoPd - see chapter VII) have proved much more difficult to saturate magnetically, applied fields $\gtrsim$15kG being necessary for alloys for which $T_c \gtrsim 1^{\circ}K$; as already described it was unfortunate the palladium metal from which the samples were made proved to be so heavily contaminated. However, since the ferromagnetic transition is not the simple co-operative phenomenon which occurs in pure iron, see specific heat measurements[110] on FePd, the random interaction analysis should still provide a valid viewpoint in this case.

The different 'saturation' behaviour of two ferromagnetic samples could arise from different demagnetizing factors, but the samples used were of approximately similar dimensions.

Our results may also be compatible with an impurity-impurity interaction, via e.g. the R-K-K-Y mechanism whose magnitude varies as $1/r_{ij}^3$ i.e. as the concentration.

A measurement of the impurity content of the melted sample as also study of a selection of similar, particularly more dilute, alloys varying in impurity content and measured in lower applied fields would render possible a more quantitative analysis of the interaction mechanism; the ^{54}MnPd system is particularly suited to this purpose

in view of the large anisotropy attained at easily accessible temperatures. Further experiments are proceeding along these lines.

Chapter VII.

^{60}Co in Palladium.

Contents:

VII.1. Sample Preparetion.

VII.2. Thermometry.

VII.3. Results.

VII.4. The Sign of the Hyperfine Field at ^{60}Co Nuclei in Palladium.

VII.5. Discussion.

VII.6. Conclusion.

Figures:

VII.1. Variation with Temperature of 'Apparent' Hyperfine Field at ^{60}Co Nuclei in Palladium (diffused).

VII.2. Variation with Temperature of 'Apparent' Hyperfine Field at ^{60}Co Nuclei in Palladium (melted in H_2 and N_2).

VII.3. Variation with Temperature of 'Apparent' Hyperfine Field at ^{60}Co Nuclei in Palladium + 0.002Co.

VII.4. Variation with Temperature of 'Apparent' Hyperfine Field at ^{60}Co Nuclei in Palladium + 0.0005Co.

VII.5. Approach to 'Saturation': ^{60}Co in Palladium + 0.0005Co.

VII.6. Variation with Temperature of 'Apparent' Hyperfine Field at ^{60}Co Nuclei in Palladium (diffused) at High $H_{applied}$.

We report in this chapter experiments using the technique of nuclear orientation on ^{60}Co nuclei in various CoPd alloys.

VII.1. Sample Preparation.

Two samples of very dilute ^{60}Co in Pd were prepared in entirely different ways to check solubility (as in the case of MnPd alloys) though cobalt metal is known to be readily soluble in palladium at all concentrations. Also made were two samples containing sufficient cobalt to be ferromagnetic in the temperature range of measurement. All samples were prepared from the palladium wire used for the MnPd (melted) sample and from $^{60}CoCl_2$ in 0.1N HCl (activity 100→ 250 Curies/gmCo); spectroscopically pure stable cobalt was used for the more concentrated samples.

a. Melted Sample. The active solution was dried onto a flattened and etched piece of the palladium wire, reduced at 900°C, melted at 1600°C and cooled slowly to room temperature, all under an atmosphere of hydrogen. The ball of metal was then squashed, etched and annealed at 900°C under H_2; part of this sample was further annealed at 900°C under a continuously flushing atmosphere of nitrogen in order to drive out any absorbed hydrogen. From the activity of this sample a cobalt content of $\sim$2ppm Pd was estimated.

b. Diffused Sample. This sample was prepared in the same way as the melted sample up to the reduction of the chloride under a hydrogen atmosphere at 900°C. The activity was then diffused into the metal at 1200°C for 18hrs under vacuum ($< 10^{-3}$mmHg) (vacuum work kindly performed by I. Bowers of the Metallurgy Lab., Oxford) then the sample was quenched to room temperature and thoroughly cleaned to remove surface activity. Estimated cobalt content was $\sim$1ppm Pd.

c. Ferromagnetic Samples. Sufficient cobalt to make a 0.002CoPd

sample was melted, together with a piece of palladium coated with the active solution, under a hydrogen atmosphere at 1600°C. This sample was later diluted by melting with three parts of palladium metal to form a 0.0005CoPd alloy.

None of these ^{60}CoPd samples has yet been analyzed spectroscopically; however, the palladium wire from which all were made was analyzed by C.S.I.R.O. (Australia) and found to contain 1300ppm Fe. As for the MnPd samples, this analysis only became available long after the experiments were completed, and it had been intended that the magnetic impurity content be well below that known to cause magnetic ordering.

VII.2. Thermometry.

An alloy of 0.1% FeCu containing ^{54}Mn activity was used as the thermometer throughout the work reported herein on the CoPd alloy system, since the degree of anisotropy v.s. temperature and applied field was roughly similar for both systems. The copper alloy was calibrated against ^{60}Co in Fe and results showed the typical temperature-dependent trend of the hyperfine fields reported herein for both ^{54}Mn and ^{60}Co in Pd[127].

VII.3. Results.

Anisotropy data from the two very dilute samples was corrected for background, overlap and pile-up (see chapter III) then analyzed using the unattenuated eq. II.3. Figures VII.1 and 2 respectively show the experimental points for the diffused sample, and for the melted sample before and after annealing in N_2, for various applied fields (no correction made for applied field). The data for both samples (annealed in H_2) in H_a = 5.4kG can be seen to agree to within the experimental error. Unfortunately the maximum applied field available for the nitrogen-annealed sample was 4.3kG and the lowest temperature ~0.02°K, owing to a temporary malfunctioning of the cryostat; however in spite of this

VARIATION WITH TEMPERATURE OF 'APPARENT' HYPERFINE FIELD AT ^{60}CoPd (DIFFUSED).
'Apparent' Hyperfine Field in kG.
1/T, °K⁻¹ °
160
140
120
100
80
60
40
10
20
30
40
50
60
70
80
90
X H_a = 5.4kG.
O H_a = 4.3kG.
x H_a = 3.2kG.
o H_a = 2.1kG.
Y H_a = 1.1kG.
H H_a = 0.54kG.

Figure VII.1.

VARIATION WITH TEMPERATURE OF 'APPARENT' HYPERFINE FIELD AT ^{60}CoPd (melted in H_2, annealed in N_2).

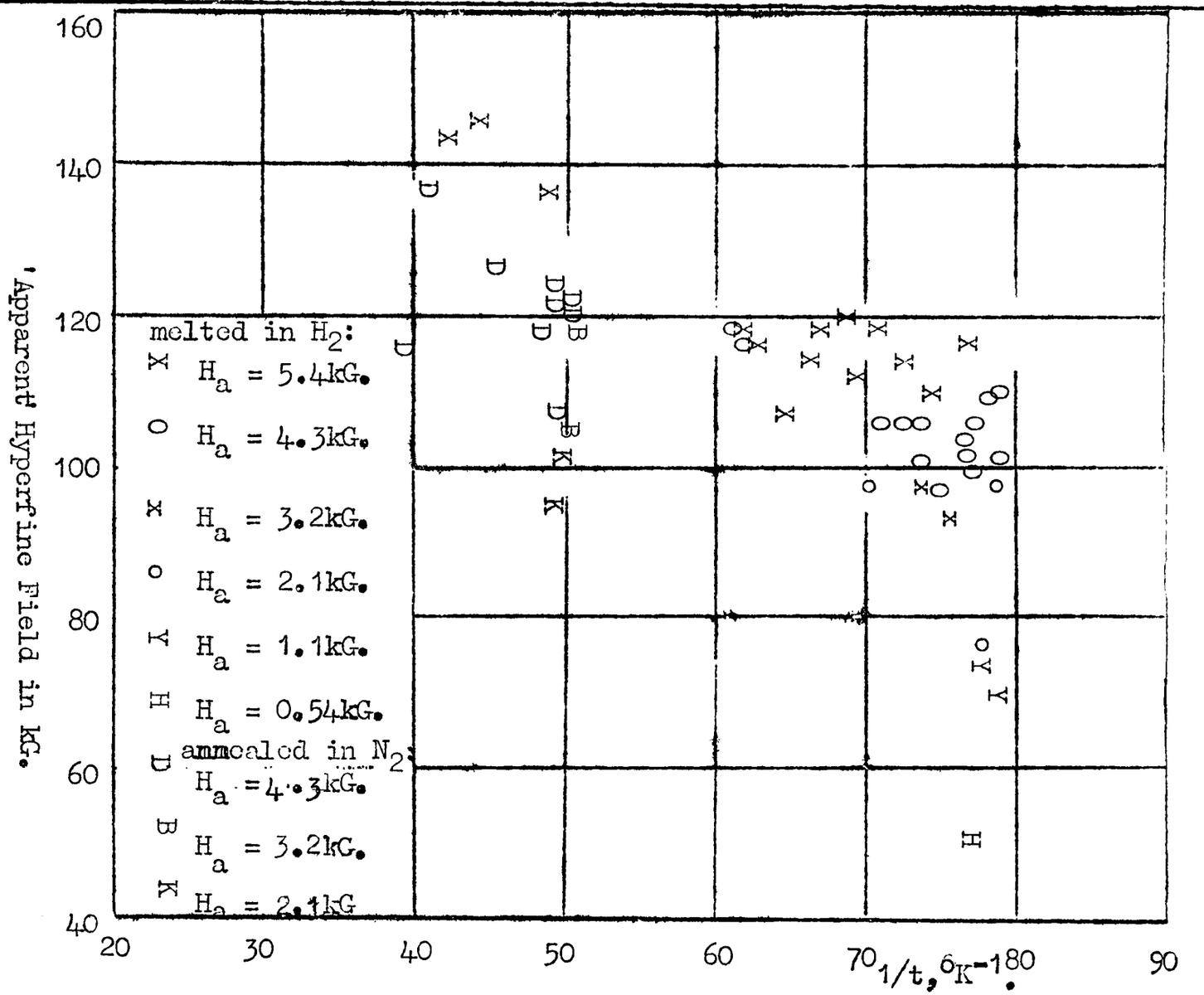


Figure VII.2.

drawback the data from the sample annealed in N_2 follows the general trend of that from both the other samples rendering consideration of the hydrogen content unecessary. The observed reduction in the gamma radiation intensity emitted axially by the ^{60}Co nucleus in pure palladium was always less than 10% which limited the accuracy attainable, particularly for the H_e values in low applied fields. All 'apparent' hyperfine field values at a constant applied field decrease with decreasing temperature and for a constant temperature decrease with decreasing applied field - both trends as observed in the MnPd data. Accordingly the anisotropy data was re-analyzed for various cut-off values H_{max} of a 'square-wave' distribution in random fields as described in chapter VI and the results are given in tables VII.1 and 2 (data corrected for applied field assuming H_e positive - see § VII.4).

Table VII.1.

H_e values: ^{60}CoPd (diffused).

H_{max} \ H_a	5.4kG	4.3kG	3.2kG	2.1kG	1.6kG	1.1kG	0.54kG
1.0kG	110kG	111kG	112kG	104kG	104kG	102kG	105kg
1.1kG	110kG	112kG	113kG	105kG	106kG	106kG	109kG
1.2kG	111kG	112kG	113kG	106kG	107kG	109kG	115kG
1.3kG	111kG	112kG	114kG	107kG	110kG	113kG	119kG
1.4kG	111kG	113kG	114kG	108kG	112kG	117kG	121kG
1.5kG	111kG	113kG	115kG	109kG	114kG	120kG	129kG
no. of points	34	8	1	2	2	3	2
Av. 1/T	$63^{o-1}K$	$48^{o-1}K$	$68^{o-1}K$	$68^{o-1}K$	$59^{o-1}K$	$63^{o-1}K$	$62^{o-1}K$

$H_e = 112 \pm 10$kG; $H_{max} = 1.4 \pm 0.2$kG.

Table VII.2.

	H_e values: ^{60}CoPd (melted).					
H_{max} \ H_a	5.4kG	4.3kG	3.2kG	2.1kG	1.1kG	0.54kG
1.0kG	117kG	104kG	94kG	93kG	85kG	79kG
1.1kG	117kG	104kG	95kG	94kG	88kG	82kG
1.2kG	117kG	105kG	95kG	95kG	91kG	86kG
1.3kG	117kG	105kG	96kG	96kG	94kG	88kG
1.4kG	117kG	105kG	96kG	97kG	97kG	92kG
1.5kG	118kG	106kG	97kG	98kG	100kG	96kG
no. of points	9	16	2	3	2	1
Av. 1/T	68°	$73^{\circ}K^{-1}$	$75^{\circ}K^{-1}$	$76^{\circ}K^{-1}$	$78^{\circ}K^{-1}$	$77^{\circ}K^{-1}$

$H_e = 107 \pm 10$kG; $H_{max} > 1.5$kG.

Thus the hyperfine field at the ^{60}Co nucleus in pure palladium was found (after the 'square-wave-distribution random field' analysis) to be $H_e = 110 \pm 8$kG, roughly a factor of two smaller than the value of 213 ± 5kG found for the n.m.r. of the ^{59}Co nucleus in (ferromagnetic) alloys of palladium containing 2, 1 and 0.5% Co at $4.2^{\circ}K$[128]. This was a little worrying, so the CoPd samples containing 0.2% and 0.05% stable cobalt were prepared and their ^{60}Co nuclei oriented to check agreement with the n.m.r. results. The first sample, containing 0.002Co, proved impossible to saturate in applied fields up to 15kG - see fig. VII.3 - and so was diluted by 1:3 parts Pd and the results for the hyperfine field in this 0.0005CoPd sample are given in fig. VII.4. (The data in figs. VII.3 and 4 has not been corrected for the applied field.) Notice the temperature dependence of the 'apparent' hyperfine field is less in the more dilute sample as one would expect for the approach to saturation. By taking the 'apparent' hyperfine field

VARIATION WITH TEMPERATURE OF 'APPARENT' H_e AT ^{60}Co IN Pd + 0.002Co.

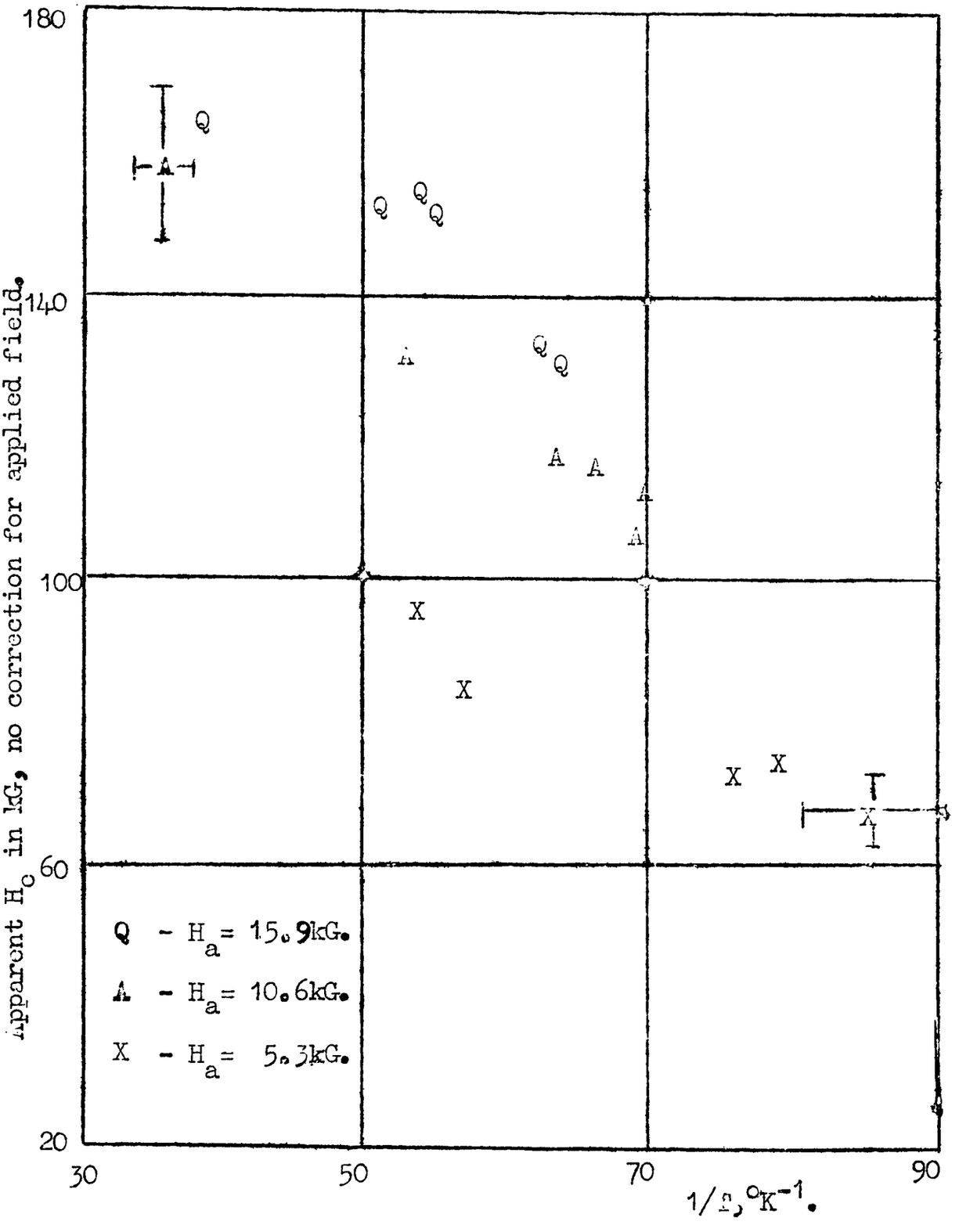


Figure VII.3.

VARIATION WITH TEMPERATURE OF 'APPARENT' H_e AT ^{60}Co IN Pd + 0.0005Co.

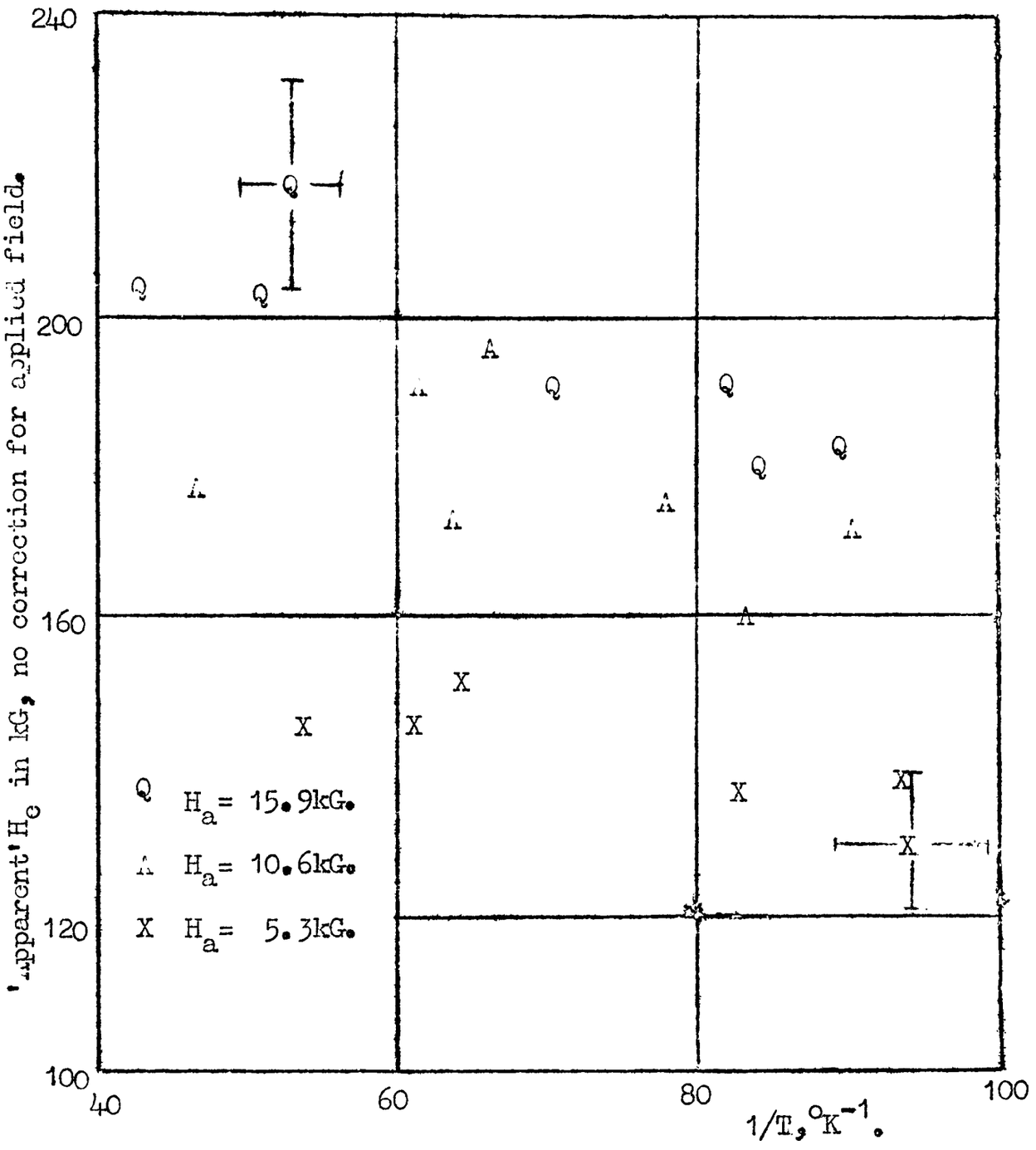


Figure VII.4.

values for the 0.0005CoPd sample at 1/60th°K (0.017°K), subtracting the applied field (see §VII.4) and plotting the resulting values against the applied field it can be shown that the 'apparent' hyperfine field approached assymtotically the value 200±20kG - see fig VII.5- , which is in agreement with the n.m.r. value of 213±5kG.

The ^{60}Co (diffused) sample was also measured in applied fields up to 15kG and the results are shown in fig VII.6 together with (for comparison) some data taken using the smaller superconducting magnet. These 'apparent' hyperfine field values are consistent, to within experimental errors, with the value obtained earlier for the hyperfine field, H_e = 110±8kG, as can be seen from table VII.3.

Table VII.3.

H_e+H_a	H_a	H_e
131±6kG	15kG	116±6kG
127±7kG	10kG	117±7kG
120±12kG	5kG	115±12kG
mean value 116±10kG		

(Errors quoted include all sources.)

VII.4. The Sign of the Hyperfine Field at ^{60}Co Nuclei in Palladium.

The sense of the circular polarisation of gamma radiation emitted by the ^{60}Co nuclei aligned in the melted palladium and 0.002CoPd samples was measured as described in chapter IV and compared with that from ^{60}Co nuclei aligned in iron. The results are given in table VII.4.

It can be seen that the sense of circular polarisation of the gamma radiation from the ^{60}Co nuclei in both palladium alloys was opposite to that from ^{60}Co nuclei in iron and so we are forced to conclude that the hyperfine fields at cobalt nuclei in CoPd alloys

APPROACH TO SATURATION: ^{60}Co in (Pd + 0.0005Co).

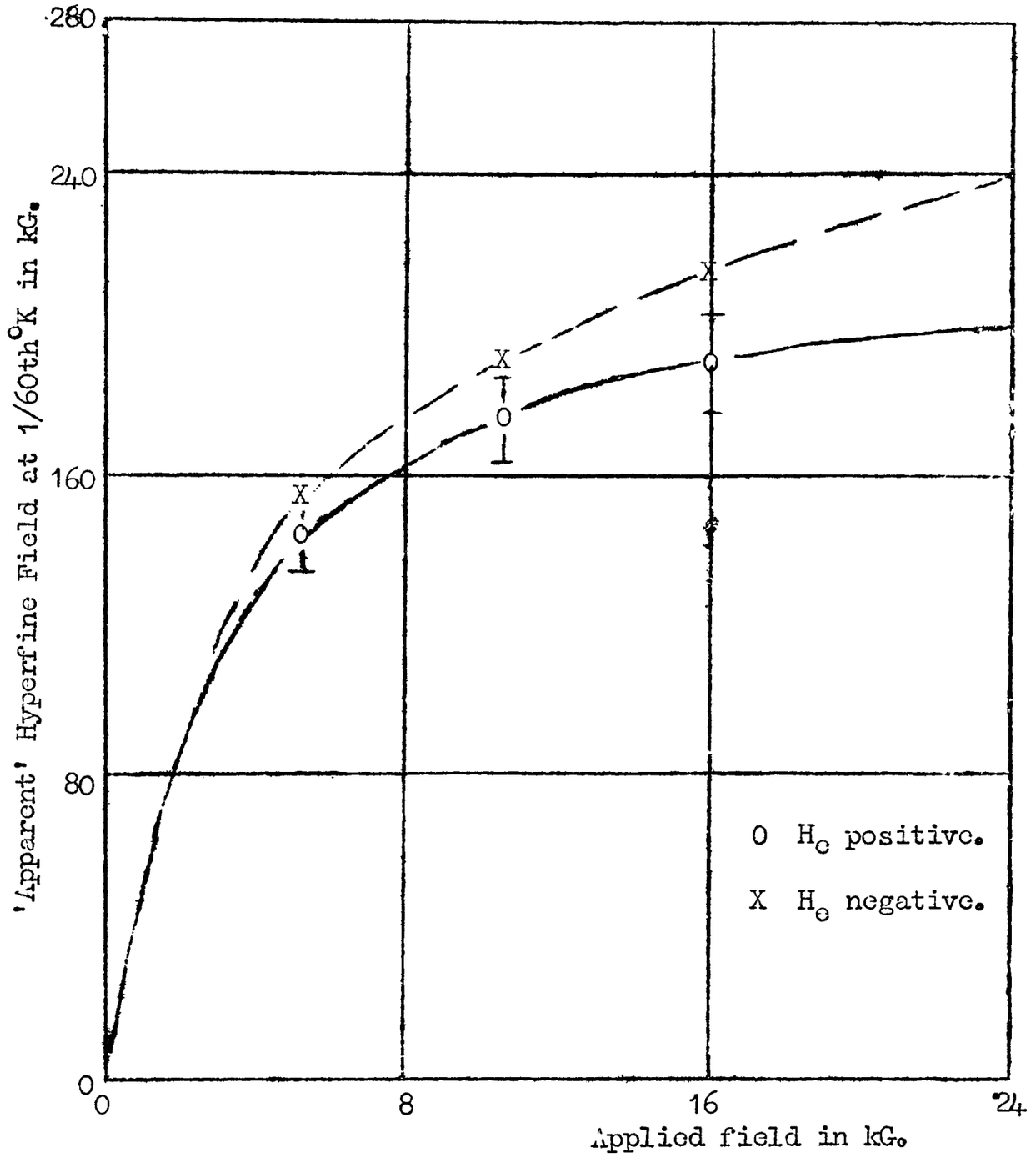


Figure VII.5.

VARIATION WITH TEMPERATURE OF 'APPARENT' H_e AT ^{60}Co IN Pd(diffused).

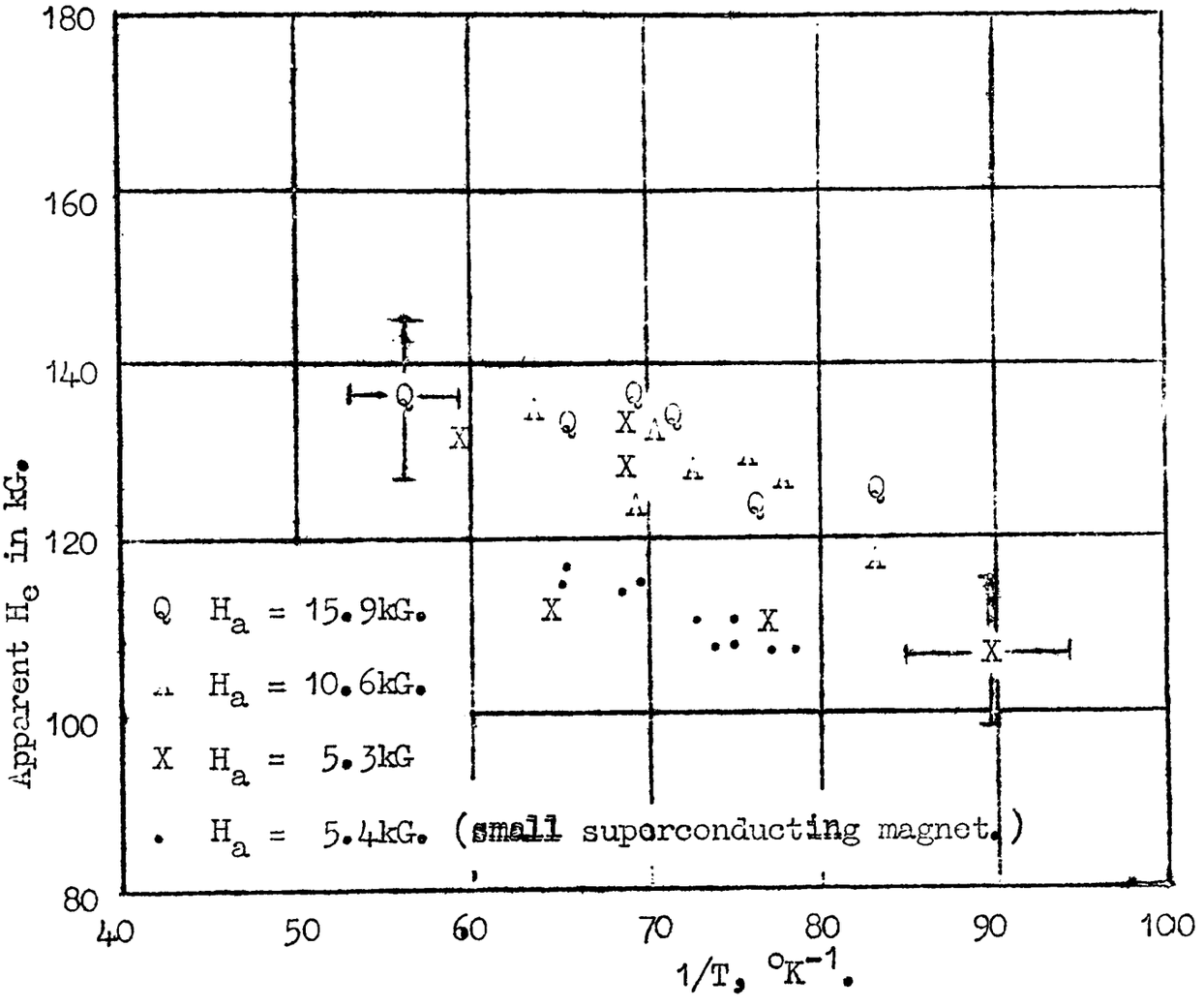


Figure VII.6.

Table VII.4.

H_a	$C(^{60}CoFe)$	$C(^{60}CoPd)$ (melted)	$C(^{60}Co + 0.002CoPd)$
+5kG	0.992±0.004	1.010±0.004	1.005±0.004
-5kG	1.010±0.003	0.986±0.004	0.991±0.004
+5kG	0.987±0.004	1.005±0.004	1.005±0.004
-5kG	1.004±0.002	0.986±0.004	0.993±0.004
+5kG	0.988±0.002	1.001±0.004	1.004±0.004
-5kG	1.011±0.002	0.989±0.004	0.991±0.004

C = counting rate when polarimeter field is negative / ditto positive.

---

are positive - a somewhat unexpected and unusual result. These circular polarisation measurements were repeated some months later on the $^{60}CoFe$ and $^{60}CoPd$ (melted) samples by J.G.Gallop and led to the identical conclusion.

VII.5. Discussion.

a. The sign of the hyperfine field. The saturation values of the hyperfine fields at ^{60}Co nuclei in iron and cobalt are large (290kG and 226kG respectively) and negative; hence the result obtained herein of a large positive hyperfine field at ^{60}Co nuclei in palladium is somewhat suprising and some doubt has been cast on the reliability of the circular polarisation measurement[129]. As mentioned above, this result was rechecked several months later by a different experimentalist to reduce the risk of human error, but using the same apparatus. No defect in the technique comes easily to mind and of course the expected negative hyperfine field was observed at Mn nuclei in palladium. For the CoPd alloys the anisotropy of the gamma radiation depended on the size of the applied magnetic field over the range of measurement ($H_a \sim 5kG$) whereas

the CoFe and MnPd samples were effectively saturated, their anisotropy being a function of temperature only. The applied field was the sum of the field due to the current passed through the superconducting magnet and the unknown field due to flux trapped in the superconducting wire during the demagnetisation of the paramagnetic salt - a process always carried out in the same sense for all the measurements herein - and of course only the current field was reversible. However, the measurements were taken by frequent reversal of the polarimeter's field, known to be negligible at the sample, and infrequent reversal of H_a, so no change with the polarimeter's field in the intensity of the radiation transmitted through the polarimeter could be attributed to such a remanent field.

The positive sign for the hyperfine field at ^{60}Co nuclei in the diffused palladium sample is consistent with saturation of this sample in applied fields ~5kG - see table VII.3. Also, a negative sign would destroy the agreement with the n.m.r. data of the saturation hyperfine field at cobalt nuclei in the 0.0005CoPd sample - see fig VII.6. Thus in the absence of any alternative experimental measurement for the sign of H_e at Co nuclei in CoPd we somewhat hesitantly accept the positive result and eagerly await the findings from n.m.r. in applied fields.

Craig et Al.[112] measured the Mössbauer spectra of ^{57}Fe in pure palladium over a range of temperatures and applied magnetic fields and found a value for the saturation hyperfine field at the ^{57}Fe nucleus of -295kG to be consistent with their data; the sign was not directly measured but was argued to be negative from the continuity in the magnitudes of H_e at ^{57}Fe nuclei in a series of CoPd alloys, the hyperfine field at ^{57}Fe in pure Co being known negative[130]. This large negative value is somewhat difficult to reconcile with the values of +110±8kG and +220±20kG found here at the ^{60}Co nucleus in CoPd alloys since from the other available information it seems these two alloy systems (FePd

and CoPd) behave in a similar fashion. The extra '3d' electron on the cobalt atom would have to cause a contribution of $\sim$+(400 to 500)kG to the hyperfine field; the sign of this contribution is in the expected sense, but of course if our result is spurious and H_e at Co nuclei in dilute CoPd is in fact negative, then the extra pairing core-electron contributes only $\sim$+(80 to 200)kG to the hyperfine field, which is again in the expected sense.

Our result is consistent with the otherwise somewhat puzzling n.m.r. spin echo intensity measurements of Kobayashi and Itoh (1965)[131] on Co nuclei in a series of CoPd alloys ranging over the full concentration. As palladium was added to cobalt the Co resonance was seen to decrease from 217Mc/s and to spread out and center about 140Mc/s for the 50% alloy; as the Pd content was further increased beyond 50%, another resonance appeared at 217Mc/s until at 99% Pd only this second resonance at 217Mc/s remained. Thus although the hyperfine field at Co nuclei in pure Co is known to be large and negative ($\sim$-220kG), this spin echo data precludes any 'continuity' arguments for the sign of H_e at Co nuclei in palladium.

b. The magnitude of the hyperfine field. The hyperfine field at the ^{60}Co nucleus in nominally pure palladium was measured to be +110 ±8kG and in palladium plus (nominally) 0.0005Co to be 200±20kG. The latter sample is expected to be in the ferromagnetic state below $\sim$0.5°K, and it was hoped the former samples remained paramagnetic to 0°K but the impurity content of 0.13%Fe in the palladium wire, measured long after completion of the experiments, indicated the likelihood these samples also were ferromagnetically ordered below $\sim$1°K. Attempts to have the magnetic susceptibility of both samples measured as a function of temperature by a colleague have so far failed. It is certain, however, that the transition ion concentration was less in the melted and diffused samples

than in the nominally 0.002Co and 0.005Co samples.

Neutron diffraction experiments on CoPd alloys [103] indicate that the magnetic moment on the Co ion site remains approximately constant but that the degree of conduction electron polarization varies with transition ion concectration and is parallel to the transition ions. Thus our results are consistent with a contribution of ~+100kG to the hyperfine field due to an increase in the conduction electron polarization with transition ion content, as long as the hyperfine fields are positive. It may be that the magnitude of the hyperfine field at ^{60}Co nuclei in palladium reduces gradually as the cobalt content of the alloy, and therefore the degree of conduction electron polarization, is reduced in the very dilute range of concentration. In this respect it is worth noting that the n.m.r. data of Ehara et Al. (1962)[128] in ferromagnetic 0.005CoPd, 0.001CoPd and 0.02CoPd samples showed a slight reduction ($\sim \frac{1}{2}\%$) in the magnitude of the hyperfine field as the cobalt content was reduced. Also Mössbauer data by Craig et Al. (1965)[132] showed the magnitude of the saturation hyperfine field at ^{57}Fe nuclei in a range of ferromagnetic FePd alloys to reduce with reducing iron content, the rate of change increasing with dilution to pure Pd; however, in the FePd case the hyperfine field is believed to be negative, so this would require the degree of conduction electron polarization in FePdto increase with decreasing iron content.

Preliminary results using the technique of nuclear orientation on ^{60}Co nuclei in a 0.003CoPd alloy have been reported by Alekseevskii et Al. (1966)[133]; however entirely different results were obtained. In particular they found the hyperfine field at the ^{60}Co nuclei in 0.003CoPd in an applied field of 5.7kG to be 260±20kG, whereas we found a 0.002CoPd sample impossible to saturate using applied fields ~15kG and the 'apparent' hyperfine field in an applied field of 5.4kG was only

$\sim$100kG. This discrepancy may be intrinsic to the CoPd alloy system, but is more likely due to the small anisotropy (lowest T $\sim 0.033^{\circ}K$) coupled with indirect thermometry (susceptibility of the cooling salt) involved in Alekseevskii et Al!s data.

There is still apparent in the high applied field data for the diffused 'paramagnetic' CoPd sample a slight temperature dependence of the hyperfine field, although this sample seems to be well saturated at Ha$\sim$5kG; this could result from an appreciable 'spread' in the values of the hyperfine field at cobalt nuclei in pure paramagnetic palladium as illustrated in fig VI.9, although such a spread would obviously have to range over $\sim \pm$50kG to describe the experimental results. The slight temperature dependence in fig VII.6 may anyway be within the combined statistical and systematic errors, remembering that the thermometer itself (^{54}Mn in Cu+0.001Fe) showed a temperature dependence of H_e which was averaged over the available calibration data in order to analyze the ^{60}CoPd results.

c. The interaction strengths. For the dilute alloys the interaction strengths were determined to be 1.4$\pm$0.2kG and $>$ 1.5kG, corresponding to interaction temperatures $\gtrsim 0.5^{\circ}K$, i.e. well above the temperatures at which the measurements were taken as in the MnPd alloys. As already discussed, owing to circumstances beyond our control, the impurity content of the initial palladium metal was such that these estimates of the interaction strength may well indicate the samples to be magnetically ordered over the temperature range of measurement. It is interesting that the concentrated alloys, known to be ferromagnetic over the temperature range of measurement, showed a temperature dependence of the 'apparent' hyperfine field similar to the dilute alloys. These two concentrated alloys proved considerably more difficult to saturate than the familiar ferromagnets Fe (sat. $H_a \sim$ 2kG),

Co (sat. $H_a \sim 15$kG) and Ni (sat. $H_a \sim 5$kG) and the cause of this is not well understood; one possibility is a highly anisotropic crystalline structure and in this connection we note that Bagguley et Al.[134] observed a contribution to the ferromagnetic resonance linewidth in CoPd alloys which they attributed to crystal anisotropy effects. However, it may just be that the internal fields in these alloys, being much smaller than those in pure Fe, Co and Ni ($\gtrsim$ two orders of magnitude), are strongly affected by the applied fields used.

VII.6. Conclusion.

The anisotropy of the gamma radiation emitted by the ^{60}Co nucleus aligned in several CoPd alloys was measured as a function of temperature and applied magnetic field over the range $\sim$(0.03 to 0.011)°K and $\sim(\frac{1}{2}$ to 5)kG; also the sense of circular polarisation of the gamma radiation relative to the applied field axis was measured. The anisotropy data for all samples was first analyzed assuming the nuclear spin axis to have been parallel to the applied magnetic field and for all samples was found to be described by a magnetic field at the nucleus which decreased with decreasing temperature and which varied in magnitude with the cobalt concentration. The alloys containing an appreciable quantity of stable cobalt were known from other data to be in the ferromagnetic state where a well-defined hyperfine field $H_e = 213 \pm 0.5$kG acts on the cobalt nuclei, so it was assumed they were not magnetically aligned. In fact it was shown that the magnetic field values determined from the above analysis at a fixed temperature, when plotted against the applied field, approached assymptotically the value $+200 \pm 20$kG for applied fields greater than 20 kG.

The positive sign for the hyperfine field was deduced from a comparison between the sense of circular polarisation of the gamma

radiation from ^{60}Co nuclei aligned in the alloys and in pure iron.

The dilute alloys clearly behaved differently from the concentrated alloys in that the magnetic field values obtained from the above analysis approached asymptotically a saturation value of 110±8kG at applied fields $\sim$ 5kG. However it is believed these samples also were magnetically ordered in the temperature range of measurement, owing to contamination of the supplied pure palladium metal. Analysis of the data assuming a 'square-wave' distribution for the strength of the interaction between the Co ions yielded interaction temperatures of the order expected for any Curie temperature of the alloys. The difference of 100kG in the two hyperfine field values is attributed to a reduction in the degree of conduction electron polarization with dilution of the Co content of the CoPd alloys. Also, some evidence of a 'spread' in the hyperfine field values was apparent in the data from one dilute sample in applied fields well above 'saturation'.

To facilitate a more complete understanding of the CoPd alloy system, more experiments are necessary, particularly over a range of alloy concentrations in the very dilute ($<$0.001Co) region. A sample analysis prior to the arduous nuclear orientation experiments would greatly assist in accelerating the collection of pertinent data.

Chapter VIII.

Hyperfine Fields in Neutron Irradiated Cobalt.

Contents:

Introduction.

VIII.1. Special Features of the Cryostat.

VIII.2. Samples.

VIII.3. Parameters for Data Analysis.

VIII.4. Experimental Procedure.

VIII.5. Results.

VIII.6. Discussion.

VIII.7. Conclusion.

Figures:

VIII.1. Decay Scheme for ^{58}Co.

VIII.2. Axial v.s. Equatorial Data from ^{58}Co, Various Annealing Temperatures.

VIII.3. Axial Data for ^{58}Co v.s. Axial Data for ^{60}Co, Various Annealing Temperatures.

VIII.4. Isochronal Annealing of Thermal Neutron Damage in Irradiated Cobalt.

Introduction.

In this chapter we describe results somewhat different in character from those discussed in chapters V to VII. A single crystal of cobalt metal was irradiated at 4°K by thermal neutrons and the ^{60}Co nuclei so formed aligned statically; the object of this experiment was to obtain some information concerning the dynamics of radiation damage.

When stable ^{59}Co is irradiated with thermal neutrons the ^{60}Co nuclei formed in an excited state promptly decay to the ground state by emission of $\sim$5-6Mev gamma rays. This gives a recoil energy to the ^{60}Co nucleus of $\sim$300ev ($\equiv 2\times10^{6}$ °K) which is considerably larger than the binding energies of ions in solids, so radiation damage such as the formation of pairs of 'holes' and 'interstitials' (Frenkel pairs) generally occurs. The splitting of nuclear spin energy levels is sensitive to the local environment so annealing processes in solids may be studied via measurements of the anisotropy of the gamma radiation emitted during the decay of the ^{60}Co nucleus.

The nuclear orientation technique was first applied to the study of irradiation damage in a Tutton salt, $(Co_{0.1}Zn_{0.9})(NH_4)_2(SO_4)_2.6H_2O$, by Grace et Al.[135] in 1955 and later by Dagley and Chapman (unpublished 1960). The gamma radiation from decaying ^{60}Co nuclei in correct lattice sites in a single crystal of the Tutton salt exhibits considerable anisotropy because of the alignment of the radioactive nuclei with respect to the crystal axes, the crystalline anisotropy causing an 'effective magnetic field' $\sim$300kG to act at the cobalt nuclei in a direction dictated by the local symmetry. If irradiation is carried out below the temperatures at which annealing of defects occurs this local symmetry is destroyed and isotropic emission of the gamma radiation at all temperatures is to be expected. In fact after irradiation with

thermal neutrons at 90°K the ^{60}Co gamma radiation anisotropy at 0.03°K from a single crystal of the Tutton salt was only $\sim\frac{1}{2}\%$, and increased monotonically with annealing temperature to be $\sim$13% for 393°K - almost the full value. The very low anisotropy observed before annealing indicates that after recoil hardly any of the ^{60}Co nuclei occupied normal lattice sites and that the hyperfine fields on them were either very small or randomly oriented. Quantitative interpretation of the annealing curve for such a coupled system in terms of activation energies associated with each type of defect is not however feasible and experiments in simpler systems were suggested.

We describe here the results of similar experiments on a much simpler system, hexagonal cobalt in which each cobalt nucleus in a lattice site sees a field H_e = -226kG directed along the hexagonal axis.[136] This system was first suggested by C. Froidevaux in 1962. Since the annealing of point defects in metals becomes appreciable above $\sim$10→20°K (see resistivity measurements on irradiated metals) the irradiation was carried out at 4.2°K and the cryostat, described in chapter III, was specifically designed for this purpose (by I.A. Campbell).

VIII.1. Special Features of the Cryostat.

In order to minimise the attenuation of the thermal neutron beam and also minimise any induced background activity (i) the various jackets in the vicinity of the sample were made from high purity aluminium tubing, (ii) a plain aluminium 'cap' replaced the superconducting magnet, (iii) the top of the sample was soldered to the lower end only of the copper rod from the cooling salt and (iv) the neutron beam was collimated with cadmium sheet to avoid the copper rod, this being the item most susceptible to irradiation. The source of thermal neutrons was some 15 miles distant from the adiabatic demagnetisation and

counting equipment so the cryostat was also designed to be portable.

VIII.2. Samples.

In the absence of a superconducting magnet, single crystals of hexagonal cobalt had to be used and to measure the sample temperature sufficient ^{58}Co activity to minimise overlap corrections, etc., was diffused into the metal from which these crystals were grown by Metals Research Ltd. The gamma radiation from ^{60}Co has energy $\sim$1.3Mev while that from ^{58}Co has energy $\sim$0.8Mev so they are easily resolvable using NaI(Tl) scintillation counters. Unfortunately the ^{58}Co activity contained an appreciable ^{60}Co contamination, $\sim$10% on receipt, which multiplied proportionately during the time which elapsed ($\sim$2 half-lives of ^{58}Co) between its purchase and the actual irradiation. However by comparing spectra from the irradiated and some unirradiated crystals the fraction of ^{60}Co 'contamination' could be estimated; of course these ^{60}Co nuclei can be expected to occupy normal lattice sites even after the irradiation, as can all the ^{58}Co nuclei since their concentration was only $\sim 10^{-13}$ and comparable with the fraction of ^{60}Co nuclei formed during irradiation.

Several single crystals, all approx. $7.5 \times 2.5 \times 3.5 mm^3$, were cut from the 'melt' by spark machining, with their long sides parallel to the c-axis.

VIII.3. Parameters for Data Analysis.

a. ^{58}Co. The decay scheme of ^{58}Co is shown in fig. VIII.1, the 0.81 and 0.805Mev gamma rays being unresolved so monitored jointly. The 0.805Mev transition is pure electric quadrupole, 99.5% of all decays contributing to the observed intensity; 1.6% of all decays contribute to the 0.81Mev transition which is a mixture of magnetic dipole (M1) and

DECAY SCHEME FOR $^{58}_{27}Co$.

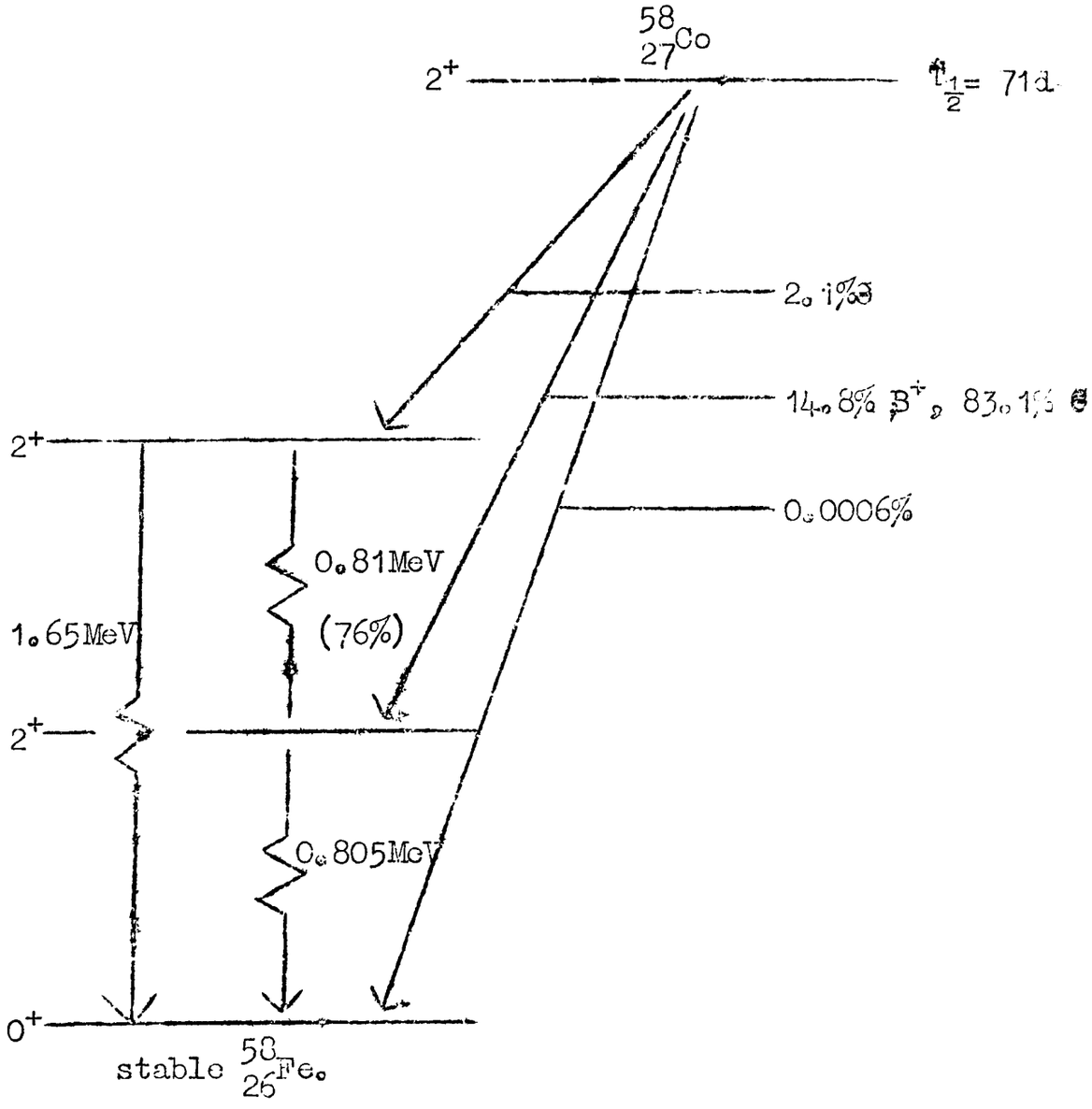


Figure VIII.1.

electric quadrupole (E2) radiation with mixing ratio[137]

$$\delta(E2/M1) = +2.2 \pm 0.3.$$

The beta decays are also mixed transitions with the mixing ratio for the transition to the 1.65Mev level of ^{58}Fe given by Δ_1 (=Amp.(δ L=1)/Amp.(δ L=0)) where[138]

$$1/(1+\Delta_1^2) = 0.45 \pm 0.11$$

and that to the 0.805Mev level of ^{58}Fe by Δ_2 where[139]

$$1/(1+\Delta_2^2) = -0.003 \pm 0.005.$$

Using these values we obtain for the non-zero parameters $U_\nu F_\nu(^{58}Co)$ in eq. II.3

$$U_2F_2 = -0.293 \pm 0.002 \text{ and } U_4F_4 = 0.693 \pm 0.010.$$

The magnetic moment of the ^{58}Co nucleus was determined from paramagnetic resonance to be 3.996 ± 0.011nm[140] relative to the value 4.583 ± 0.003nm for the ^{59}Co nucleus and the hyperfine field at Co nuclei in normal lattice sites was determined by n.m.r. to be -226kG[141] when extrapolated to 0°K.

b. ^{60}Co. These parameters are given in § II.4.

c. Closure Domains. In such short single crystals there may be an appreciable volume taken up by 'closure' domains and in these the hyperfine field will not be parallel to the long side. If all closure domains, constituting a fraction X of the total volume, are assumed to be magnetized perpendicularly to the long side and randomly oriented in their plane then the observed axial anisotropy W'(0) and observed equatorial anisotropy W'(90) are given by

$$W'(0) = (1-X)W(0) + XW(90)$$

$$W'(90) = (1-X)W(90) + X \qquad \ldots\ldots\ldots \text{VIII.1}$$

VIII.4. Experimental Procedure.

Two of the single crystals were mounted side by side on the copper rod with their long axes vertical, and cooled as in chapter III

to $\sim$0.015°K to check for thermal insulation, etc. The cryostat was then transported to the neutron beam at the face of BEPO reactor, A.E.R.E., Harwell, (neutron flux $\sim 2\times10^{7}$ neutrons cm^{-2} sec^{-1}) and the sample irradiated for 8 days. Daily refilling of the helium reservoir and $\sim$5hourly refilling of the nitrogen reservoir were necessary in order to maintain the sample temperature at 4.2°K throughout this period. After irradiation the cryostat, still containing liquid helium, was returned to the laboratory. Gamma spectra of the sample revealed some induced ^{64}Cu activity (half-life = 12.8h) and this was allowed to decay for $\sim$2 days before the nuclear orientation experiments proceeded.

Three 'runs' - counting for 3 to 4 hrs after demagnetization and again for $\sim$2hrs after warming up to 1.3°K - were made on the sample before warming it above 4.2°K, then one 'run' after $\sim\frac{1}{2}$ hr annealing at 20°K (data from another 'run' at this stage had to be abandoned due to appreciable drift in the H.T. supply), two 'runs' after 1 hr at 77°K and finally two 'runs' after annealing at 300°K for 36 hrs.

Cobalt has a large heat capacity below $\sim$0.1°K and cooling of the crystals was apparent for up to 1 hr after each demagnetisation.

VIII.5. Results.

After irradiation the ^{58}Co and ^{60}Co count rates were $\sim$80 and $\sim$40 cps respectively, but only 40±2% of the ^{60}Co activity was formed during irradiation.

Figure VIII.2 shows, using expanded scales with an offset origin, a plot of values of W'(90)-1 against 1-W'(0) for the ^{58}Co gamma radiation; the curves were obtained from eq. II.3 and VIII.1 for the fractional volume of closure domains X = 0, 0.05 and 0.1. The experimental points correspond to a temperature range from 0.014 to 0.02°K

AXIAL V.S. EQUATORIAL DATA FROM ^{58}Co, VARIOUS ANNEALING TEMPERATURES.

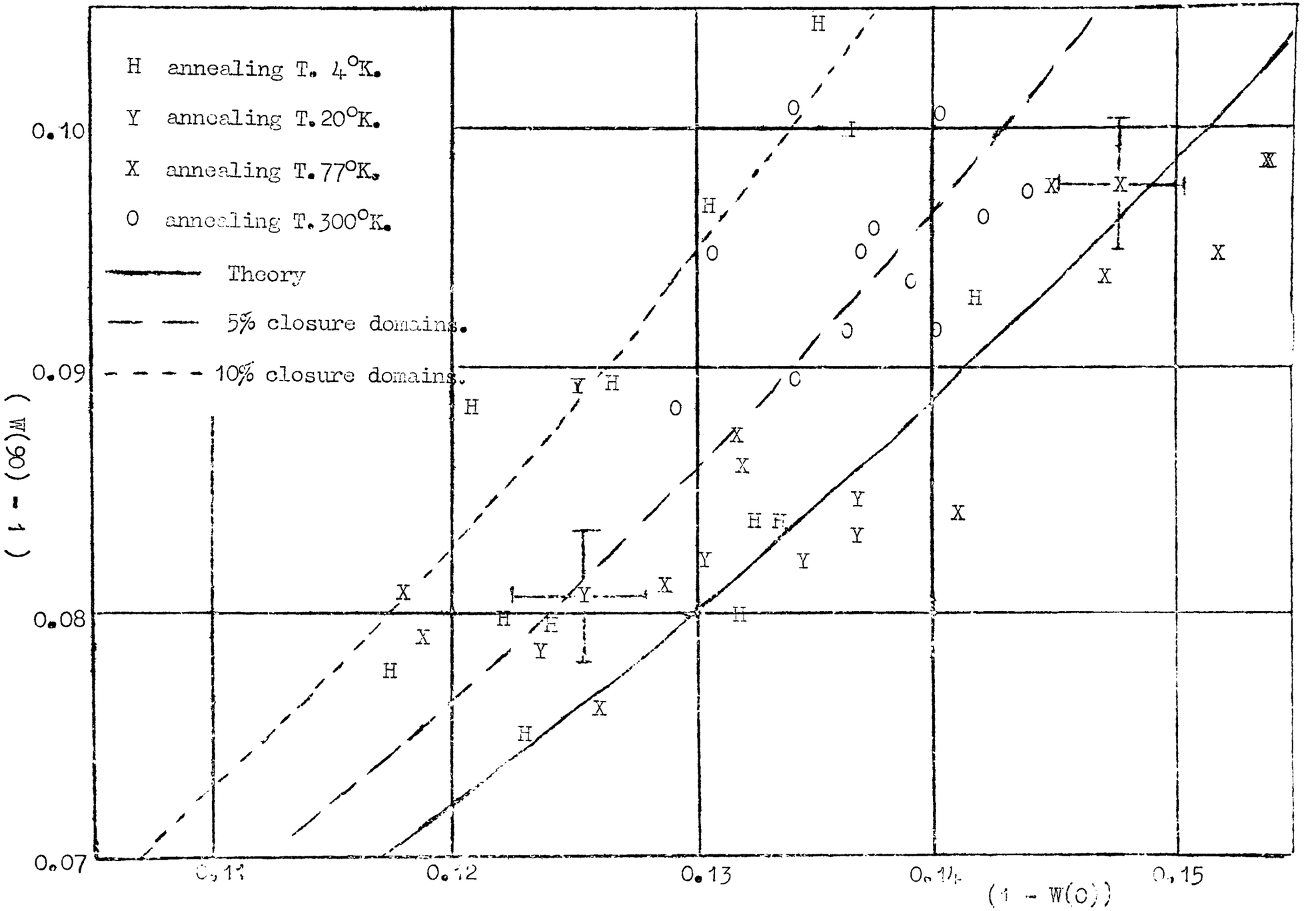


Figure VIII.2.

and each point represents 1600s of 'cold' counting time. A plot of the axial v.s. equatorial anisotropy of the ^{60}Co gamma radiation is not so sensitive to closure domains owing to the smaller U_4F_4 term. From fig VIII.2. we see that, using our simple model, 4±2% of the crystals consisted of closure domains.

Fig VIII.3 shows the values of $1 - W'(0)$ for ^{58}Co against the corresponding values for ^{60}Co, again with an offset origin. If the ^{60}Co nuclei formed during irradiation experienced a hyperfine field very much different from 226kG then the experimental points should deviate from the theoretical curves, drawn for 0 and 4% closure domains; however, there is clearly no appreciable difference between the results taken after the various annealing temperatures, to within the experimental accuracy.

Each quartet of 800s anisotropy measurements was analyzed as described in §§III.14 and III.16 to determine the hyperfine field at the ^{60}Co nuclei, assuming several possible values for the fraction of closure domains X, and the results are summarised in the table VIII.1.

Table VIII.1.

Mean Values of H_e for ^{60}Co.

X / Anneal. Temp.	0	0.02	0.04	0.06	uncertainty
4°K	231kG	228kG	226kG	223kG	±2kG
20°K	220kG	218kG	215kG	212kG	5.5kG
77°K	228kG	225kG	222kG	217kG	3.5kG
300°K	227kG	224kG	221kG	216kG	3kG

These results show that there can only be a small change, if any, in the hyperfine field on the ^{60}Co nuclei upon annealing and that the fraction of closure domains assumed does not affect this conclusion.

AXIAL DATA FOR ^{58}Co V.S. AXIAL DATA FOR ^{60}Co, VARIOUS ANNEALING TEMPERATURES.

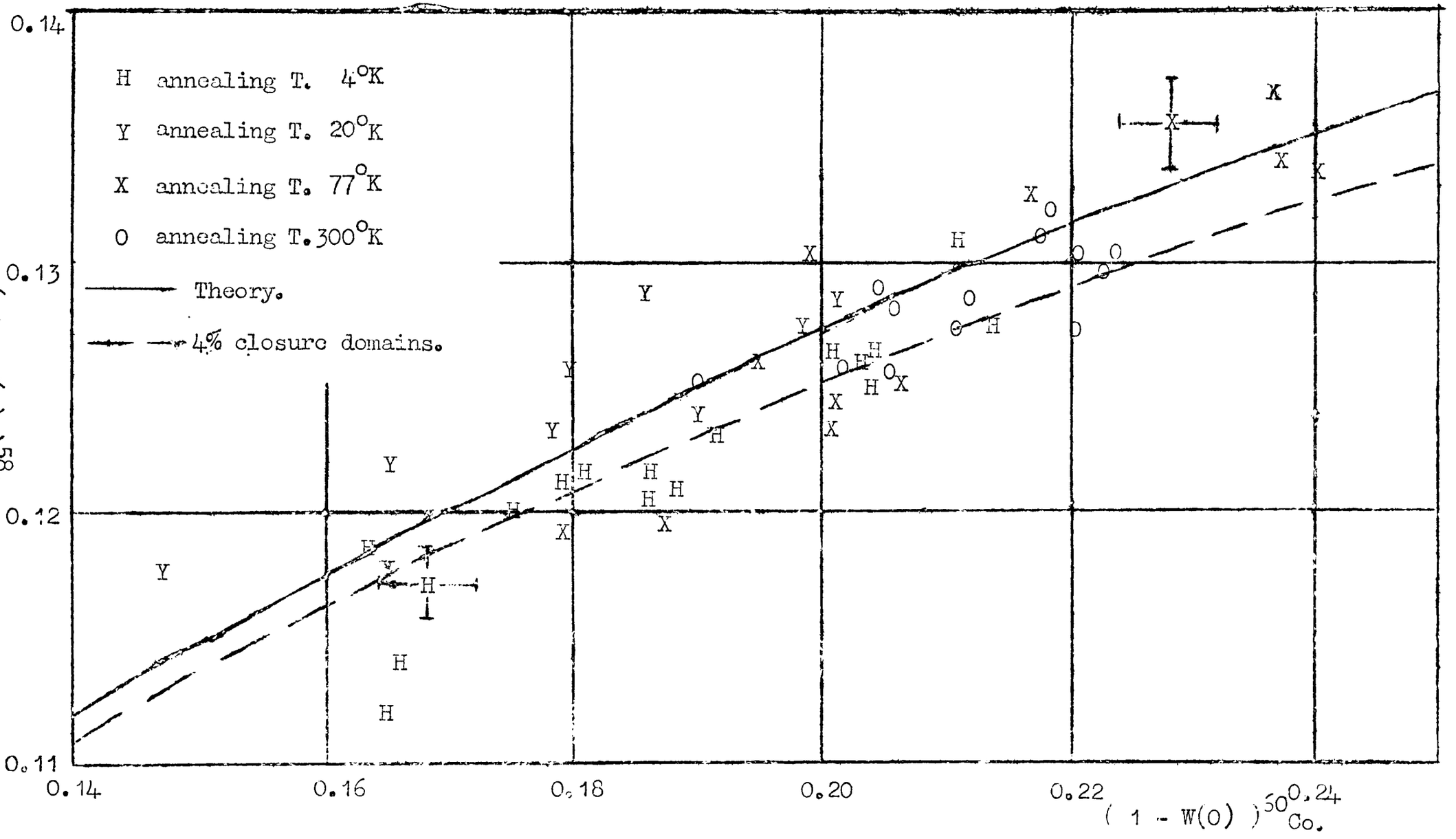


Figure VIII.3.

Comparing the H_e values for annealing temperatures of 4°K and 300°K, we see an increase of 4±3kG i.e. 2±1.5% in the average field on the ^{60}Co nuclei before annealing at 300°K. Since only 40% of the ^{60}Co nuclei were formed during irradiation at 4°K the change in hyperfine field on these nuclei before annealing at 300°K is +(5±3.8)% and is almost within our experimental errors.

VIII.6. Discussion.

Resistivity measurements on thermal neutron-irradiated cobalt by Coltmann et Al.[142] reveal considerable radiation damage which begins to anneal at temperatures ~10°K and is almost completely annealed at 300°K - see fig VIII.4; these results are consistent with thermal neutron damage in cobalt which is "uniform and simple and consists of a few Frenkel pairs per capture event". If the ^{60}Co atoms occupied interstitial positions after recoil then one would expect a large reduction in the observed hyperfine field before annealing due to destruction of the local symmetry, so this possibility can be ruled out. There remains then the question of whether the recoil atom has any nearest neighbour vacancies or interstitial atoms. We can obtain some indication of the change to be expected in the hyperfine field at a lattice site with a nearest neighbour vacancy from measurements on alloys of magnetic hosts containing non-magnetic impurities. Mössbauer measurements by Wertheim et Al. (1964)[143] and by Stearns (1966)[144] on iron containing aluminium, manganese or silicon were consistent with a reduction of 8% in the hyperfine field at an iron nucleus having a nearest neighbour non-magnetic atom, a reduction of 4% for a non-magnetic next n.n. and an increase of ~2% for a non-magnetic third nearest neighbour. Nuclear magnetic resonance measurements in cobalt-based alloys by Itoh et Al. (1964)[145] also gave a reduction of 8% in

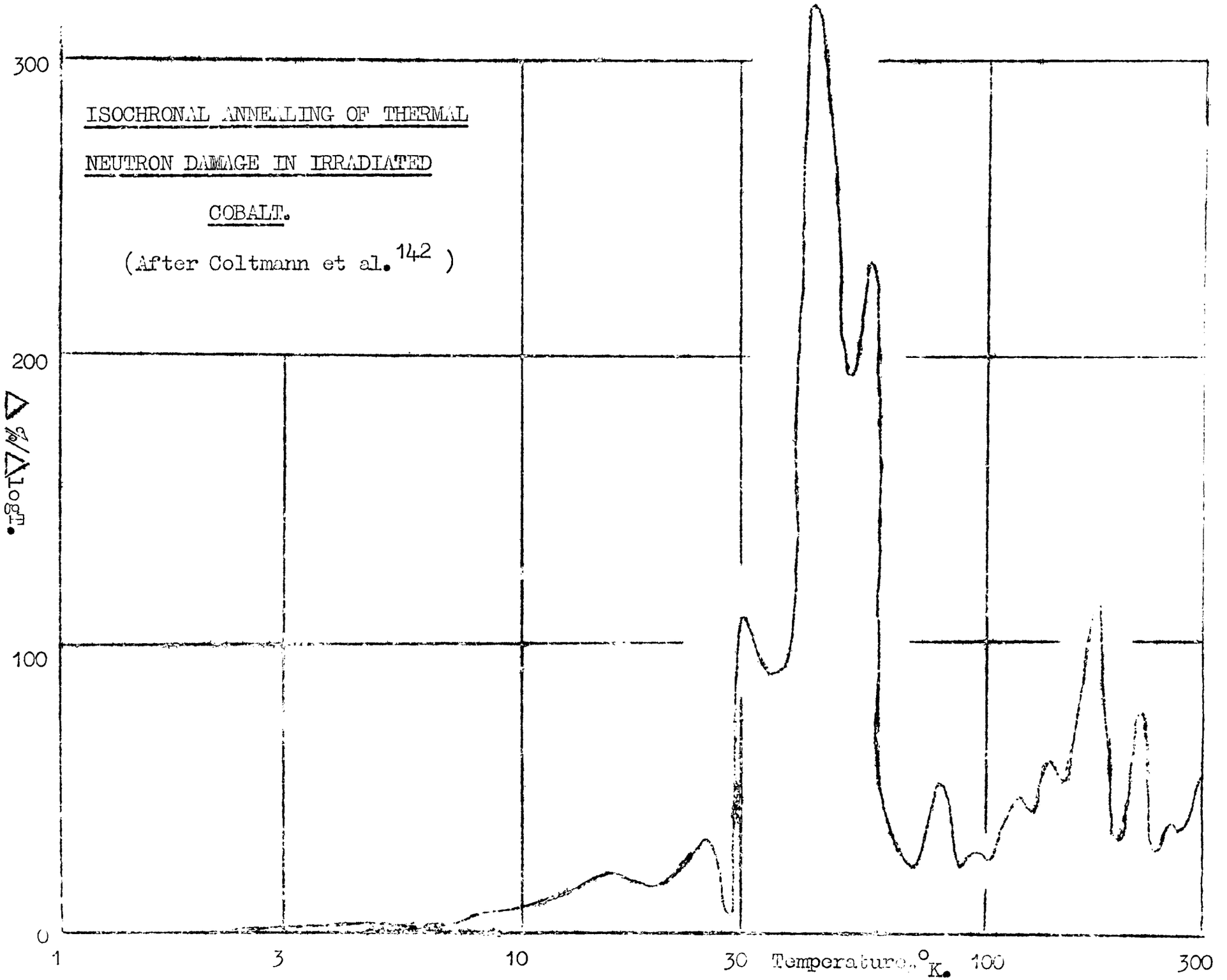


Figure VIII.4.

the hyperfine field on cobalt nuclei having one nearest neighbour aluminium, copper or silicon atom. If the thermal neutron damage took the form of a cobalt atom occupying a nearest neighbour interstitial position to the ^{60}Co atom one might expect an increase in the hyperfine field at the ^{60}Co nucleus, but fractionally greater than the 8% reduction per n.n. non-magnetic atom since the interstitial is much closer to the ^{60}Co nucleus. Thus it seems the results indicate the primary 'knock-on' nuclei to occupy lattice sites and that any radiation damage, which certainly exists at $4.2^{o}K$, is confined to regions further than one lattice constant from the primary 'knock-on' atom.

Calculations have been carried out to study radiation damage mechanisms in copper (fcc)[146] and in αFe-(bcc)[147]. The classical equations of motion of a set of several hundred to a thousand atoms with appropriate interactions were solved for large numbers of sequences, each initiated by the sudden transfer of some momentum to one atom (the 'primary knock-on'), the other atoms initially being at rest in normal lattice sites. This is analogous to the present experimental situation where the ^{60}Co atom corresponds to the primary knock-on atom with an initial energy of $\sim$300eV. The calculations showed that the most common sequence occuring was one in which the primary knock-on replaced one of its neighbours which then could replace a further neighbour until finally an interstitial was formed several atomic distances away from the original knock-on atom. It was found that with knock-on energies as low as $\sim$70eV, for which the most detailed calculations were carried out, the knock-on could replace a first, second or third neighbour. Thus for energies $\sim$300eV the primary knock-on could well come to rest in a lattice site several atomic distances away from any vacancies or interstitials caused by these chains of correlated replacements. Moreover, the calculations of Erginsoy et Al.

(1965)[147] indicated that 'channelling', in which the primary knock-on moves along a trajectory between normal lattice sites and may well end up in an interstitial site, is not a very likely mechanism below 1500eV.

The results of the experiment reported here seem to confirm these calculations and particularly are consistent with a vacancy three lattice constants from the ^{60}Co nuclei. It had been hoped to derive from the present experiment some direct information concerning hyperfine fields in a damaged lattice; however we can see from the calculations that a primary knock-on energy less than 20eV ($\equiv 1.3 \cdot 10^5$ °K) is necessary to acheive this end. It is almost certainly impossible to find a nucleus which will absorb a thermal neutron and emit less than $\sim\frac{1}{2}$MeV of prompt gamma rays, since the binding energy of a nucleon, $\sim$8MeV, must be dissipated in the process.

VIII.7. Conclusion.

The hyperfine field at ^{60}Co nuclei formed in thermal neutron-irradiated hcp cobalt metal at 4°K was found to be $5 \pm 3.8\%$ larger than the same after annealing at room temperature. Although there is no available direct information about the effects of vacancies or interstitials upon the hyperfine fields of atoms in ferromagnetic metals, it is argued that after recoil the ^{60}Co nuclei exist in normal lattice sites with any vacancy or interstitial formed at a distance of more than one lattice constant. This supports the results of recent theoretical calculations about the mechanisms of radiation damage.

Appendix A.

The High Tension Stabiliser.

A schematic diagram of the counting equipment plus stabiliser unit is shown in Fig A.Ia. The stabiliser served to 'lock-in' one discriminator 'window' onto a 'peak' in the gamma ray spectrum, and functioned as follows.

A 20c/s voltage modulation was added to the amplified voltage pulses before the discriminator; this had the effect of 'wobbling' the gamma ray spectrum along its energy/voltage axis. If the discriminator window were set near a peak in the gamma ray spectrum, the output pulse rate from the discriminator would vary considerably at the modulation frequency of 20c/s. The discriminator output pulses were broadened by a monostable flip-flop, converted to a continuous ('d.c.') signal with 20c/s modulation in amplitude, using a smoothing circuit having a time constant between the frequency of the pulses and of the modulation, then amplified and fed to a phase-sensitive detector. The phase of this 'modulated counting rate' signal would change by π as the discriminator window passed from one side of a peak to the other, see Fig. A.Ib. The reference signal to the phase sensitive detector was provided by the original 20c/s signal (with an appropriate compensating phase shift), which acted as a reversing switch every half cycle. Thus the output d.c. signal from this unit changed sign as the discriminator window passed from one side of a peak to the other. Another smoothing circuit, having a very long time constant ($\sim$10sec.), filtered out all remaining modulation from the phase sensitive detector output, which was then fed to the grid of the triode supplying the high tension to the photomultiplier tube, and was of the correct sign to restore the nearest peak in the gamma ray spectrum to the center of

BLOCK DIAGRAM OF ONE SCINTILLATION COUNTER WITH TWO "WINDOWS" TO SPECTRUM, ONE USED FOR STABILISATION.

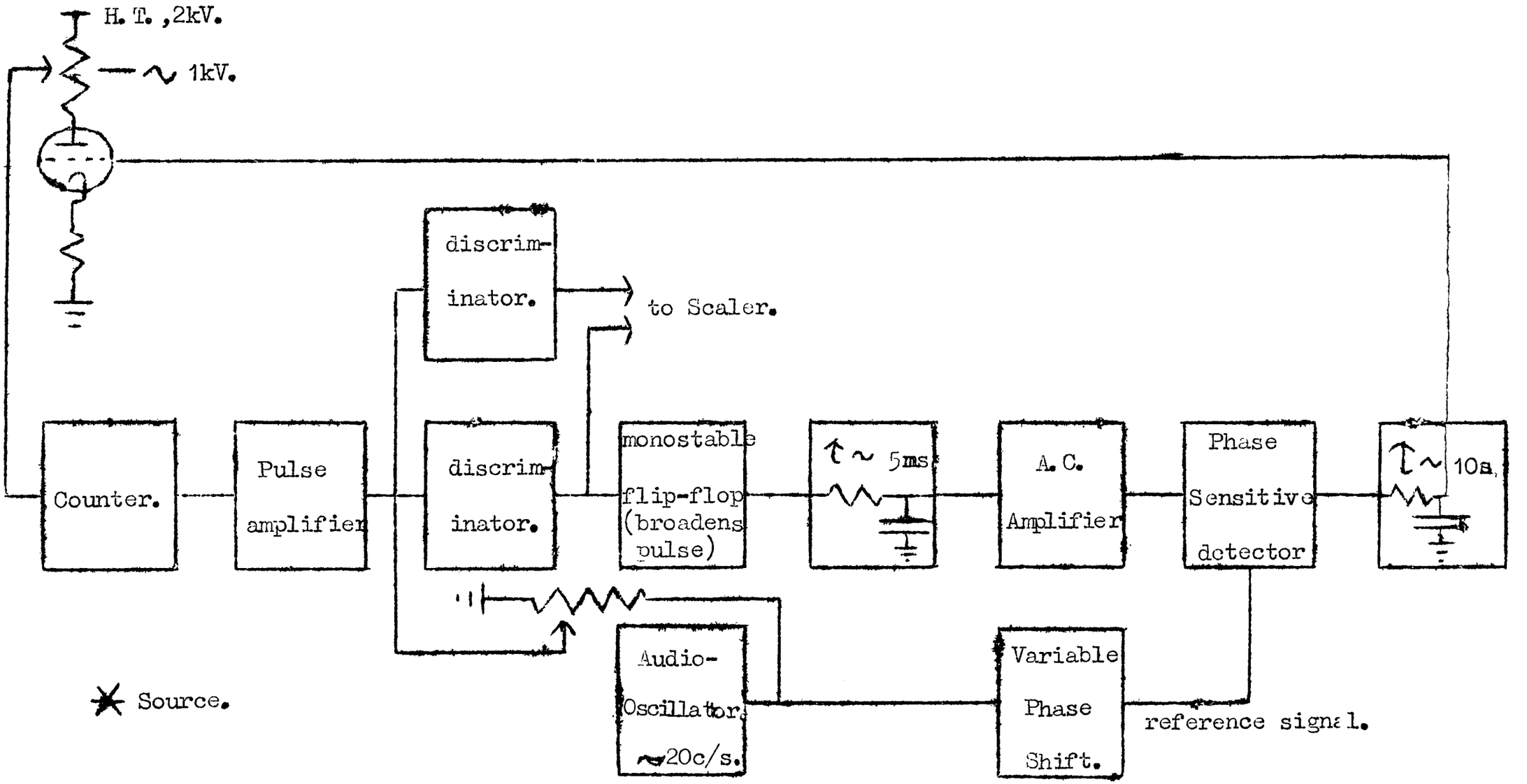


Figure A. 1a.

the discriminator window. Once a spectrum peak was in the center of the window, the correcting signal to the triode grid would, of course, be zero.

This stabiliser was designed and built by Dr G.V.H.Wilson.

Discriminator Output After Modulation.

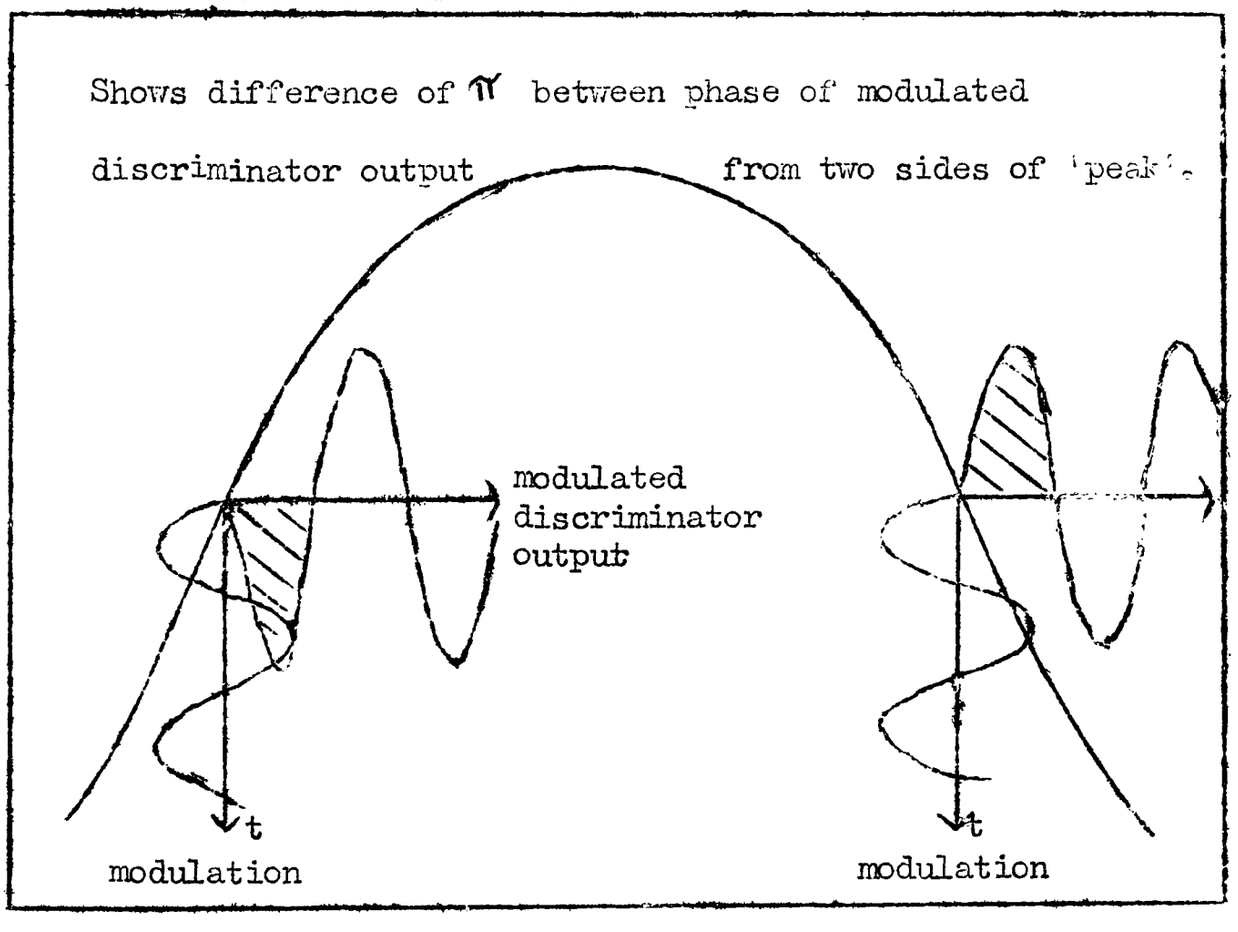


Figure A.1b.

Appendix B.

Corrections Applied to the Observed Anisotropy.

We give here the equations used to correct the observed anisotropy for the contributions from any background radiation, and from Compton scatter of any higher energy radiation (overlap) or double coincidence of any lower energy radiation (pile-up).

We consider the case of a two gamma ray spectrum A, B in which the observed 'effects' are E_A^o, E_B^o respectively and the true 'effects' are E_A^t, E_B^t and the 'effects' $E(\theta,T)$ are related to the anisotropy $W(\theta,T)$ by

$$E(\theta,T) = \left| 1 - W(\theta,T) \right| .$$

Then the true 'effects are given by

$$E_A^t = \frac{(E_A^o N_A - \beta R_B E_B^o N_B)}{(N_A - \beta(N_B - B_B) - B_A)} \times \frac{(1 - \alpha\beta)}{(1 - \alpha\beta R_B R_A)}$$

$$E_B^t = \frac{(E_B^o N_B - \alpha R_A E_A^o N_A)}{(N_B - \alpha(N_A - B_A) - B_B)} \times \frac{(1 - \alpha\beta)}{(1 - \alpha\beta R_A R_B)}$$

where N_A, N_B are the 'warm' counting rates in the A, B 'windows' respectively, B_A and B_B are the background counting rates,

$$\alpha = \frac{\text{number of counts in window B due to nucleus A}}{\text{number of counts in window A due to nucleus A}} ,$$

and the anisotropy due to A in window B is a fraction R_A of the anisotropy due to A in window A.

For β interchange A for B and B for A in α, and for R_B interchange A for B and B for A in R_A.

Appendix C.

Explicit Expression for the Degree of Circular Polarisation.

In this appendix we give an explicit expression for the polarisation of the gamma radiation emitted during an electric quadrupole transition from a level I to I-2 (^{54}Mn, $2^+ \rightarrow 0^+$; ^{60}Co, $4^+ \rightarrow 2^+ \rightarrow 0^+$.) by aligned nuclei.

If $\chi_{//}$ and χ_c are respectively the linearly and left-circularly polarised vectors ($-\chi_c$ is the right-circularly polarised vector), and the degree of polarisation is given by $W(\theta)\underline{E}_o$, then

$$W(\theta)\underline{E}_o = A\chi_{//} + B\chi_c \qquad \ldots\ldots\ldots \text{IV.1.}$$

where for an E2 transition $I \leftrightarrow I-2$,[45]

$$A = (45/7)N_2 f_2(\cos^2\theta - 1) + (25/4)N_4 f_4(-7\cos^4\theta + 8\cos^2\theta + 1)$$

$$B = 2N_1 f_1 \cos\theta + 5N_3 f_3(-5\cos^3\theta + 3\cos\theta)$$

and

$$N_k = b_k I^k (2I-k)!/2I! \quad , \quad b_k = 2^{\frac{1}{2}k} \text{ for k even,}$$
$$= 2^{\frac{1}{2}(k+1)} \text{ for k odd.}$$

$$f_1 = I^{-1}\sum_m m c_m; \qquad f_2 = I^{-2}(\sum_m m^2 c_m - \tfrac{1}{3}I(I+1));$$

$$f_3 = I^{-3}(\sum_m m^3 c_m - (1/5)(3I^2 + 3I - 1)\sum_m m c_m);$$

$$f_4 = I^{-4}(\sum_m m^4 c_m - (1/7)(6I^2 + 6I - 5)\sum_m m^2 c_m + (3/35).$$

$$.I(I-1)(I+1)(I+2)).$$

The c_m are the population probabilities of the levels m of the state immediately preceeding the observed gamma decay. These f_k can be rewritten in terms of the population probalities a_m of the levels of

the initial nucleus, spin I_o, in thermal equilibrium with its surroundings before any decay which may immediately precede that observed (β in the case of ^{54}Mn and ^{60}Co). The relation between $f_k(I_o)$ and $f_k(I)$ is particularly simple for the types of decay in which we are interested, namely stretched decays, when[45]

$$N_k(I)f_k(I) = N_k(I_o)f_k(I_o).$$

Only the sense of the circular polarisation, that is the sign of B, the coefficient of χ_c, was detected in the experiments. We see that B changes sign if the angle θ of observation changes by π. Also it can be shown that this sign depends on the differences $a_m - a_{-m}$, that is on the sign of the hyperfine field relative to the applied magnetic field, for any given angle θ.

References.

1. W. A. Heisenberg, Z. Physik 49, 619, 1928.

2. R. Stuart, W. Marshall, Phys. Rev. 120, 353, 1960.

3. A. J. Freeman, R. Nesbet, R. E. Watson, Phys. Rev. 125, 1978, 1962.

4. E. Fermi, Z. Physik 60, 320, 1930.

5. R. M. Sternheimer, Phys. Rev. 86, 316, 1952.

6. D. R. Hartree, Proc. Camb. Phil. Soc. 24, 89, 1928.

   V. Fock, Z. Physik 61, 126, 1930.

   J. C. Slater, Phys. Rev. 35, 210, 1930.

7. R. E. Watson, A. J. Freeman, Magnetism 2A, 235, 1965. Ed. G. T. Rado, H. Suhl.

8. R. E. Watson, A. J. Freeman, Phys. Rev. 123, 2027, 1961.

9. R. E. Watson, A. J. Freeman, Magnetism 2A, 167-305, 1965. Eds. Rado & Suhl.

10. R. E. Watson, A. J. Freeman, Phys. Rev. 131, 250, 1963.

11. E. C. Stoner, "Magnetism and Matter", Methuen.

12. F. Frohlich, F. R. N. Nabarro, Proc. Roy. Soc. A175, 382, 1940.

13. C. Zener, Phys. Rev. 81, 440; 83, 299, 1951.

14. M. A. Ruderman, C. Kittel, Phys. Rev. 96, 99, 1954.

15. T. Kasuya, Prog. Theor. Phys. (Kyoto) 16, 45, 1956.

16. K. Yosida, Phys. Rev. 106, 893, 1957.

17. G. Vertogen, W. J. Caspers, Zeitschrift für Physik 198, 37, 1967.

18. J. Kondo, Prog. Theor. Phys. 36, 429, 1966; Phys. Rev. 154, 644, 1967.

19. Y. Nagaoka, Phys. Rev. 138, A1112, 1965; Prog. Theor. Phys. 37, 13, 1967.

20. A. W. Overhauser, J. Phys. Chem. Sol. 13, 71, 1960; Phys. Rev. 128, 1437, 1962; J. Applied Phys. 34, 1019, 1963.

21. J. Friedel, Il Nuovo Cimento suppl 7, 287, 1958; J. Phys. Rad. 23, 692, 1962.

22. D. E. Nagle, H. Frauenfelder, R. D. Taylor, D. R. F. Cochran, B. T. Matthias,

Phys. Rev. Lotts. 5, 364, 1960.

P. P. Craig, D. E. Nagle, W. A. Steyert, R. D. Taylor, Phys. Rev. Letts. 9, 12, 1962.

23. E. Mathias, R. J. Halliday, Phys. Rev. Letts. 17, 897, 1966.

J. E. Templeton, D. A. Shirley, Phys. Rev. Letts. 18, 240, 1967.

24. B. Bleaney, Proc. Phys. Soc. A64, 315, 1951., Phil. Mag. (7), 42, 441, 1951.

25. A. Abragam, M. H. L. Price, Proc. Roy. Soc. A205, 135, 1951.

26. C. J. Gorter, Phys. Zeit. 35, 923, 1934.

27. N. Kurti, F. E. Simon, Proc. Roy. Soc. A149, 152, 1935.

28. J. W. T. Dabbs, L. D. Roberts, S. Bernstein, Phys. Rev. 98, 1512, 1955.

29. C. J. Gorter, Physica 14, 504, 1048.

M. E. Rose, Phys. Rev. 75, 213, 1949.

30. E. Ambler, M. A. Grace, H. Halban, N. Kurti, H. Durand, C. Johnson, H. R. Lemmer, Phil. Mag. 44, 216, 1953.

S. Bernstein, L. D. Roberts, C. P. Stanford, J. W. T. Dabbs, T. E. Stephenson, Phys. Rev. 94, 1243, 1954.

31. B. N. Samoilov, V. V. Sklyarevskii, E. P. Stepanov, J. E. T. P. 9, 448, 1959; J. E. T. P. 11, 261, 1960.

G. R. Khutsishvili, J. E. T. P. 2, 744, 1956.

32. J. A. Cameron, L. A. Campbell, J. P. Compton, R. A. G. Lines, G. V. H. Wilson, Phys. Letts. 20, 569, 1966.

33. B. Bleaney, J. M. Daniels, M. A. Grace, H. Halban, N. Kurti, F. N. H. Robinson, F. E. Simon, Proc. Roy. Soc. A221, 170, 1954.

34. R. V. Pound, Phys. Rev. 76, 1410, 1949.

35. J. Blok, D. A. Shirley, Phys. Rev. 143, 911, 1966.

35a. J. W. T. Dabbs, L. D. Roberts, G. W. Parker, Bull. Am. Phys. Soc. ser II, 1, 207, 1956.

36. J. A. Spiers, Nature 161, 807, 1948.

37. N. R. Steenberg, Phys. Rev. 84, 1051, 1951.

38. H. A. Tolhoek, S. R. de Groot, Physica 17, 81, 1951.

39. N. R. Steenberg, Proc Phys Soc A65, 791, 1952.

40. H. A. Tolhoek, J. A. M. Cox, Physica 18, 357, 359, 1952.

41. H. A. Tolhoek, Physica 18, 1257, 1952.

42. N. R. Steenberg, Proc. Phys. Soc. A66, 391, 399, 1953.

43. N. R. Steenberg, Can. J. Phys. 31, 204, 1953.

44. H. A. Tolhoek, J. A. M. Cox, Physica 19, 101, 1953.

45. J. A. M. Cox, H. A. Tolhoek, Physica 19, 673, 683, 1953.

46. J. A. M. Cox, S. R. de Groot, C. D. Hartogh, Physica 19, 1119, 1123, 1953.

47. G. R. Satchler, Proc. Phys. Soc. A66, 1081, 1953.

48. G. R. Satchler, Phys. Rev. 94, 1304, 1954.

49. C. D. Hartogh, H. A. Tolhoek, S. R. de Groot, Physica 20, 1310, 1954.

50. J. P. Gray, G. R. Satchler, Proc. Phys. Soc. A68, 349, 1955.

51. M. A. Grace, R. J. Blin-Stoyle, Handbuch der Physik 42, 555, 1957.

52. N. R. Steenberg, Proc. Phys. Soc. A66, 399, 1953.

53. M. Tinkham, "Group Theory and Quantum Mechanics", p121-2, Mc Graw-Hill, 1964.

54. A. Simon, Oak Ridge National Laboratory rept ORNL-1718, 1954.

55. L. C. Biedenharn, ORNL rept 1098, 1952.

56. A. Simon, J. H. Vandersluis, L. C. Biedenharn, ORNL rept 1679, 1954.

57. L. C. Biedenharn, M. E. Rose, Rev. Mod. Phys. 25, 729, 1953.

58. M. Ferentz, N. Rosensweig, Argonne National Laboratory Report 5324, 19 .

59. D. R. Bland, "Solutions of Laplace's Equation", p68, Routledge and Kegan Paul, London, 1961.

60. L. A. Campbell, N. J. Stone, B. G. Turrell, Proc. Roy. Soc. A283, 379, 1965.

61. P. Dagley, M. A. Grace, J. S. Hill, C. V. Sowter, Phil. Mag. 3, 489, 1958.

62. J. Blok, D. A. Shirley, Phys. Rev. 143, 911, 1966.

63. Landolt-Börnstein 1961. Group 1, vol. 1., Berlin: Springer-Verlag.

64. W. Dubrov, C. D. Jeffries, Phys. Rev. 108, 60, 1957.

65. I. Lindgren, "Perturbed Angular Correlations", Ed. Karlsson et Al., North Holland, 1964.

66. J. P. Compton, Thesis, Oxford, 1965.

67. F. E. Hoare, L. C. Jackson, N. Kurti, "Experimental Cryophysics", London, 1961.

68. L. A. Campbell, Thesis, Oxford, 1964.

69. Hobden, 20-10-1959, Oxford.

70. M. H. L. Yates, "Perturbed Angular Correlations", Eds E. Karlsson, E. Matthias, K. Siegbahn., North Holland: Amsterdam, 1964.

71. W. Franz, Ann. Physik. 33, 689, 1938.

72. U. Fano, J. Opt. Soc. Amer. 39, 859, 1949.

73. S. B. Gunst, L. A. Page, Phys. Rev. 92, 970, 1953.

74. F. W. Lipps, H. A. Tolhoek, Physica 20, 85, 395, 1954.

75. J. C. Wheatley, W. J. Huiskamp, A. N. Diddens, M. J. Steenland, H. A. Tolhoek, Physica 21, 841, 1955.

76. D. A. Shirley, G. A. Westenbarger, Phys. Rev. 138, A170, 1965.

77. G. M. Stinson, R. G. Summers-Gill, Physics in Canada 22, 43, 1966.

78. M. Kontani, K. Asayama, J. Itoh, J. Phys. Soc. Japan. 20, 1737, 1965.

79. R. J. Blin-Stoyle, Rev. Mod. Phys. 28, 75, 1956.

80. J. A. Cameron, L. A. Campbell, J. P. Compton, R. A. G. Lines, Phys. Letts. 10, 24, 1964.

81. G. A. Westenbarger, D. A. Shirley, Phys. Rev. 138, A161, 1965.

82. S. G. Schmelling, V. J. Ehlers, H. A. Schugart, Phys. Rev. 154, 1142, 1967.

83. L. D. Roberts, J. O. Thomson, Phys. Rev. 129, 664, 1963.

84. Vogt, Ergebnisse d. Exakt Naturwiss 11, 323, 1952.

85. F. E. Hoare, J. C. Walling, J. C. Matthews, Proc. Roy. Soc. (London) A216, 502, 1953.

86. N. F. Mott, D. Jones, "Theory of the Properties of Metals and Alloys" p194, 1936, O. U. P.

87. S. C. Abrahams, J. Phys. Chem. Sol. (G. B.) 24, 589, 1963.

88. A. Arrot, J. Appl. Phys. (U. S. A.) 36, 1093, 1965.

89. F. E. Hoare, J. C. Matthews, Proc. Roy. Soc. A212, 137, 1952.

90. J. A. Seitchik, A. C. Gossard, V. Jaccarino, Phys. Rev. A136, 1119, 1964.

91. K. Clusius, L. Schachinger, Z. Naturforsch 2A, 90, 1947.

92. G. L. Picard, F. E. Simon, Proc. Phys. Soc. 61, 1, 1948.

93. J. Crangle, T. F. Smith, Phys. Rev. Letts. (U. S. A.) 9, 86, 1962.

94. J. A. Rayne, Phys. Rev. 107, 669, 1957.

95. N. K. Hindley, P. Rhodes, Proc. Phys. Soc. (G. B.) 81, 717, 1963.

96. J. Wucher, Compte Rendu 242, 1143, 1956.

97. J. Friedel, P. Lenglart, G. Leman, J. Phys. Chem. Sol. 25, 781, 1964.

98. P. Lenglart, G. Leman, J. P. Lelian, J. Phys. Chem. Sol. 27, 377, 1966.

99. J. W. Cable, E. O. Wollan, Phys. Rev. 140, 2003, 1965.

100. R. M. Bozorth, P. A. Wolff, D. D. Davis, V. B. Compton, J. H. Wernick, Phys. Rev. 122, 1157, 1961.

101. J. Crangle, Phil. Mag. ser 8, 5, 335, 1960.

102. J. W. Cable, E. O. Wollan, W. C. Koehler, J. Appl. Phys. 34, 1189, 1963.

103. G. G. Low, T. M. Holden, Proc. Phys. Soc. 89, 119, 1966.

104. Duk-Joo Kim, Phys. Rev. 149, 434, 1966.

105. M. Peter, J. Phys. Rad. 23, 730, 1962.

106. M. Peter, D. Shaltiel, J. H. Wernick, H. J. Williams, J. B. Mock, R. C. Sherwood, Phys. Rev. Letts. 9, 50, 1962.

107. D. Shaltiel, J. Appl. Phys. 34, 1190, 1963.

108. D. Mattis, Phys. Rev. Letts. 12, 561, 1964.

109. B. Giovanni, M. Peter, J. R. Schrieffer, Phys. Rev. Letts. 12, 736, 1964.

110. B. W. Veal, J. A. Rayne, Phys. Rev. 135A. 442. 1964.

111. B. M. Boerstoel, C. Du Chatenier, Proc. Ninth Int. Conf. in Low Temp. Physics, Ohio, U. S. A., paper CU12, 1964.

112. P. P. Craig, D. E. Nagle, W. A. Steyert, R. D. Taylor, Phys. Rev. Letts. 9, 12, 1962.

113. F. W. D. Woodhams, R. E. Meads, J. S. Carlow, Phys. Letts. 23, 419, 1966.

114. J. A. Gonzalo, M. I. Kay, J. Phys. Soc. Japan 21, 1626, 1966.

115. E. Krén, J. Solyom, Phys. Letts. 22, 273, 1966.

116. H. Sato, R. S. Toth, Phys. Rev. A139, 1581, 1965.

117. D. H. Shaltiel, J. H. Wernick, Phys. Rev. A136, 245, 1964.

118. M. Hansen, "Constitution of Binary Alloys", Mc Graw-Hill, New York, 1958.

119. Svensson, Ann. der Physik 18, 294, 1933.

120. Y. Kôi, A. Tsujimura, T. Hihara, T. Kushida, J. Phys. Soc. Japan 16, 1040, 1961.

121. W. Marshall, Phys. Rev. 118, 1519, 1960.

122. T. A. Kitchens, W. A. Steyert, R. D. Taylor, Phys. Rev. 138A, 467, 1965.

123. R. M. Housely, J. G. Dash, Phys. Letts. 10, 270, 1964.

124. J. P. Compton, I. R. Williams, G. V. H. Wilson, Proc. Conf. Hyp. Interact., Antomar, California, 1967.

125. Y. Nagaoka, Prog. Theor. Phys. 37, 13, 1967.; Phys. Rev. 138, A1112, 1965.

126. J. Kondo, Prog. Theor. Phys. 36, 429, 1966; Phys. Rev. 154, 644, 1967.

127. I. R. Williams, Thesis, Oxford, 1968.

128. S. Ehara, Y. Tomomo, J. Phys. Soc. Japan 17, 726, 1962.

129. D. A. Shirley, Private Communication, 1967.

130. D. E. Nagle, P. P. Craig, P. Barret, D. R. F. Cochran, C. E. Olsen, R. D. Taylor, Phys. Rev. 125, 490, 1962.

131. S. Kobayashi, J. Itoh, J. Phys. Soc. Japan 20, 1741, 1965.

132. P. P. Craig, B. Mozer, R. Segnan, Phys, Rev. Letts. 14, 895, 1965.

133. N. E. Alekseevskii, V. N. Anishenko, A. L. Erzinkyan, V. P. Parfenova, V. S. Shpinel, Z. E. T. P. 3, 318, 1966.

134. D. M. S. Bagguley, W. A. Crossley, J. Liesegang, Proc. Phys. Soc. 90, 1047, 1967.

135. M. A. Grace, C. E. Johnson, N. Kurti, R. G. Scurlock, R. T. Taylor, Comm. Conf. Basses Temperatures, Paris. Annexe 1955-3, 1955. Bull. Inst. Int. du Froid, p261.

136. M. A. Grace, C. E. Johnson, N. Kurti, R,G,Scurlock, R. T. Taylor, Phil. Mag. 4, 948, 1959.

137. H. Frauenfelder, N. Levine, A. Rossi, S. Singer, Phys. Rev. 103, 352, 1956.

138. D. F. Griffing, J. C. Wheatley, Phys. Rev. 104, 389, 1956.

139. P. Dagley, M. A. Grace, J. S. Hill, C.V.Sowter, Phil. Mag. 3, 489, 1958.

140. V. Dubrov, C. D. Jeffries, Phys. Rev. 108, 60, 1957.

141. Y. Koi, A. Tsujimura, T. Hihara, T. Kushida, J. Phys. Soc. Japan 17, Suppl. B-I, 96, 1962.

142. R. R. Coltmann, Jr, C. E. Klabunde, J. K. Redman, 1966, to be published.

143. G. K. Wertheim, V. Jaccarino, J. H. Wernick, D.N. E. Buchanan, Phys. Rev. Letts. 12, 24, 1964.

144. M. B. Stearns, Phys. Rev. 147, 439, 1966.

145. J. Itoh, K. Asayama, S. Kobayashi, Proc. Int. Conf. Magnetism., Nottingham, 1964.

146. J. B. Gibson, A. N. Goland, M. Milgram, G. H. Vineyard, Phys. Rev. 120, 1229, 1960.

147. C. Erginsoy, G. H. Vineyard, A. Englart, Phys. Rev. 133A, 595, 1964; Phys. Rev. 139A, 118, 1965.

Acknowledgements.

I am indebted to the following for their help:

Professor B. Bleaney for extending to me the facilities of the Clarendon Laboratory.

Dr R. W. Hill for his very helpful supervision.

Dr N. Kurti for much encouragement.

Dr G. V. H. Wilson for his close collaboration throughout the work described herein.

My 'comrades in arms', Dr L. A. Campbell, Dr J. P. Compton, Mr R. A. G. Lines, Mr J. Gallop, Mr I. R. Williams, for their considerable help.

The Technical staff of the Clarendon Laboratory for their understanding and rapid assistance, particularly Mr E. R. Tilbury, Mr K. Robinson, Mr A. Hazel, Mr C. W. Band and many others.

Lastly I would like to thank all the friends and colleagues who made my stay in Oxford so enjoyable.

My thanks are also due to the Science Research Council for the award of a three year maintenance grant.
